Universidade de Aveiro
2015

Departamento de
Electrónica, Telecomunicações e Informática

ALI SHAHPARI

Redes Ópticas de Acesso de Nova Geração: Tecnologias e Economia

Next Generation Optical Access Networks: Technologies and Economics

Universidade de Aveiro Departamento de
2015 Electrónica, Telecomunicações e Informática

ALI SHAHPARI

Redes Ópticas de Acesso de Nova Geração: Tecnologias e Ecónomia

Next Generation Optical Access Networks: Technologies and Economics

Tese apresentada à Universidade de Aveiro para cumprimento dos requisitos necessários à obtenção do grau de Doutor em Engenharia Electrotécnica / Telecomunicações, realizada sob a orientação científica do Doutor António Luís Jesus Teixeira, Professor Associado com Agregação do Departamento de Electrónica, Telecomunicações e Informática da Universidade de Aveiro, e do Doutor Mário José Neves Lima, Professor Auxiliar do Departamento de Electrónica, Telecomunicações e Informática da Universidade de Aveiro.

Apoio financeiro da Fundação para a Ciência e a Tecnologia - FCT atravésda bolsa FRH/BD/71667/2010 e do FSE no âmbito do Programa Operacional Potencial Humano (POPH) do QREN.

o júri

presidente

Doutor Manuel João Senos Matias
Professor Catedrático da Universidade de Aveiro

Doutor Josep Joan Prat Goma
Professor Catedrático da Universitat Politècnica de Catalunya

Doutor José Rodrigues Ferreira da Rocha
Professor Catedrático da Universidade de Aveiro

Doutor Adolfo da Visitação Tregeira Cartaxo
Professor Associado com Agregação do Instituto Superior Técnico da Universidade de Lisboa

Doutor António Luís Jesus Teixeira
Professor Associado com Agregação da Universidade de Aveiro (orientador)

Doutor Abel Jorge Antunes da Costa
Professor Auxiliar da Faculdade de Engenharia da Universidade do Porto

Acknowledgments

My PhD thesis has given me the pleasure and privilege of learning from people around the world with different believes and backgrounds. With the utmost sincerity, I wish to thank my academic supervisors, Prof. António Luís Jesus Teixeira and Prof. Mário José Neves de Lima, who have provided me with this wonderful opportunity to study at the University of Aveiro and I appreciate them for sharing their unique knowledge and experience.

I also extend my sincere thanks to all my colleagues and friends at Instituto de Telecomunicações for many fruitful discussions and pleasant times. I take this opportunity to especially thank to Ricardo Ferreira, Jacklyn Reis, Vitor Ribeiro, Giorgia Parca, João Prata, Zoran Vujicic, Fernando Guiomar, Alvaro Almeida, José Girão, Liliana Costa and Nelson Muga, among others. Particularly Ricardo Ferreira and Jacklyn Reis for explaining and rectifying many DSP related issues. I am very appreciated to Professors Dr. Armando Pinto, Dr. Rogério Nogueira, Dr. Paulo Monteiro and Dr. Paulo André for their friendship and help.

I would like to thank the University of Aveiro, in particular to the Department of Electronics, Telecommunications and Informatics (DETI) and Instituto de Telecomunicações (IT) for providing me fantastic working conditions. I also acknowledge Fundação para a Ciência e a Tecnologia for invaluable support in funding. I would also like to acknowledge SARDANA, GPON-in-a-BOX, TOMAR-PON, NG-PON2, DiNEq, PANAROMA2 and Real-PON projects as well as COST Action IC110 for providing some of the equipment used in this work.

I would like to thank Dr. Naoya Wada, Dr. Ruben Luís, Dr. Benjamin Puttnam and Dr. José Mendinueta for giving me the opportunity to work at National Institute of Information and Communications Technology, in Tokyo (Japan). I spent three unforgettable full time weeks in NICT working on some of my experimental works.

I am also very appreciated to Dr. Giorgio Tosi Beleffi from Ministry of Economic Development in Rome (Italy), Dr. Harald Rohde from Nokia Siemens Networks (Optical Networks) in Munich (Germany) for the opportunity to work with them on state-of-the-art technologies.

My special thanks to my parents, Sakineh and Mohammadreza and my wife Somayeh for unceasing support throughout my studies. You will have my love and gratitude, always.

palavras-chave Redes óticas de acesso de próxima geração, eficiência energética, redes óticas passivas, eficiência espetral, multiplexagem por divisão de comprimento de onda, comunicações óticas em espaço livre, formato de modulação avançado, comunicação coerente.

resumo O trabalho aqui apresentado estuda redes óticas de acesso de próxima geração (NG-OAN) nas vertentes económica (consumo de energia) e tecnológica (taxa, alcance e largura de banda dedicada/partilhada). O trabalho está dividido em quatro grandes temas de investigação: a eficiência energética em arquiteturas de acesso ótico, as redes óticas passivas de longo alcance (LR-PON) com nova eficiência espetral, o impacto da diafonia em redes de acesso heterogéneas e homogéneas e as transmissões ópticas híbridas com tecnologias sem fio.

Investiga-se o impacto dos perfis dos utilizadores, as tipologias da rede de distribuição ótica, as características do equipamento de partilha de recursos e o consumo de energia em LR-PON. Para se ter uma visão clara sobre o consumo de energia de cada parte das NG-OAN, é proposto um modelo para avaliar a eficiência energética das tecnologias de acesso óticas.

Desenvolve-se uma arquitetura PON bi-direcional com elevada eficiência espetral, recorrendo a multiplexagem por divisão de comprimento de onda ultra-densa (UDWDM), modulação de amplitude em quadratura com formato de impulso de Nyquist, oferecendo até 10 Gb/s por utilizador/comprimento de onda. O desempenho deste sistema em termos de sensibilidade do recetor e da tolerância à resposta não linear do canal de comunicação, sob diferentes condições de transmissão, é avaliado experimentalmente. Em transmissão bi-direcional, utilizando desvio de frequência (cima/baixo) do impulso com formato de Nyquist relativo à portadora ótica conseguiu-se uma alocação de largura de banda completa e uma manutenção mais simplificada de redes UDWDM, bem como a redução do espalhamento de Rayleigh. Além disso, a deteção auto-homodina é usada para relaxar o requisito de largura de linha do laser e a complexidade do processamento digital de sinal nas unidades da rede ótica.

Propõe-se um modelo numérico simplificado para estimar o impacto da diafonia de Raman em sistemas PON de próxima geração, com sobreposição do sinal de vídeo. É analisada a coexistência da série G.98X ITU-T e são considerados e avaliados sistemas coerentes multi-comprimento de onda.

Adicionalmente avaliam-se os desempenhos de PONs bi-direcionais híbridas, considerando tecnologia coerente e propagação por espaço livre, para diferentes balanços de potência e taxas de repartição na rede ótica de distribuição.

key words Next generation optical access network, energy efficiency, passive optical networks, spectral efficiency, wavelength-division multiplexing, free space optics, advanced modulation formats, coherent communication.

abstract

The work presented herein, studies Next Generation Optical Access Networks (NG-OAN) economically (e.g. energy consumption) and technologically (e.g. rate, reach and dedicated/shared bandwidth). The work is divided into four main topics: energy efficiency in optical access architectures, novel spectrally efficient Long-Reach Passive Optical Networks (LR-PON), crosstalk impacts in heterogeneous and homogenous access networks and hybrid optical wireless transmissions.

We investigate the impact of user profiles, optical distribution network topologies and equipment characteristics on resource sharing and power consumption in LR-PON. To have a clear vision on the energy consumption evolution of each part of NG-OAN, a model is proposed to evaluate the energy efficiency of optical access technologies.

A spectrally efficient bidirectional Ultra-Dense Wavelength Division Multiplexing (UDWDM) PON architecture is developed using Nyquist shaped 16-ary quadrature amplitude modulation, offering up to 10 Gb/s service capabilities per user or wavelength. Performance of this system in terms of receiver sensitivity and nonlinear tolerance under different network transmission capacity conditions are experimentally optimized. In bi-directional transmission, using frequency up/down-shifting of Nyquist pulse shaped signal from optical carrier, a full bandwidth allocation and easy maintenance of UDWDM networks as well as reduction of Rayleigh back-scattering are achieved. Moreover, self-homodyne detection is used to relax the laser linewidth requirement and digital signal processing complexity at the optical network unit.

Simplified numerical model to estimate the impact of Raman crosstalk of multi-system next generation PONs in video overlay is proposed. Coexistence of considered G.98X ITU-T series and coherent multi-wavelength systems is considered and assessed.

Additionally, the performances of bidirectional hybrid optical wireless coherent PONs over different optical distribution network power budgets and hybrid splitting ratios are evaluated.

"You have to learn the rules of the game. And then
you have to play better than anyone else."
Albert Einstein

I would like to dedicate this thesis to my lovely wife, Somayeh, and my parents, Sakineh and Mohammadreza.

CONTENTS

LIST OF TABLES

LIST OF FIGURES

LIST OF ACRONYMS

ADC	Analogue-to-Digital Converter
AON	Active Optical Network
ASE	Amplified Spontaneous Emission
AWG	Arbitrary Waveform Generator
BER	Bit Error Rate
BM	Burst Mode
BTB	Back-to-Back
CapEx	Capital Expenditures
CATV	Cable Television
CD	Coherent Detection
CE	Co-existence Element
CNR	Carrier-to-Noise Ratio
CO	Central Office
COC	Code of Conduct
CoRX	Coherent Receiver
CPE	Carrier Phase Estimation
CW	Continuous Wave
DAC	Digital-to-Analogue Converter
DFB	Distributed Feedback
DM	Direct Modulation
DML	Directly Modulated DFB Lasers
DS	Downstream
DSP	Digital Signal Processing
DWDM	Dense Wavelength Division Multiplexing
EB	Extender Box
ECL	External Cavity Laser
EDFA	Erbium Doped Fiber Amplifier
EML	Electro-absorption Modulated Laser
EPON	Ethernet PON
ESA	Electrical Spectrum Analyzer
EVM	Error Vector Magnitude
FE	Fast Ethernet
FEC	Forward Error Correction
FOAN	Future Optical Access Networks
FP	Fabry-Perot
FSAN	Full Service Access Network
FSO	Free Space Optics
FTTx	Fiber to the Node, Curb, Building, or Home
FWM	Four-Wave Mixing
FXS	Foreign eXchange Station
GE	Giga Ethernet
GPON	Gigabit PON
GRIN	Graded -Index
HD-TV	High Definition Television
IEEE	Institute of Electrical and Electronics Engineers
IM-DD	Intensity Modulation – Direct Detection
ILMZ	Integrated Laser Mach-Zehnder
ITU-T	International Telecommunication Union Telecommunication
LO	Local Oscillator
LR-PON	Long Reach-Passive Optical Network
LSI	Large Scale Integration
MZM	Mach-Zehnder Modulator
M-QAM	M-ary Quadrature Amplitude Modulation
NG-OAN	Next Generation Optical Access Network

NG-PON	Next Generation-Passive Optical Network
NRZ	Non-Return to Zero
OAN	Optical Access Networks
ODN	Optical Distribution Network
OFDMA	Orthogonal Frequency Division Multiple Access
OFDM-PON	Orthogonal Frequency Division Multiplexing PON
OLT	Optical Line Terminal
ONU	Optical Network Unit
OOK	On-Off Keying
OpEx	Operational Expenditures
OSA	Optical Spectrum Analyzer
OSNR	Optical Signal-to-Noise Ratio
OTG	Optical Transceiver Group
OWC	Optical Wireless Communication
OW	Optical Wireless
PBC	Polarization Beam Combiner
PBS	Polarization Beam Splitter
PC	Polarization Controller
PD	Photo Detector
PDF	Population Distribution Function
PDM	Polarization-Division Multiplexing
PON	Passive Optical Network
PRBS	Pseudo Random Binary Sequence
PSD	Power Spectral Density
PT	Pilot Tone
PtP	Point to Point
PtMP	Point to Multi-Point
PTVM	Pilot Tone Vector Modulator
QAM	Quadrature Amplitude Modulation
QPSK	Quadrature Phase Shift Keying
RBS	Rayleigh Back-Scattering
RF	Radio Frequency
RIN	Relative Intensity Noise
RN	Remote Node
RoF	Radio over Fiber
SHD	Self-Homodyne Detection
SMF	Single-Mode Fiber
SNI	Service Node Interface
SNR	Signal-to-Noise Ratio
SOA	Semiconductor Optical Amplifier
SPM	Self-Phase Modulation
SRS	Stimulated Raman Scattering
SSB	Single Side Band
TDM	Time Division Multiplexing
TRx	Transmitter and Receiver
TWDM	Time and Wavelength Division Multiplexing
UDWDM	Ultra Dense Wavelength Division Multiplexing
UNI	User Network Interface
US	Upstream
VOA	Variable Optical Attenuator
VOD	Video On Demand
WDM-PON	Wavelength-Division Multiplexing Passive Optical Network
WM	Wavelength Mux
WS	Wave Shaper
X-GPON	10-Gigabit-capable Passive Optical Network
XPM	Cross-Phase Modulation

CHAPTER 1 INTRODUCTION

Summary

Passive Optical Networks (PONs) are stemming as balanced alternatives for deploying the next generation future proof broadband. Technologically, several possibilities for PONs that offer efficient usage of bandwidth and energy per bit are being considered nowadays. Coherent based PON is envisioned to be as one of the promising candidates for Next Generation Optical Access Networks (NG-OAN). Clearly, this technology still requires maturing in order to meet the price targets for access networks as well as to meet the type of services and working conditions (rate, reach, energy consumption, dedicated/shared bandwidth). This work starts by addressing some of the factors that can be considered in the energy efficiency and resources optimization of optical access networks. Then it continues to investigate in detail the novel spectrally efficient coherent PON. This chapter details motivations, objectives and original contributions. The thesis organization is presented at the end of the chapter.

1.1 Passive Optical Networks

The proliferation of bandwidth-consuming Internet services such as cloud computing, high-definition television and mobile devices with the processing capability to consume and produce data at a high rate, has posed several challenges to network developers. Indeed, heterogeneous traffic in the networks which grow exponentially and typically are terminated in wireless terminals, has imposed a set of requirements which have pushed even standards to move faster [1]. Also, these new trends have changed the way operators are looking to the market and pushed them to innovate and rehab their networks at a faster pace to be able to cope with the competition from newcomers [2]. Therefore, with current technology, the underlying network backhaul has to be supported by fiber distribution, which may lead to the required latency and bandwidth to support more than one technology and also its growth in a sustained way. Herein, network operators are deploying fiber networks that can cover all the way to user in order to dramatically raise the data rate they can offer in efficient way. In recent years, telecom operators have shown a great interest in the development of cost-effective and reliable Fiber to the Home/Curb/Building/Cabinet (FTTx) networks based on Passive Optical Networks (PON) [3-5]. Nowadays, both IEEE and ITU-T with the Full Services Access Network (FSAN) group are working towards the standards for Next Generation PON2 (NG-PON2) and Time Division Multiple Access (TDMA) has been the preferred technology in PONs [6-8]. In the ITU-T side the path has been driven from Gigabit PON (GPON) (delivering asymmetric 1.25 Gb/s for upstream and 2.5 Gb/s for downstream) to 10-Gigabit-capable PON (XG-PON) and recently Time and Wavelength Division Multiplexing PON (TWDM-PON), G.989 [6], with four wavelengths at 10 Gb/s expandable up to 8 wavelengths, representing an aggregate rate of 40 up to 80 Gb/s. In the IEEE standards, the 802.3 series are also being tuned however for now in the line of the Ethernet PON (PON), the 10 G-EPON and its recent version the IEEE 802.3bk with extended capabilities and budget, however still on the 10 Gb/s per PON.

The benefits of TWDM approach, specifically for residential clients, are clear and immediate. However, with the increased requirements from heavy usage of residential or business users and increased mobile back and front hauling, it may be insufficient in some areas, for coping with bandwidth demands (e.g. LTE that may require from 1 up to 5 Gb/s). To solve this, it is being considered the sharing of the available bands with dedicated Point-

to-Point (PtP) WDM links. As such, WDM-PON has been presented as a solution, for higher data rate links, and at the same time supporting more users. Moreover they can provide dedicated wavelengths to each Optical Networks Unit (ONU) corresponding to each user, one PtP data link between the ONU and the Optical Line Terminal (OLT).

Extending this concept to a higher level, by an efficient and flexible spectrum utilization, Ultra Dense Wavelength Division Multiplexing (UDWDM) and Orthogonal Frequency Division Multiple Access (OFDMA) PONs have been recently proposed for future mobile backhaul/front haul systems and business users [J5], [9-11]. They offer high aggregation and flexible management of wavelengths, in a reduced bandwidth scenario, while providing high data rates.

Video overlay (analogue or digital), being one of the oldest technologies available in access networks, broadcasts a portion of the radio frequency spectrum (54 MHz to 1 GHz) at C-band (1550-1560 nm) to each customer [6, 12]. Consequently, transmitting video overlay with current PON technologies offers several benefits to operators and current PON customers at a reduced incremental cost. Even for some operators, video overlay is still one major source of revenue, or even their sole business target, therefore, this technology should be maintained in the new coming optical access deployments.

Additionally, and to comply with specific conditions which may occur, e.g. network resiliency or service outages minimization (caused by disasters, civil conflicts or terrorism acts) [13], can be overcome, under some condition, by optical wireless links. Free-Space Optic (FSO) can offer the highest capacity with license-free wireless spectrum domain and fast installation of the equipment and opens doors of opportunity in areas that are largely unexplored [14].

1.2 Optical Access Design Aspects

Due to the plurality of end user types and very heterogeneous nature of services, Internet data traffic in access network is becoming very dynamic and unpredictable. This makes the design of future optical access networks challenging and a blue ocean strategy that can create a leap in value for both buyers and the operator, using simultaneous pursuit of differentiation and low cost [15], should be considered. From cost point of view, complexity of the cost sensitive elements should be reduced, eventually by (i) keeping Optical Distribution Network (ODN) in Point-to-Multi Point (PtMP) and unchanged for as much time as possible,

(ii) reducing complexity, cost and energy consumption per bit at each part of the network, especially in the customer side and (iii) increasing barriers to providers change. From the value point of view, client's satisfaction is a key that can be achieved by (i) investing in a good technology from the first day, (ii) pay as you grow approach with enough flexibility to keep up surprising the client, (iii) innovation in the service and providing fast reaction to the markets. From what was referred, state-of-the-art optical access networks rely on both a large network capacity and scalability, together with flexible and efficient usage of spectral resources, easy maintenance, and coexistence with other existing PONs and video overlay, as shown in Fig. 1.1. In addition, extended reach is a key requirement to increase coverage area and reduce costs and energy per user.

However, when we are talking about coexistence of several technologies in a single fiber, both the electronics and optics disturb the input signal via various scattering phenomena, such as Cross-Phase Modulation (XPM), Four-Wave Mixing (FWM), Stimulated Raman Scattering (SRS) and crosstalk due to back reflections in bidirectional link [16-18]. The challenge for service providers is to find solutions that manage these distortions in an efficient way.

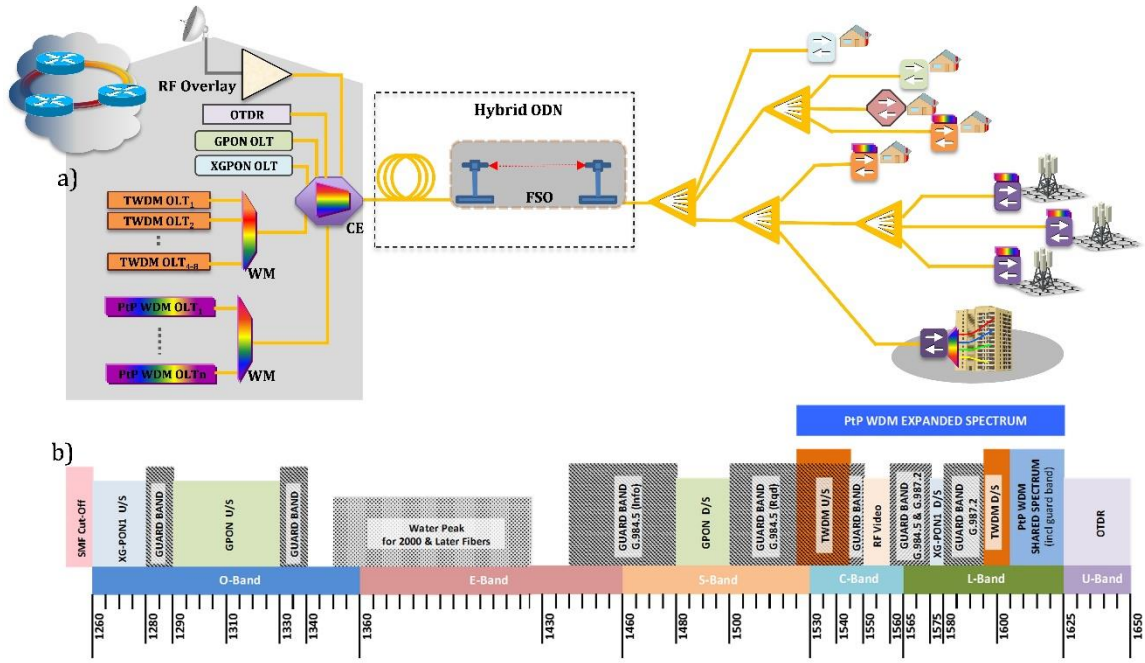

Figure 1.1 (a) Multiple system configuration for next generation optical access networks, (b) wavelength plan and coexistence representation [7]. CE: Co-existence Element, WM: Wavelength Mux (demux), FSO: Free Space Optics.

On the other side, from Fig. 1.1 (b) it can be noticed that the spectrum is already very crowded and with video overlay, there are only part of the transition bands in C, E and L bands. This situation has led to a lot of discussions when planning to support 1-10 Gb/s dedicated bandwidth per user/wavelength. Although, UDWDM system proposed in [J5, 9] uses very high channel count in very narrow channel spacing, e.g. 3 GHz, however, it can be quite challenging to upgrade to higher bit rates per channel/user when resorting to narrow channel spacing and reduced symbol rates.

1.3 Motivation and Outline

This Ph.D. thesis aims to investigate potential paths and parameters for the optimization of PONs requirements, technologically and economically. As such, the work was carried out targeting the following objectives:

1. Identify energy efficiency scenarios for optical access networks and develop a comprehensive energy consumption model that can cover all the optical access network dimensions.
2. Investigate advanced coherent PON architectures to overcome the spectrum scarcity and limitations of the existing systems, to be compatible with the specifications of future optical access networks.
3. Propose crosstalk mitigation schemes in coexistence scenarios, either via new coherent PON systems or by optimization of required guard band between coexisting systems, to comply with network coverage and capacity.
4. Develop a simple model for estimating the carrier-to-Raman-crosstalk ratio of RF-video signals caused by multi-system next generation PONs in coexistence scenario.
5. Evaluate hybrid combination of optical wireless infrastructures to address complete coverage area, optimized spectrum usage and network resiliency.

1.4 Thesis Organization

Besides this introductory chapter, the remainder of this thesis is organized as follows:

Chapter 2 addresses some of the factors that can be considered in the analysis of energy consumption in optical access networks.

Chapter 3 addresses spectrally efficient bidirectional UDWDM-PON based on Nyquist pulse shaping supporting 10 Gb/s dedicated data rate per user. The nonlinear mitigations of Nyquist pulse shaped signal are investigated theoretically and experimentally. It is also presented that Self-Homodyne Detection (SHD) enables reducing laser phase noise requirements and simplifying the Digital Signal Processing (DSP) in the proposed system.

Chapter 4 presents the performance analysis of UDWDM-PON in coexistence with legacy technologies such as GPON, X-GPON, TWDM and RF-Video in optical distribution networks. The system model and performance metric for carrier-to-Raman-crosstalk ratio of RF video are presented. Potential guard band for locations of UDWDM channels is analyzed by theoretical and practical approximations.

Chapter 5 presents a set of demonstrations over hybrid optical wireless links in metro and access networks. In particular, this chapter assesses the feasibility of bidirectional hybrid ODN coherent PON operating at 10 Gb/s per user.

Chapter 6 concludes the work with a summarization of promising future research directions.

1.5 Original Contributions

The work performed in this thesis has a set of contributions relevant to technological and economical optimization criteria of future optical access networks.

- The first part of the work, covering objective 1, contributed to analyze and optimize power consumption in optical access networks. The impact of different types of splitter structures on resource sharing and power consumption in long reach PON is analyzed. Also, some considerations are made on a set of criteria that may be used to balance between investment in a potentially more expensive technology at the interfaces (tunable Transmitter/Receiver (TRx)) versus a simpler and less expensive interface technology and some changes in the ODN. An energy consumption per user per day metric is proposed to evaluate the energy efficiency of optical access technologies. The work was described in three conference papers [C1], [C2], [C3]. Also, during these works we have participated for several contributions in FSAN NG-PON2 power consumption.

- Secondly, objective 2, a special attention was given to implement spectrally efficient PON based on coherent detection. We have been pushing the limits of optical access network capacity, by successfully demonstrating and beating records in the density and total aggregate bit rate. We numerically and experimentally demonstrated a bidirectional Terabit+ UDWDM coherent PON with Nyquist shaped 16-ary Quadrature Amplitude Modulation (16QAM), offering up to 10 Gb/s service capabilities per user/wavelength for 192 users in a total spectrum of 12.8 nm over 40 km of standard single-mode fiber. The work was described in two journal papers [J1], [J2] and 5 conference papers [C4-C8] in collaboration with Dr. J. D. Reis and Mr. R. Ferreira. In March 2013, we have demonstrated the highest spectral density ever achieved in a single PON, by fitting 1.92 Tb/s in only 12.8 nm, recognized publicly by the acceptance of the PDP at Optical Fiber Communication Conference (OFC). To extend this work, a proof of concept fully loaded bidirectional ultrahigh capacity PON (2 × 1008 × 8.3 Gb/s) is also presented. This is achieved using partial spectrum overlap, Nyquist shaping, digital frequency shifting, self-homodyne detection, and pilot tone re-modulation. The work was described in 2 journal papers [J3, J4] and 2 conference papers [C9, C10] in collaboration with Dr. R. Luis.

- Next contributions, covering objectives 3 and 4, were associated with crosstalk impact of heterogeneous optical access network. We investigated the performance of UDWDM-PON system regarding the frequency guard band and optical power of legacy technologies such as video overlay, GPON, X-GPON, TWDM-PON. We also experimentally and theoretically evaluated the impact of nonlinear Raman crosstalk on video overlay. We have considered G.98X ITU-T series and coherent multi-wavelength systems Raman crosstalk on video overlay. The contributions were reported in 2 journal papers [J3], [J5] and 5 conference papers [C11-C15] in collaboration with Dr. H. Rohde in Nokia Siemens Network and Dr. J. D. Reis. Also, during these works we contributed with FSAN in ITU-T G.989.2 recommendation in the physical layer requirements and specifications for the NG-PON2 physical media dependent layer.

- The later part of the work, objective 4, addressed the experimental demonstrations of hybrid optical wireless in optical metro and access networks. We could achieve the

transmission of a total capacity of 1.6 Terabit/s over hybrid fiber and 80 meters FSO system, with no optical-electronic-optical conversion at interfaces with air. This work was published in [J6] and one conference [C16] in collaboration with Dr. G. Parca and Dr. G. Tosi Beleffi. Later, to demonstrate capability of FSO system in optical access network, several high capacity indoor and outdoor hybrid optical wireless PONs were successfully demonstrated in half/full duplex links. Hybrid splitting based on beam splitters was also demonstrated showing a path towards FSO distribution in temporary campaigns or controlled environments. The work contributed to one journal [J7] and 7 conference papers [C15, C17-C22].

These contributions can lay down paths for spectrally efficient hybrid optical access network technologies which have capabilities to support high number of users with 10 Gb/s data rates.

1.6 List of Publications

The following is a list of original work published in the course of this research.

Journals:

[J1] J. D. Reis, **A. Shahpari**, R. Ferreira, S. Ziaie, D. Neves, M. Lima and A. Teixeira, "Terabit+ (192x10 Gb/s) Nyquist shaped UDWDM coherent PON with upstream and downstream over a 12.8 nm band," *IEEE/OSA Journal of Lightwave Tech*., vol. 32, no. 4, pp. 729- 735, January 2014. The first two authors equally contributed to this paper.

[J2] J. D. Reis, **A. Shahpari,** R. Ferreira, D. Neves, M. Lima and A. Teixeira, "Performance optimization of Nyquist signaling for spectrally efficient optical access networks [Invited]," *IEEE/OSA Journal of Optical Communications Networking*, vol. 7, no. 1, pp. A200-A208, January 2015.

[J3] **A. Shahpari,** R. S. Luís, V. Ribeiro, J. D. Reis, R. Ferreira, J. M. D. Mendinueta, Z. Vujicic, B. J. Puttnam, M. Lima, N. Wada and A. Teixeira, "Spectrally efficient enhanced performance bi-directional coherent PON with laserless 10 Gb/s ONU [Invited]," *IEEE/OSA Journal of Optical Communications Networking*, vol. 7, no. 3, pp. A403-A413, March 2015.

[J4] R. S. Luis, **A. Shahpari**, J. D. Reis, R. Ferreira, Z. Vujicic, B. J. Puttnam, J. M. D. Mendinueta, M. Lima, N. Wada and A. Teixeira, "Ultra high capacity self-homodyne PON with simplified ONU and burst-mode upstream," *IEEE Photonics Technology Letters*, vol. 26, no. 7, pp. 686 - 689, January 2014. The first two authors equally contributed to this paper.

[J5] H. Rohde, E. Gottwald, A. Teixeira, J. D. Reis, **A. Shahpari,** K. Pulverer and J. S. Wey, "Coherent ultra-dense WDM technology for next generation optical metro and access networks," *IEEE/OSA Journal of Lightwave Technology*, vol. 32, no. 10, pp. 2041-2052, April 2014.

[J6] G. Parca, **A. Shahpari,** V. Carrozzo, G. M. Tosi Beleffi and A. Teixeira, "Optical wireless transmission at 1.6-Tbit⁄s (16 × 100 Gbit⁄s) for next-generation convergent urban infrastructures," *Optical Engineering*, vol. 52, no. 11, pp. 1161021-5, November 2013.

[J7] **A. Shahpari,** A. Abdalla, G. Parca, J. Reis, R. Ferreira, M. Lima, V. Carrozzo, G. M. Tosi Beleffi and A. Teixeira, "Ultra high capacity PON systems with free-space optical communications," *Fiber and Integrated Optics*, vol. 33, no. 3, pp. 149 - 162, July 2014.

Conferences:

[C1] **A. Shahpari**, S. Ziaie, J. D. Reis, Z. Vujicic, M. Lima and A. Teixeira, "Impact of splitter configuration strategies on power consumption in PON," Proc. *Optoelectronics and Communications Conf. (OECC),* Kyoto, July 2013, paper TuPP-5.

[C2] A. Teixeira and **A. Shahpari**, "Implications of ODN on energy consumption in access networks [Invited paper]," Proc. *Access Networks and In-house Communications (ANIC),* Toronto, June 2011, paper AMB2.

[C3] A. Teixeira, **A. Shahpari** and M. Lima, "Factors in energy efficiency rating in optical access networks," Proc. International Conf. on Transparent Networks (ICTON), Stockholm, June 2011, paper Th.A3.4.

[C4] **A. Shahpari**, J. D. Reis, R. Ferreira, D. Neves, M. Lima and A. Teixeira, "Terabit+ (192 x 10 Gb/s) Nyquist shaped UDWDM coherent PON with upstream and downstream over a 12.8 nm band," Proc. *Optical Fiber Communication Conf. (OFC),* Anaheim, CA , March 2013, paper PDP5B.3.

[C5] J. D. Reis, **A. Shahpari**, R. Ferreira, D. Neves, M. Lima and A. Teixeira, "Nyquist signaling for spectrally-efficient optical access networks [Invited Paper]," Proc. *Optical Fiber Communication Conf. (OFC),* San Francisco, CA, March 2014, paper W3G3.

[C6] J. D. Reis, R. Ferreira, S. M. Rossi, G. J. Suzigan, T. M.S. Pinto, **A. Shahpari,** A. L. Teixeira, N. G. Gonzalez and J. R. F. Oliveira, "Bidirectional coherent WDM-PON performance with real-time Nyquist 16QAM transmitter," Proc. *Optical Fiber Communication Conf. (OFC),* Los Angeles, CA, March 2015, paper Th3I.5.

[C7] R. Ferreira, J. D. Reis, S. M. Rossi, T. M.S. Pinto, S. B. Amado, **A. Shahpari,** N. G. Gonzalez, J. R. F. Oliveira, A. N. Pinto and A. L. Teixeira, "Demonstration of Nyquist UDWDM-PON with digital signal processing in real-time," Proc. *Optical Fiber Communication Conf. (OFC),* Los Angeles, CA, March 2015, paper Th3I.4.

[C8] J.D. Reis, **A. Shahpari,** R. Ferreira, D. Neves, M. Lima and A. Teixeira, "Downstream and upstream Nyquist band optimization for heterodyne coherent PON," Proc. *Optical Fiber Communication Conf. (OFC),* San Francisco, CA, March 2014, paper W2A25.

[C9] **A. Shahpari**, R. S. Luis, J. D. Reis, Z. Vujicic, M. Lima, N. Wada and A. Teixeira, "Fully coherent self- homodyne bi-directional enhanced performance PON," Proc. *Optical Fiber Communication Conf. (OFC),* San Francisco, CA, March 2014, paper W4G.1.

[C10] R. S. Luís., B. J. Puttnam, J.-M. D. Mendinueta, **A. Shahpari,** Z. Vujičić, W. Klausa, J. Sakaguchi, Y.Awaji, A. Teixeira, N.Wada, T. Kawanishi and A. Kanno, "Coherent detection in self-homodyne systems with single and multi-core transmission [Invited Paper]," Proc. *SPIE Photonics West*, February 2015.

[C11] J. D. Reis, **A. Shahpari**, R. Ferreira, F. P. Guiomar, D. Neves, A. N. Pinto and A. Teixeira, "Analysis of transmission impairments on terabit aggregate PONs," Proc. *Optical Fiber Communication Conf. (OFC),*Anaheim, CA , March 2013, paper OM2A5.

[C12] **A. Shahpari**, J. D. Reis, R. Ferreira, Z. Vujicic, M. Lima and A. Teixeira, "Coherent UDWDM-PON guard band for legacy video and 10G-NRZ systems," Proc. *Optoelectronics and Communications Conf. (OECC*), Kyoto, July 2013, paper WP1-4.

[C13] **A. Shahpari,** J. D. Reis, S. Ziaie, R. Ferreira, M. Lima, A. N. Pinto and A. Teixeira, "Multi system next-generation PONs impact on video overlay," Proc. *European Conf. on Optical Communications (ECOC),* London, United Kingdom, September 2013, paper Tu.3.F.3.

[C14] A. Teixeira, **A. Shahpari,** J. D. Reis and M. Lima, "Spectral management in flexible multi-wavelength PONs," Proc. *Optical Fiber Communication Conf. (OFC),* Anaheim, CA, March 2013, paper JW2A09.

[C15] **A. Shahpari,** R. Ferreira, A. Sousa, V. Ribeiro, J. D. Reis, M. Lima and A. Teixeira, "Optimization criteria for coherent PONs with video overlay and hybrid ODN," Proc. *Optical Fiber Communication Conf. (OFC),* Los Angeles, CA, March 2015, paper Th3I.2.

[C16] G. Parca, **A. Shahpari,** V. Carrozzo, G.M. Tosi Beleffi and A. Teixeira, "Broadband free space optical urban links for next generation infrastructures and services," Proc. *International Conf. on Transparent Networks (ICTON),* Cartagena, June 2013, paper Tu.B3.2.

[C17] A. Teixeira, G. Parca, **A. Shahpari,** J. D. Reis, R. Ferreira , A. A. Mahmoud , M. Lima and G. Beleffi and V. Carrozzo, "Ultra high capacity PON systems [Invited paper]," Proc. *International Conf. on Transparent Networks (ICTON),* Cartagena, June 2013, paper Tu.C3.4.

[C18] **A. Shahpari**, A. N. Sousa, R. Ferreira, M. Lima and A. Teixeira, "Free space optical communications for ultra-high capacity PON system," Proc. *International Conf. on Applications of Optics and Photonics (AOP),* Aveiro, August 2014, paper 92861Y.

[C19] G. Parca, A. Tavares, **A. Shahpari,** V. Carrozzo, G. M. Tosi Beleffi and A. Teixeira, "FSO for broadband multi service delivery in future networks," Proc. *International Workshop on Optical Wireless Communications (IWOW),* Newcastle, October 2013, pp 67-70.

[C20] **A. Shahpari,** R. Ferreira, V. Ribeiro, Z. Vujicic, A. Tavares, S. Ziaie, A. Sousa, F. P. Guiomar, M. Lima, A. N. Pinto and A. Teixeira, "Free space optics hybrid PTMP advanced modulation bidirectional PON," Proc. *Eur. Conf. Opt. Commun. (ECOC),* Cannes, September 2014, paper P.7.16.

[C21] A. Teixeira, **A. Shahpari,** J. D. Reis and R. Ferreira, "Flexible access networks [Invited Paper]," Proc. *International Conf. on Transparent Networks (ICTON),* Graz, July 2014, paper Tu.B3.1.

[C22] R. M. Ferreira, **A. Shahpari,** S. B. Amado, P. Costa, J. D. Reis, F. P. Guiomar, A. N. Pinto and A. Teixeira, "Impact of TWDM on optional real-time QPSK WDM channels," Proc. *Eur. Conf. Opt. Commun. (ECOC),* Cannes, September 2014, paper P.7.19.

Other Contributions:

[J8] Z. Vujicic , R. P. Dionísio, **A. Shahpari,** N. P. Pavlovic and A. Teixeira, "Efficient dynamic modeling of reflective semiconductor optical amplifier," *IEEE Journal of Selected Topics in Quantum Electronics,* vol. 19, no. 5, pp. 3000310, April 2013.

[J9] A. Abdalla, R. Ferreira, **A. Shahpari**, J. D. Reis, M. Lima and A. Teixeira, "Improved nonlinear tolerance in ultra- dense WDM OFDM systems," *Optics Communications - Elsevier,* 326, pp 88-93, April 2014.

[J10] V. C. Duarte , **A. Shahpari**, M. V. Drummond, A. Teixeira and R.N. Nogueira, "All-optical OOK-to-QPSK modulation format conversion based on XPM," *Microwave and Optical Tech. Letters,* vol. 56, no. 2, pp. 355 - 359, February 2014.

[J11] A. Sousa, **A. Shahpari**, A. Teixeira, R. Nogueira and P. S. Andre, "Group velocity dispersion monitoring for QPSK signals using direct detection," *Microwave and Optical Technology Letters,* vol. 56, no. 9, pp. 2078-2080, September 2014.

[J12] Z. Vujicic, R.S. Luis, J. M. Mendinueta, **A. Shahpari**, N. P. Pavlovic, B. J. Puttnam, Y. K. Kamio, M. N. Nakamura, N. Wada and A. Teixeira, "Demonstration of wavelength shared coherent PON using RSOA and simplified DSP," *IEEE Photonics Technology Letters,* vol. 26, no. 21, pp. 2142 - 2145, November 2014.

[J13] V. Ribeiro, R. S. Luis, J. M.D. Mendinueta, B. J. Puttnam, **A. Shahpari**, N. J. Muga, M. Lima, S.Shinada, N. Wada and Antonio Teixeira, "All-optical packet alignment using polarization attraction effect," *IEEE Photonics Technology Letters,* vol. 27, no. 5, pp. 541-544, March 2015.

[C23] Z. Vujicic, N. P. Pavlovic, **A. Shahpari** and A. Teixeira, "Efficient dynamic wideband model for reflective semiconductor optical amplifier," Proc. *Optical Fiber Communication Conf. (OFC),* Anaheim, CA, March 2013, paper JW2A.34.

[C24] A. N. Pinto, F. P. Guiomar, S. B. Amado, S. Ziaie, **A. Shahpari,** R. Ferreira, N. J. Muga and A. L. Teixeira, "Digital equalization of optical Fiber nonlinearities in very high‐speed optical communication systems," Proc. *International Conf. on Transparent Networks (ICTON)*, Graz, July 2014, paper We.D1.1.

[C25] V. Ribeiro, R. S. Luís, J. Mendinueta, B. Puttnam, **A. Shahpari**, N. Muga, M. Lima, S. Shinada, N. Wada and A. Teixeira, "Sub-microsecond packet polarization alignment using all-optical polarization attraction," Proc. *Optoelectronics and Communications Conf. (OECC)*, Melbourne, July 2014, paper TU4A-3.

1.7 Concluding Remarks

This chapter presented an overall view of the thesis. The motivation and background for future optical access networks were discussed. The most relevant technical and economic aspects related to energy consumption, spectral efficiency and coexistence scenarios in design of these networks were highlighted. The main motivation of coherent passive optical network is to support high spectral efficiency with high aggregated capacity and easier network upgrade for flexible bandwidth passive optical networks. The original contribution of the thesis and also thesis organization were presented.

References

[1] CISCO VNI, "Global mobile data traffic forecast," 2013-2018 Feb. 2014. [Online]. Available: www.cisco.com

[2] A. Teixeira, "What is left in fiber access bandwidth?," Proc. *International Conf. on Transparent Networks (ICTON)*, Coventry, UK, July 2012, paper.Tu.A3.1.

[3] P. Chanclou, A. Cui, F. Geilhardt, H. Nakamura, and D. Nesset, "Network operator requirements for the next generation of optical access networks," *IEEE Netw. Mag.*, vol. 26, no. 2, pp. 8-14, March-April. 2012.

[4] E. Wong, "Next-generation broadband access networks and technologies," *J. Lightwave Technol.*, vol. 30, no. 4, pp. 597-608, February 2012.

[5] A. Teixeira, "Standardization in PONs: status and possible directions," Proc. *International Conf. on Transparent Networks (ICTON)*, Munich, Germany, July 2010, paper We.A4.7.

[6] ITU-T recommendation G.989.1, "40-Gigabit-capable passive optical networks (NG-PON2): General requirements," March 2013.

[7] ITU-T recommendation G.989.2 (draft), "40-Gigabit-capable passive optical networks: Physical media dependent layer specification," April 2014.

[8] IEEE P802.3av task force ,www.ieee802.org/3/av/.

[9] H. Rohde, S. Smolorz, K. Kloppe, and E. Gottwald, "Next generation optical access: 1 Gbit/s for everyone," Proc. *Eur. Conf. Opt. Commun. (ECOC)*, Vienna, Austria, September 2009, paper 10.5.5.

[10] J. Prat, M. Angelou, C. Kazmierski, R. Pous, M. Presi, A. Rafel, G. Vall-llosera, I. Tomkos, E. Ciaramella, "Towards ultra-dense wavelength to the user: the approach of the COCONUT

project," Proc. *International Conf. on Transparent Networks (ICTON)*, Cartagena, Spain, June 2013, paper. Tu.C3.2.

[11] N. Cvijetic, "OFDM for next-generation optical access networks," *J. Lightwave Technol*., vol. 30, no. 4, pp. 384-398, February 2012.

[12] F. Villarruel, and L. Ray, "1550 video overlay: the new old reliable," *Scientific Atlanta White paper*, 2007.

[13] I. Sugino, "Disaster recovery and the R&D policy in Japan's telecommunication," Plenary talk Proc. *Optical Fiber Communication Conf. (OFC)*, Los Angeles, CA, March 2012.

[14] V. Jungnickel, "High-speed optical wireless communica-tions technologies," Proc. *Optical Fiber Communication Conf. (OFC)*, San Francisco-CA, March 2014, paper Th1F.5.

[15] W.C. Kim, R. Mauborgne, *Blue ocean strategy*, Harvard Bus Rev, October 2004.

[16] J. D. Reis, D. M. Neves and A. L. Teixera, "Analysis on nonlinearities on coherent ultra-dense WDM-PONs using Volterra series," *J. Lightw. Technol.*, vol. 30, no. 2, pp. 234-241, January 2012.

[17] M. R. Phillips and D. M. Ott, "Crosstalk due to optical fiber nonlinearities in WDM CATV lightwave systems," *J. Lightwave Technol.*, vol. 17, no. 10, pp. 1782-1792, October 1999.

[18] D. Lavery, C. Behrens, S. J. Savory, "On the impact of backreflections in a bidirectional 10 Gbit/s coherent WDM-PON," Proc. *Optical Fiber Communication Conf. (OFC)*, Los Angeles, CA, March 2012, paper OTh1F.3.

CHAPTER 2 ENERGY EFFICIENCY IN OPTICAL ACCESS NETWORKS

Summary

The concept of energy efficiency in optical access networks can be addressed from different perspectives such as network design, user profiles, optical distribution network topologies and equipment characteristics. Since the lifecycle of wireline access deployment is rather long (typically more than 10 years), a set of criteria in optimization of optical distribution network should be defined. Moreover, it is an important advantage for network operators, even at specification time, a clear vision on the energy consumption horizon of each part of their system. The purpose of this chapter is to provide some of the factors that can be considered in the analysis and optimization of current and next generation optical access networks.

2.1 Introduction

Nowadays, high energy costs, climate change concerns, energy preservation and efficiency start to play a central role in the design and operation of industry and telecom equipment. Besides, studies on network energy usage have shown that access networks consume around 70% of overall Internet power consumption and consequently, reduction of energy consumption in these networks has significant influence on power consumption reduction in all telecom equipment [1].

Data rate hungry applications, whether domestic or business, are permanently pushing operators to develop their access network to Fiber-To-The-Home (FTTH) based on Point-to-Multi-Point (PtMP) Passive Optical Networks (PON) [2]. However, the deployment of fiber, type of splitter configurations as well as Optical Distribution Networks (ODN) topologies should be defined in the first phase of fiber installation. Moreover, the need or not to redress the installed fiber plants in PONs, are an important point in the current techno-economic context. For example, users continue asking higher accessibility and so coverage of all regions makes operator's network more compatible. In an effort to provide higher coverage in a cost-effective manner, Long-Reach PON (LR-PON) with several optical amplification technologies has been proposed [3]. Consequently, using optical amplification in PON is resulting on more power consumption. This is even more dramatic in a first phase deployment of suburban and rural scenarios, where the number of potential users for new services is low. Therefore, a network optimization to make balance between cost-effective PON and best efficiency in terms of resource sharing and power saving, should be applied.

In addition, due to long lifecycle of PON deployment, some considerations should be made on the investment and interface technology level in ODN. Herein, a set of criteria that may be used to balance between investment in a potentially more expensive technology at the interfaces (e.g. tunable TRx) versus a simpler and less expensive interface technology and some changes in the ODN, should be defined.

Also, most vendors limit their energy specifications to the consumption of the equipment. As such, it is necessary to define a model that can put together all factors and try to set a fair and consolidated rating of each technology, which should account both with sustainability

of the system for its life time as well as benefit the most durable and appropriate solutions for each specific scenario.

In this chapter, we analyze the impact of different types of splitter structures on resource sharing and power consumption in long reach PON. In Section 2.3, a set of analysis and methodology, based on nonspecific protocol or transmission technology in ODN, is presented. A model for energy efficiency rating of access network equipment is considered with complete figure of metric in section 2.4. Section 2.5 concludes the chapter.

2.2 Energy Efficiency Scenarios for LR-PON (paper C1)

From the above mentioned, it is clear that for having cost-effective and competitive network for the low potential user area, resource sharing and energy consumption needs to be optimized for easy migration to Next Generation PON (NG-PON). Authors in [4] present a simple plan for power saving in long reach PON and in [5] power saving for several nodes of consolidation is considered. We introduce a power saving method for PON in terms of fiber distribution and Optical Line Terminal (OLT) port loading, optimized for several population distributions with using Semiconductor Optical Amplifiers (SOAs) technology as a reach extender. Especially, in this part an attempt to establish a cost-effective deployment method for reducing the power consumption during long life time of access network is presented.

The population distribution model is schematically presented in Fig. 2.1 (a). This model attempts to achieve the important relationship between population characteristics and network topology. We assume a coverage area with 6 population distributions, all normally distributed but with different means, which determines the geographic places of central offices, and different standard deviations for spreading of each distribution. In this case main Central Office (CO) is located at the most populated city. Also, in this example the city A (50000, 4) with 50000 potential users and population standard deviation of 4 km is located as a main city and B (30000, 4), C (10000, 4), D (5000, 3), E (10000, 2) and F (20000, 5) are used as a suburban or rural scenarios. For clustering of each distribution area we divided each city into 5 or 6 circular regions, depending on standard deviation and optimization of splitter placement and fiber length.

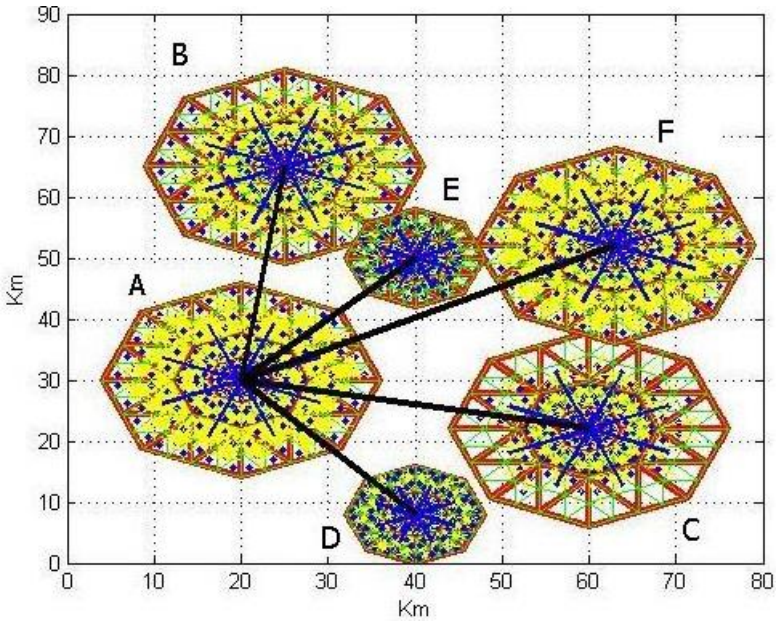

(a)

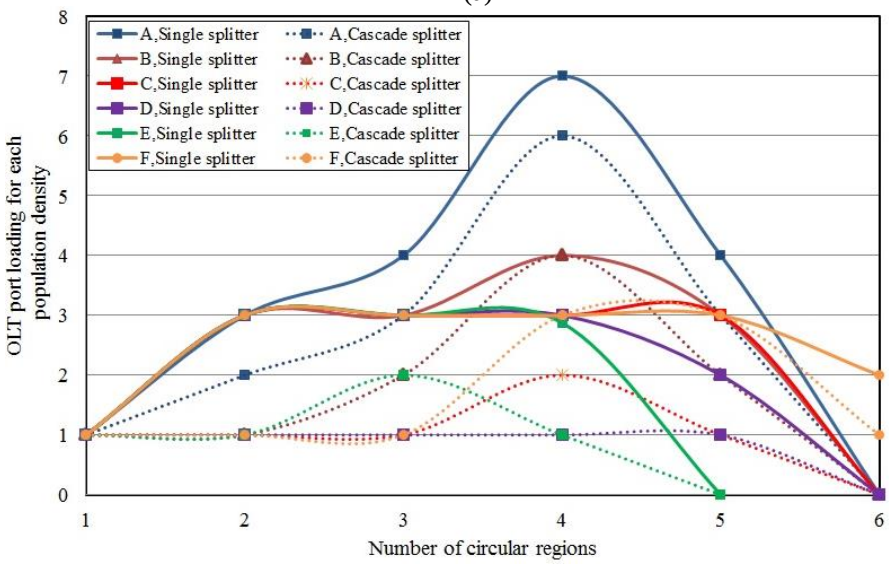

(b)

Figure 2.1 (a) Coverage area with six population distributions, (b) OLT port loading versus number of regions for 10% take rate.

As the location of splitters at the edge of the serving area is considered to be more convenient than in the middle of it, we can use triangle geometric model that has been suggested by [6]. With this model, calculation of fiber length and splitter placement for cascaded strategy are more efficient. Fig. 2.1 (b) presents the number of OLT port loading for each area of above mentioned areas with single and 3-stage cascaded splitter strategies for 10% take rate (subscription rate) as achieved by triangle model. As observed in this figure, the number of OLT ports in case of cascaded structure for all regions is decreased slightly. For higher population areas we used GPON OLT chassis, which supports 18 OLT cards for 9216 GPON

subscribers using class B+ while supporting industry-standard 2.5 Gb/s downstream and 1.25 Gb/s upstream bandwidth. A chassis with 14 OLT cards and 7168 users was used for thinly populated areas. Note that, each OLT card supports 8 GPON ports. In the first case, power consumption per chassis in full load is 1896 W and second one is 1544 W [7].

Although reach extender is used, the number of central offices and aggregation nodes will be decreased in big cities, but in small and separated areas this method can play more important role in case of Operational Expenditures (OpEx) reduction [5]. Actually, when the number of suburban or rural users is very low, designing a dedicated CO for them may not be economical. In this case, we used an Extender Box (EB) based on SOA for GPON that can support 64 users up to 60 km reach with 25 W power consumption.

In best scenario and with best OLT port efficiency, minimum power consumption per user without using EB is around 0.21 W ($0.21 \cong 1896/9216$) and with EB is 0.6 W ($0.6 \cong 1896/9216 + 25/64$). In order to get some numbers near these values in real cases, several use scenarios are studied in this work:

- Scenario 1: GPON OLT for all distribution areas with single splitter structure (1:64).
- Scenario 2: GPON OLT for all distribution areas with 3-stage (1:2, 1:8 and 1:4) cascaded splitter structure. In this case 1:2 splitter is located at OLT.
- Scenario 3: GPON OLT for all distribution areas with 3-stage (1:4, 1:4 and 1:4) cascaded splitter structure.
- Scenario 4: consolidated GPON OLT in CO of city A and using EB for other areas with using single splitter structure.
- Scenario 5: consolidated GPON OLT in CO of city A and using EB for other areas with using 3-stage (1:2, 1:8 and 1:4) cascaded splitter structure in all areas
- Scenario 6: consolidated GPON OLT in CO of city A and using EB for other areas with using 3-stage (1:4, 1:4 and 1:4) cascaded splitter structure in all areas.

However, the work and concepts are valid for other scenarios compositions and different splitter configurations. Fig. 2.2 is obtained by dividing the two values with and without EB. As depicted in Fig. 2.2 (a), when the number of potential subscribers is high, for instance more than 50%, the benefits for the cascaded and single structure are the same, but in low take rates by using 3-stage cascaded structure we can increase power saving up to 50% specially for spread distributions same F area. As shown in Fig. 2.2 (b) controlling the power

consumption is an important aspect. Therefore, it is obvious that we cannot decrease the power consumption of user with EB, due to the use of two active components, even with best OLT port loading, but we can decrease the related energy consumption of cooling, light and aggregation nodes and consequently OpEx.

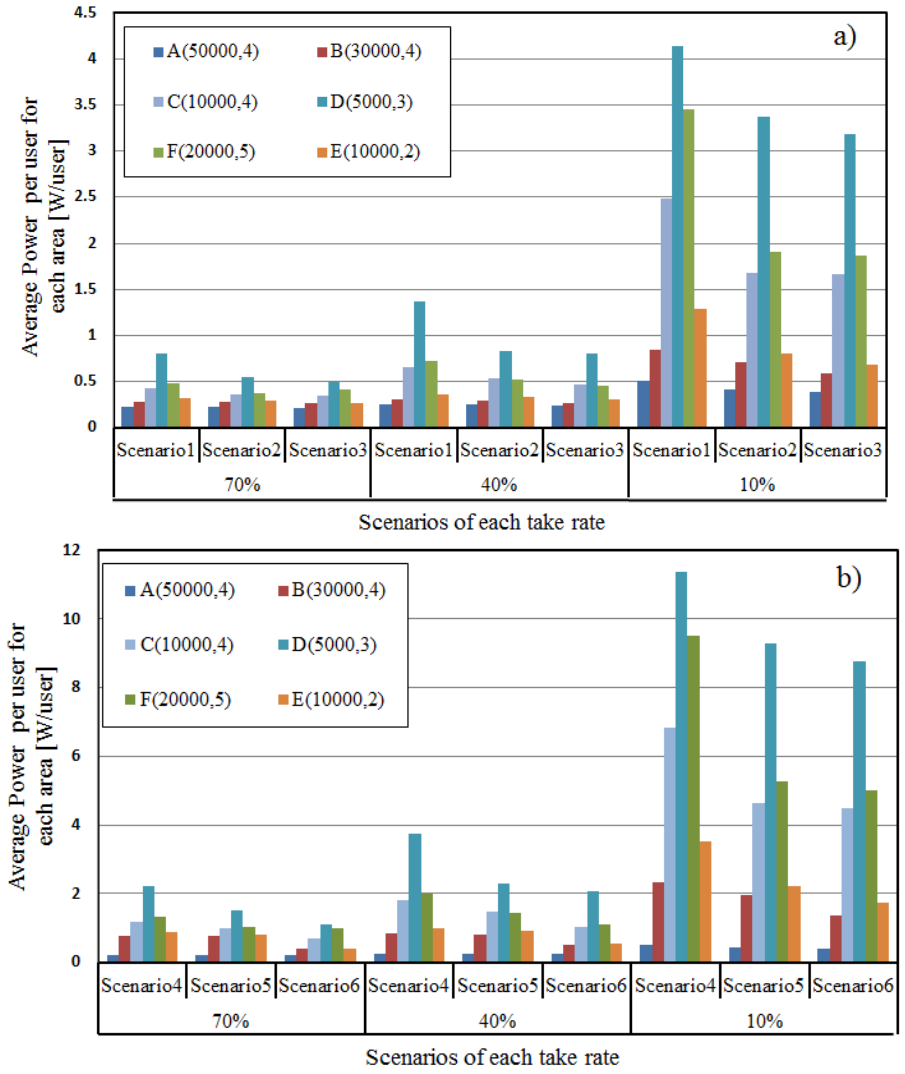

Figure 2.2 Power consumption per user for 6 scenarios of all population density (a) using GPON OLT in each distributions, (b) using extender box.

The message kept from this analysis is that there is a big power saving potential in the cascaded structure (scenario 6), when the operators upgrade their network to NG-PON like Ultra Dense Wavelength Division Multiplexing PON (UDWDM-PON) splitter based PON. These benefits can be taken into account, in the spread population, greater average than 40% power efficiency without any change in outside plan and therefore decreasing the migration costs.

2.3 Implications of ODN on Energy Consumption in PON (paper C2)

As mentioned before, the actual point of development of FTTH is very critical, since there are several efforts ongoing all over the world to deploy new fiber to each and every requiring household. This can mean this investment is very important, which will, in most cases, be co-funded by the governmental authorities, local, national and even transnational. We may notice the interests of legacy operators, in keeping as much as possible the control on access to the infrastructures, to allow their model to prolong as much as possible; the regulators, willing to break the previous model without creating other vertical possible models, and increasing competition and space for innovation; the newcomers which want to find their own models and entries; and others with the more diverse intentions [2].

From the above mentioned, it is clear to observe the size and number of forces involved in the definition of the new deployments. One of the questions which have been dividing the technology and scientists is the deployment of transparent one-to-many or opaque, being it space, Point-to-Point (PtP), or wavelength piped, e.g. one-to-many arrayed waveguide grating based solutions.

Several are the arguments being brought up for any of the presented solutions, being these more harsh between the fiber spatial PtP and the other two technologies, mostly based on arguments, valid, like freedom for future solutions and independency from technology. However, in what respects the two most common one-to-many solutions, splitter and non-splitter based solutions, the arguments center mainly in the losses which grow with the number of users for the splitters and are kept in a limited range, for the case of arrayed waveguide gratings, typically between 2-7 dB [8]. In any of the cases the arguments are valid, however in this work an attempt one to establish a more operational, long term criteria, which will help structuring strategies, encompassing also the ecological impact, a stringent criterion to be ultimately considered as major. The criterion to be used is related to power consumption of fundamental states of the system, which are mostly independent of the protocols overlapping to the TRx technology, and will only be focused on the basic physical topology decision concepts, transparent ODN + tunable (Transmitter/Receiver) TRx vs. opaque. The operation of the two above mentioned concepts is schematically presented in Fig. 2.3.

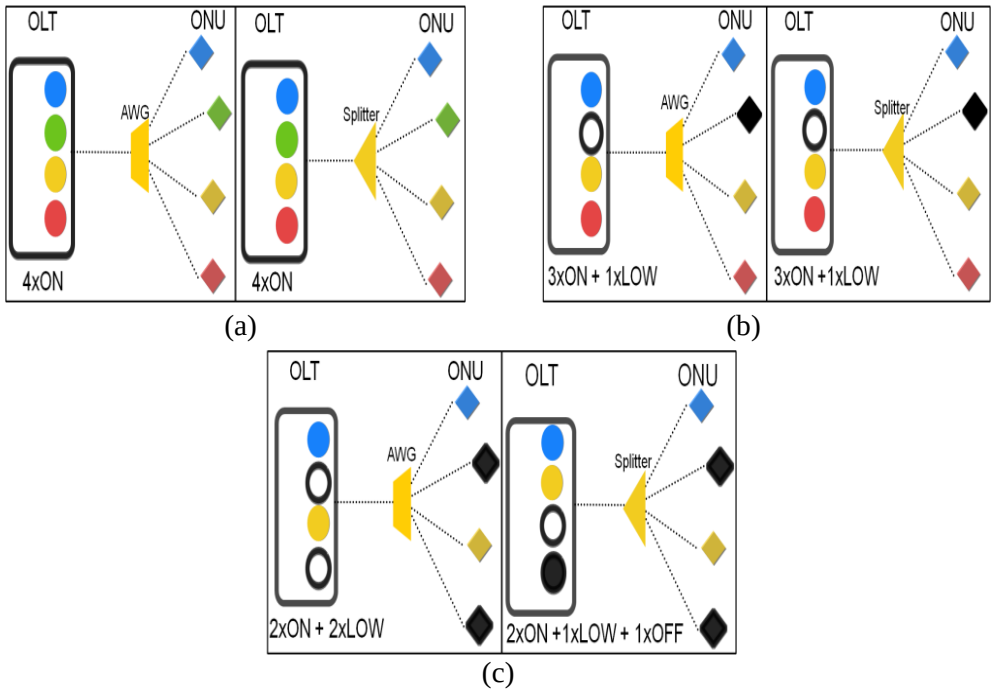

Figure 2.3 (a) Typical operation for all subscribers simultaneously in an arrayed waveguide grating and splitter version, (b) one of the ONUs shuts down or idles, (c) two idle or shut down ONUs.
Caption: O - idle OLT user interface; filled O - shut down OLT interface; black diamonds- shut down or idle ONU. Colored O - lightened OLT interfaces; colored diamonds - active ONUs.

In normal operation, the two defined scenarios are similar in terms of power consumption, assuming that the power exhausted to compensate for the ODN losses will, with technology evolution, be of minor significance due also to the limited sets of scenarios where this factor will effectively make a difference, e.g. long reach. From there, the potential differentiation will mostly stem from the potential to reduce operational energy costs for the non-negligible off time of these types of Optical Network Units (ONUs). In a piped opaque solution, PtP or arrayed waveguide grating based solutions, there is no simple way to monitor the ONUs off state and willingness to regain activity, either than pinging it at a defined speed or listening, being therefore an OLT state, named from now in this work as LOW, which will consume a certain amount of energy, since is a "lifetime" commitment.

In a transparent solution, e.g. tunable technology plus splitter in the ODN, there is a potential for re-dimensioning the whole wavelength attribution and shut down all non-used OLT user interfaces but one, which will be monitoring or waiting for activity from any state changing ONU, and will represent the gate in for each of the ONUs re-gathering service. For questions of feasibility at technical or economic levels, one may require to have groups of transmitters, named here as Optical Transceiver Group (OTG), stemming from the same laser or TRx

which may bind some level of activity even in the transparent tunable solution, also analyzed in this work.

For the sake of getting to some numbers which can be easily understood, a use case scenario is considered in this work, however the concept is valid for other scenarios. Out of the consideration in the model is single wavelength TDM solutions, since they will not work in the case of arrayed waveguide grating based ODNs or make any sense in the PtP solution. In this use case, we considered the LOW power state as 20% of the full ON power state and the OFF state has a null power consumption. A next generation network, where consolidation or high density of subscribers is present, is considered having the maximum 1000 clients physically connected to the network.

Fig. 2.4 (a) is obtained by adding the number of ON, LOW and OFF ONUs accounting its weight, 1, 0.2 and 0 respectively, according to the number of active users. The method is simple for the opaque solutions, where

$$P(\%) = ((N_{total} - N) \times LOW + N)) / N_{total} \qquad (2.1)$$

For the other solution, transparent ODN + tunable TRx,

$$P(\%) = (LOW + N) / N_{total} \qquad (2.2)$$

where N is the number of active subscribers, N_{total} is the number of connected subscribers

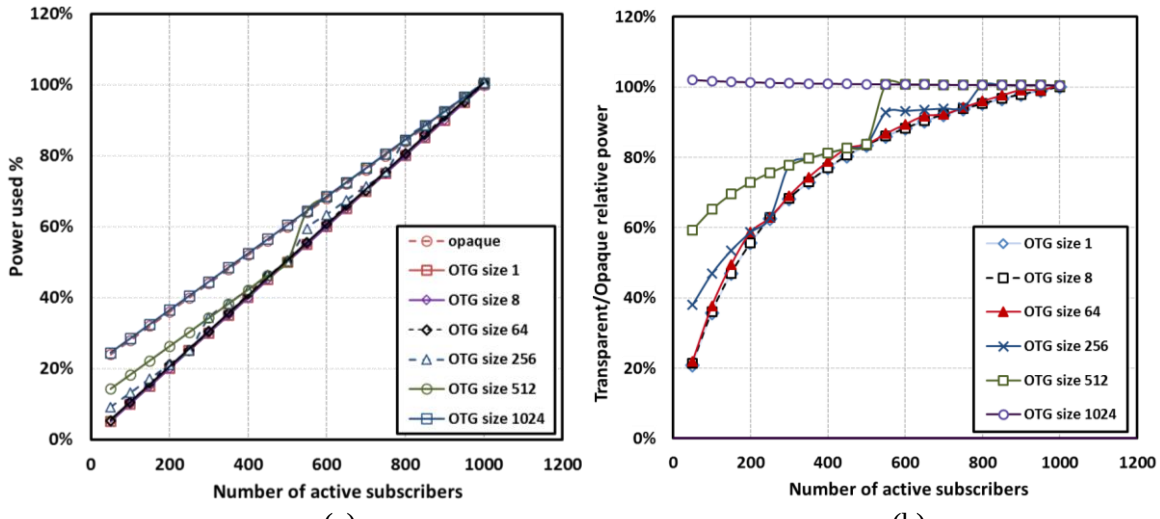

(a) (b)

Figure 2.4 (a) Relative power as a function of the number of active subscribers, (b) transparent/opaque relative power as a function of the number of active subscribers. Both graphs are drawn in the transparent case for several OTG array size.

and LOW is the number of OLTs in low state. If OTGs are used, the complexity grows but can be simplified as: the number of OTGs ON is the integer division of N and the OTG size. The remaining channels will be ON up to the point N is filled, and the remaining up to the size of the OTG, will be in LOW state.

Fig. 2.4 (b) is obtained by dividing the two values for easy reading of the relation between the two. Observing Fig. 2.4 (b), as expected, when the number of active subscribers is low, below 50%, the benefit for the transparent-tunable technology is, in the use case scenario, greater than 15%.

In order to extract the real implications of the technology, the energy benefit, has to be graded. In the present work, the intraday average percentage number of active users pattern was considered for the purpose and presented in Fig. 2.5 (a), and named as heavy. From this pattern other 2 patterns (e.g. medium (the same pattern x 50%) and low (the same pattern x 20%) are also considered. The message kept from the analysis of Fig. 2.5 (b) is that there is high energy efficiency potential in the transparent-tunable case, when compared with the opaque cases. These benefits can be, in the example patterns, greater than 60% for small OTG sizes a low usage patterns, tending to be null in the case of high OTG sizes. The pattern used plays only as a scaling factor in the obtained curves.

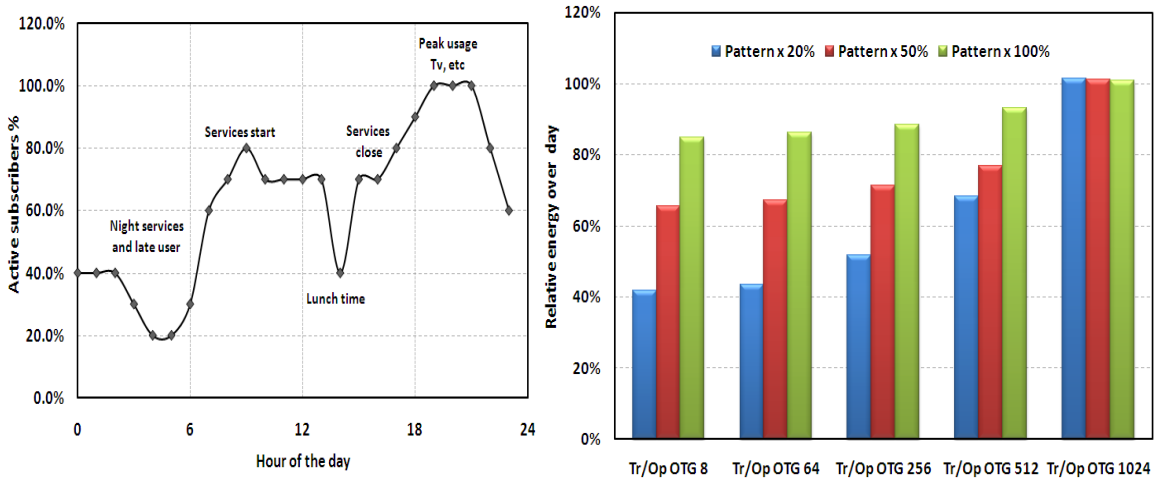

Figure 2.5 (a) Reference usage user pattern and (b) relative energy over a day for each OTG group size and pattern (transparent/opaque).

2.4 Factors in Energy Efficiency Rating in Optical Access Networks (paper C3)

In the course of the years, the major driving force for deployment of digital infrastructures was the digital divide. This idea was typically pushed by central governments, specifically as example, European Union, as a means to provide equal access to information and communication. The objective was leveraging the society, and from there obtain indirectly a fairer society. Independently of the policy results, which, anyhow, are visible everywhere through the abundant access to a variety of IT solutions, it also speeds up the costs and benefits of globalization. This trend made possible to create business around almost any solution or idea. From this economical interest a lot of pressure was put on faster and better access to IT and to the development of many solutions mostly focusing the channel bandwidth increase. The latter has led to early and, sometimes, not so efficient and ecologically developments. These developments were able to fly since there was none or sparse impact regulation. Short term solutions were stemming and having market just because there was the continuous need for information and connectivity. As example, one can analyze the number of mobile phone versions that each one has had in average and how fashionable they became, appearing as fashion accessories, not being sold by its efficiency, disposal capability, or ecological and social cost.

It is common to read standards where no considerations about efficiency or power saving modes are made. Lately, this has started to be taken in major consideration, since, also, the main policies have now changed. The actual economic scene favors ecologic and low power consumption solutions, due to resource exhaustion, willingness to minimize the oil dependence and to protect the planet balance. For achieving this, Code of Conduct (CoC), which is not a standard or even produced by any standardization body but by policy makers, is being created and is expected to be respected independently of the technology, therefore is being used as a political tool to drive conscientious technological development defining new ecosystems for business development [9].

In the field of telecommunications, and due to the previous infrastructure capacity exhaustion of the copper access (meaning reach and bandwidth), it came the opportunity to generate a whole new set of developments and trends in the field. Of course, as in any field, there are the fast technology adopters, where these ecological considerations were not

minded upon deployment, however are now being taken seriously when redesigning the new solutions. But, it is a sustained vision that new systems should be as efficient as possible for allowing the minimal cost per bit, and promoting the faster upgrade allowing some margins for redesigning the operators traditionally large profit margin per bit business, that nowadays has been eroded by the overlaying of killer profitable service layer applications. This new business ecosystem brings certainly a lot of tension and care when deploying the new infrastructures, therefore, in many cases, either an independent actor enters as infrastructure holder or there is an association, where the public entities also partnership, to deploy such a future common use utility.

However, when deploying equipment, the concerns may change, since, in that case, OpEx plays an important role and should be taken as an investment and a mean to control areas of users and clients, therefore, market position. Considering this, a different mindset comes directly to many of the different types of players, namely the traditional incumbents, the newcomers and the recent players.

There are several publications which provide approximate estimations of energy consumption in different types of access networks [10-15]. In [12, 13] a basic power consumption model for generic access networks is presented. In [14] they improve their model and reveal energy consumption model in different networks with respect to traffic projection and the average access bit rate and have considered power consumption of PON and active optical access depending on the degree of node consolidation. The authors of [16] present new model for power consumption in long reach access network and compare all technology vs. peak data rate and number of users. Although numerous works have been done to review the power consumption of telecommunication networks [10, 11, 14], little attention has been paid to suggest and provide a comprehensive model for energy consumption rating in Next Generation Optical Access Networks (NG-OAN). In all literatures, power consumption normalized to throughputs and user are a metric, which is only good benchmark for switch or router in core; also there is no adequate effort to consider all effective dimensions in energy consumption. However, it is mandatory to introduce suitable power and energy-efficiency metrics for access networks to select green technologies.

2.4.1 Duality: Green-Performance

It has been identified, long ago and in many types of business, a duality which in many cases drive oppositely: be fully green; or be more performance (Fig. 2.6). Clearly, if some environmental concerns are put aside, the margins for profit grow, since there are reduced costs on controlling the impact of a certain product or service. In telecom, the main concerns are related to the terminals, which are typically frequently prone to updates and changes, and to the energy consumption of all processes which support the business. As what regards power, numbers rate high nowadays, 4% plus of total power consumption in developed countries, tending to grow as the cloud applications and virtualization of hardware grow. It is, for the above reasons not as simple decision as before, when it concerns defining a new technology to deploy, since, performance parameters may not be enough. OpEx, related to the increasing energy cost, becomes somehow dependent on the energy consumption of the system. However, for upgrading technology and/or making long term investments, typically 10+ years in the field for telecommunications and networking, a high margin in the data rates granted by the technology should also be considered and brought up front, with the risk of outperform in a short timescale and from there consequent market share loss. From the considerations above, one should define wide enough criteria to allow a clear definition of the path forward when investing in Telco business. This will lead certainly to a more complex figure of merit for these systems, which should encompass most of the parameters involved in this market and not only performance or energy. Also, in the future we will, most probably, have to adopt flexible ONUs which may easily encompass the interworking with several different technologies in the OLT and ODN. These trends will allow the required

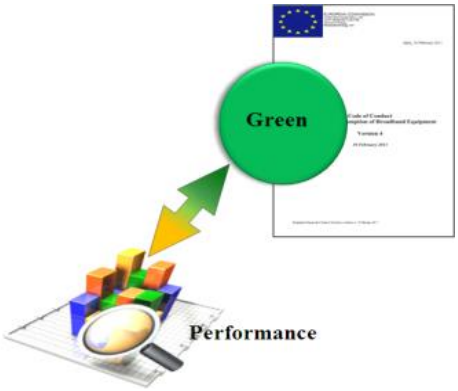

Figure 2.6 Duality: Green-Performance.

flexibility for energy optimization and OpEx and Capital Expenditure (CapEx) reduction and optimization allowing enough margins for the operators to have further margins for putting in innovation, which is one fundamental driving force for this market.

2.4.2 ODN Topologies

Every year the amount of subscribers connected and using broadband services is increasing and it is clear that due to variety of cultures and differentiation of environments, there are topologies dependent on the number of subscribers and the area where these subscribers are distributed. These topologies, being the market input of many operators, can be categorized, as example, in four different types, as what regards users/area:

- Highly dense urban (>2k/km^2, e.g. Delhi, Seoul, New York, …)
- Dense urban (>1k/km^2, e.g. most big cities)
- Sparse (>200/km^2, small cities, large villages)
- Highly sparse(<=200/km^2, rural areas, small village)

A figure of merit for the next generation, ODN topologies, user profiles, and technology performance in terms of power and data rate should all be considered. Of course, for sake of sanity, subsets of the possible parameters arrangements should be considered to allow limited conceptual design and choice time. This is the type of methodology that is outlined in this work.

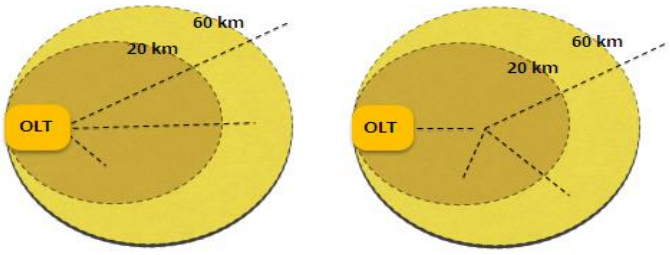

Figure 2.7 ODN topologies, point to point and point to multi point.

It is clear that in urban areas any physical topology will fit the requirements, since typically, considering 2 k clients per aggregation office, we may need one per km^2. Going down in density, dense urban, 1 of those 2 k clients aggregation offices per 1 km^2 will be needed. For sparse, 1 for each 100 km^2, and very seldom such a high aggregation would be needed for the highly sparse cases. These numbers are indicative and consider estimations with variable

penetration. As shown in Fig. 2.7 this is just to lead to the fact that any topology, PtP or Point to Multi Point (PtMP), will fit the first 2 scenarios, due to involved distances therefore, other factors, like fiber aggregation and handling, Central Office (CO) area, management, energy, etc., will weight in the decision for one or the other. In the remaining scenarios, easily one can reach fiber spans of 10 km, 20 km, or more specifically in the highly sparse case. This subject has already been observed by the related entities and standards, and two ranges were defined for access networks, up to 20 km and up to 60 km, and a new one, up to 100 km which is stemming with the increased stress on CO consolidation. It is understandable that technologies are more or less energy efficient with the ranges involved; therefore, this parameter should also come to play, and, for sake of simplicity, be considered in the already existing presented ranges (Fig. 2.7). Regarding the topology, this should be open since it could represent in some cases a clear benefit to opt for one or the other topology, depending on the radius of covered area, the client density for each area accounting from the CO location and eventually for characterizing demand.

2.4.3 Equipment Characteristics

It is clear that equipment is the one that effectively consumes the power in passive ODNs, if we disregard for now the cooling and due to numbers, customer premise equipment is even more critical. Although the customer premises power does not account for the operators costs and could be a little misleading trying to insert this factor into the equation, but for deciding upon a certain technology and contribution to the global emission of carbon oxygen, this factor should also be accounted. There are common sense environmental regulations in terms of energy consumption, however in Europe a CoC is being developed and updated for creating a firm compromise with some target numbers.

Equipment in operator and customer sides have a number of parameters, and in what concerns the power consumption, it is clear that the power that the equipment inputs into its plug is a determining factor. As shown in Fig. 2.8 ONU is divided into transmitter and receiver optics and electronics, Large Scale Integration (LSI: MAC, CPU, etc.), User Network Interface (UNI: Fast Ethernet (FE), Giga Ethernet (GE), Wi-Fi, Foreign eXchange Station (FXS), USB) and OLT in CO includes TRx, LSI and Service Node Interface (SNI) for uplink. Considering increasing data rates, clock frequencies and density in chips, power

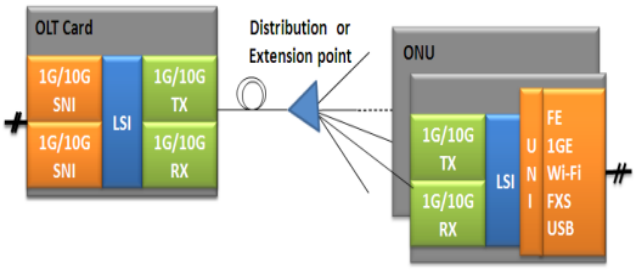

Figure 2.8 OLT and ONU functions.

dissipation and control becomes a must to be considered in any system. If these values are available they should also be accounted in a per subscriber basis.

However, referring to CoC general guidelines, literature [9,15,16], and for sake of simplicity the value of power consumption in each part can be estimated and accounted individually, since different providers will certainly come with certain very specific solutions.

The principal function modes in CoC are [9]:

- Idle mode
- On state mode (low load mode, full load mode).

These absolute power values per subscriber cannot help us in analyzing the future proof robustness of the system. This is due to the fact that there is not enough information on the performance of such equipment in terms of data rate. From this latter requirement, another set of factors should come with the technology as a tag, which are the peak, sustained and low power performance data rates. The peak data rate is relevant as a selling point, therefore should be taken for marketing purposes, however, in our vision, the sustained data rate is a more eligible metrics for the objective of power rating a technology, since it will grant, at design time, the minimum quality of transmission granted to the every user. One may bring many arguments to the table, like the probabilities, e.g. best effort service delivery techniques, which maximize, and should be used in operational matters, however should, in a first phase, be considered out of the equation for sake of equity. Therefore, for comparison basis, from the technical part of the system, vendors should provide the CoC driven effective power consumption and sustainable bandwidth in the referred operational modes, on a per subscriber basis for the ONU and OLT.

A. Services

According to bottom-up business model, services are key requirements for each system and architecture design. Type and quality of service, total traffic and data rate scales can be the

metrics for classification of system adaptability to the user profiles, and help us projecting traffic, aiming at predicting the time limit for a certain technology. Therefore, besides growing a large set of data, it can also be understood that there are too many metrics possible to be used, which in the end may result in confusing or unclear roadmaps both for technology and power consumption. If one considers the total traffic, the results could be positive if, for that sum, single value, there were not many contributors which depend greatly on the type of usage. To keep it simple, let's just take the example of business and home user, complete different patterns and potential for demand and production, therefore requiring different type of design and concepts for optimum service delivery. When considering abstract data rate scales, one is disregarding the application and the usage of it, since different applications will lead to certain known amount of user time, and therefore interfaces which consume different amounts of energy, e.g. voice and high-definition compressed video.

Hence, one should move to a more application driven metrology, since, from there, even not knowing exact user profiles, one can extrapolate the usage from the type of business and activities and population living in the area. With information of user profiles, minimal sustained data rate for that type of user can be determined.

As a first guess a certain number of profiles come to mind:

- Light user - voice, VOIP, gaming, data and IPTV small part of the time
- Heavy user - voice, video conference, gaming, data, cloud computing, Video On Demand (VOD) dedicated, live VOD, peer to peer, IPTV a great part of the time
- Business - high data during working hours
- Mobile back hauling - heavy traffic during zone activity hours
- Datacenter - serving at all times optimized by other machines to be as optimum as possible.

For forecasting of the service bandwidth evolution and types of user, traffic study in [17, 18] has been used in the user profile. We assume the service type usages of each user for our duration study is constant and follow Fig. 2.9. Types of service for each user are defined using the requirements and traffic dimensioning in [17].

Several types of PON architectures have been or are being developed, such as Gigabit PON (GPON) and XGPON specified by the ITU-T, Ethernet PON (1G/1G-EPON, 1G/10G-EPON) and 10 Gb/s Ethernet PON (10G-EPON), which are standardized by the IEEE. 1G PtP and 10G PtP are options which can sustain data rate for end users. Also Wavelength-Division Multiplexing (WDM) PON and hybrid WDM/TDM PON are new solutions with high bandwidth for business and heavy users and are growing quickly for extended data rate and/or reach [18]. In addition, Ultra Dense WDM PON (UDWDM PON) will potentially emerge in future [19]. In this study, due to focus on the CoC, we will address TDM PON and PtP technologies. In Fig. 2.10, the downstream and upstream bandwidth data

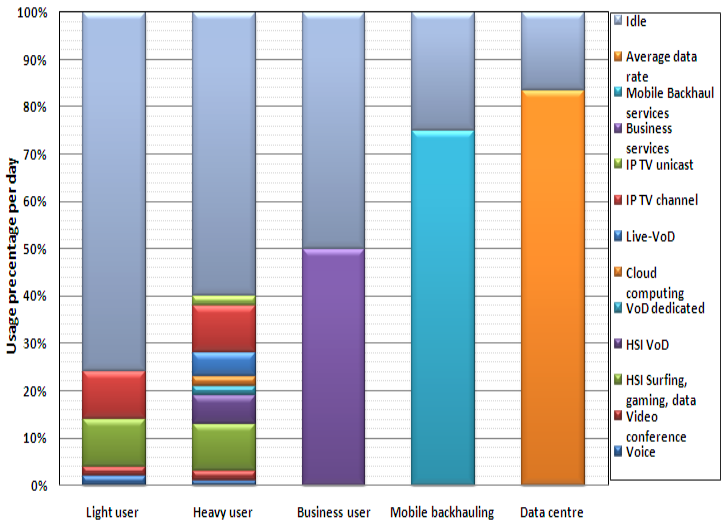

Figure 2.9 Service type usage per day.

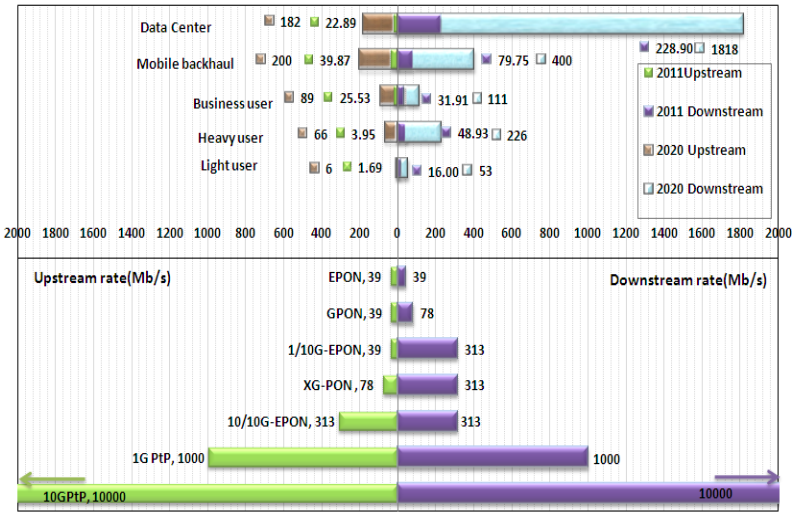

Figure 2.10 Today and future bandwidth requirements and solutions.

requirements for each user type are demonstrated, together with the bandwidth of some of today's access solutions. Table 2.1 gives an overview of the power consumption values and the peak data rate of the most relevant technology based on CoC [9] and [15, 16].

Table 2.1 Key parameters used in the model for power consumption and sustained bandwidth [9, 15, 16].

Access network	Peak data rate per user [Gb/s]		Number of user per OLT port	Reach extender option	OLT power per user in each year [W]			ONU power in each year [W]		
	US	DS			2010	2014	2020	2010	2014	2020
EPON	1	1	32	SOA+EDFA	0.37	0.22	0.15	16.3	10.3	7.8
GPON	1.25	2.5	32	SOA+EDFA	0.47	0.25	0.15	17	10.6	7.4
GEPON	1	10	32	SOA+EDFA	0.84	0.44	0.29	16.6	11.8	9.3
XGPON	2.5	10	32	SOA+EDFA	1	0.43	0.28	17.3	12.3	9.5
10 GEPON	10	10	32	SOA+EDFA	0.88	0.43	0.26	17.3	13.3	10.3
1G PtP	1	1	24	SOA	5	4	3.3	14.4	10.6	8.3
10G PtP	10	10	12	SOA	28	20	11.4	19.3	11.2	8.9

The case study assumes four FE, a Wi-Fi, two FXS and one USB interfaces for residential users and two FE, two GE, a Wi-Fi, two FXS and one USB for the other user profiles chosen. Also the reach extender technologies can be achieved using optical amplifiers such as SOA, Erbium-Doped Fiber Amplifier (EDFA) or both. We extended all these power consumption trends to 2014 and 2020 having as trend the CoC.

B. Model and results

From the previous sections, a set of profiles and guidelines for defining a pattern for consistently rate a technology in terms of energy consumption, having in mind both performance and topology, were discussed. Several types of network topology and access system may be employed in delivering the various user profiles and the traffic they need. With a set of traffic projections currently available, the model of Fig. 2.11 can anticipate the time validity of a certain type of technology as well as its power consumption trend.

For calculation of energy per day for each user we have,

$$E_{User}(y, MaxD, rB) = \sum_{\substack{op.modes \\ @\, MaxD \wedge rB \times \beta(y)}} \left(\left[\alpha_{ONU}(y) \times P_{ONU}^{op.mode_i} \right] \times T_{op.mode_i} \right) + \sum_{\substack{op.modes \\ @\, MaxD \wedge rB \times \beta(y)}} \left(\left[\alpha_{OLT}(y) \times 2 \times P_{OLT}^{op.mode_i} \right] \times T_{op.mode_i} \right) \quad (2.3)$$

where *y*, *rB* represent the case study year and required sustained data rate at first year, respectively, and β(y) represents traffic evolution function for each year. Operating modes

are: off, idle, low and full mode while $T_{op.mode_i}$ denotes the time of each mode i. $P_{ONU}^{op.mode_i}$ and $P_{OLT}^{op.mode_i}$ are the powers consumed per user by the ONU and OLT for each operating modes, respectively and α_{ONU} (y) and α_{OLT}(y) denote power evolution function for ONU and OLT in each year. Distances are sectioned in typical ranges (0-20 km; 0-60 km; 0-60 km+) and are determined by MaxD. Using extended reach, the corresponding extra power is added to $P_{OLT}^{op.mode_i}$. We note that factor 2 in OLT terms takes cooling requirements, service provisioning and external power supply losses into account [13]. Number of users per each PON is assumed to be 32 in all use cases.

From the current model, one can estimate the energy rating of the considered access network options. An analysis using a business use case based in our model was performed to understand the result and lessons stemming. As shown in Fig. 2.12, the trend shows an improvement of the power efficiency for each new application specific integrated circuit and

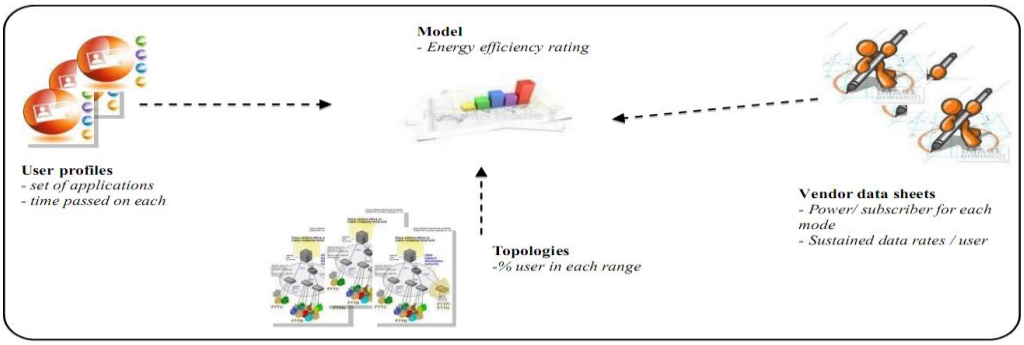

Figure 2.11 Energy efficient model ingredients.

technology used in access network. Moreover, sleep modes and power shedding as power saving strategies in ONU and OLT are introduced to lower the energy dissipation. Based on these trends, we confront to increase in traffic capacity, but using new technology is seen as decreasing in energy consumption per user in access network. Other important lesson is the spotting of the time life of some technology after 2014 for heavy and business users. In this use case, GPON and EPON cannot support the requirement of these users for the given considerations, e.g. 32 users, and so, for solving these problems operator must decrease the number of user per PON and consequently increase the cost and power consumption. Therefore a new technology as XGPON, and 10G EPON with more energy-efficient hardware architectures and technology in OLT and ONU will emerge. But these may not be

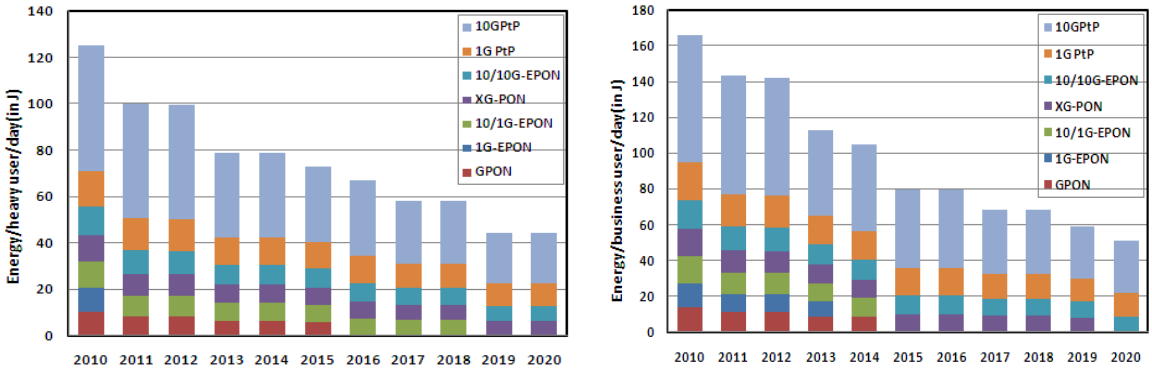

(a) (b)

Figure 2.12 Energy consumption per user as a function of technology and time for short reach: (a) heavy user, (b) business user.

enough. For mobile backhaul and data center after 2015, next generation optical accesses such as(U)(D)WDM technologies may be required.

Fig. 2.13 shows the evolution of the total energy-per-user-per-day for 2010, 2014 and 2020 and demonstrates maximum potential for efficient access network utilization within the model network architecture. Herein, two scenarios are considered for distance 20 km and 60 km, providing insight into the future impact of access networks on green topology and high performance. According to our model the total energy-per-user can be reduced by a base line in CoC, but the energy consumption increase with using PtP technology. 10 G PtP networks support sustained data rate very well for up to several users, however it becomes the most inefficient as energy efficiency. Also 1G PtP network and 10G EPON are other possible solutions, which are able to support user up to 60 km but these are relatively power-inefficient for business user, mobile backhaul and data center. Soon after, a new generation of PON (WDM-PON and UDWDM-PON) with even higher aggregate rates can be employed. But market adoption and cost performance for these green technologies has a tangible risk regarding to profits. In fact this is the benefit of our model that can easily evaluate best-case or pushing-to-the-limit scenarios for each user profile in respect to time evolution.

As it can be seen in Fig. 2.13, this model only considers state-of-the-art technology continuously upgraded each year. In the event that operators practically use equipment for long term. However the model looks to the future of networking from a new perspective, where energy rating and economic concerns are viewed as fundamental design criteria and helps us to select the green solution that use for long life time and gives a plan to migration

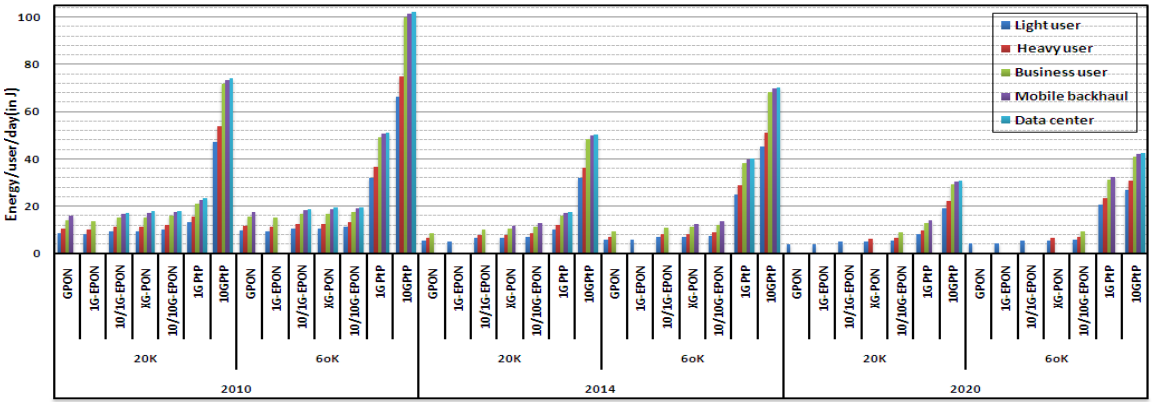

Figure 2.13 Energy consumption per user as a function of technology and reach for several user profiles.

to new technology to provide more profit. For the best-case scenario, one can realize higher demand user will require higher energy and the trends of some technologies, considering technology and traffic evolution, will not sustain if used by the considered user count for all user profiles.

2.5 Concluding Remarks

In this chapter, a numerical model for power consumption optimization in long reach optical access networks, which is based on population distributions and network topology, was presented. The work led us to the conclusion that the combination of reach extension technologies in conjunction with cascaded splitter structure reduces energy consumption of OLT in low take rate areas and provides better OLT port loading than a single splitter architecture. Then, a set of analysis and methodology for the investment and interface technology levels in ODN, were presented. In order to quantify the relative benefits of tunable TRx+ transparent ODN vs opaque, three different usage patterns and different OTGs sizes were considered in terms of energy consumption. It was established that there is a big power saving (60%) from the combination of tunable TRx + transparent ODN. Finally, some of the most relevant parameters such as equipment characteristics, topologies and user profiles that can be considered in the analysis of current access networks were addressed and a model for energy efficiency rating of optical access network equipment was presented. The application of the model to several technologies envisaged several limitations in some of the future application scenarios and technologies (e.g. GPON) that resulted future technology with higher data rate and more energy efficient architectures will cover these limitations.

References

[1] R. Bolla, R. Bruschi, F. Davoli and F. Cucchietti, "Energy efficiency in the future Internet: a survey of existing approaches and trends in energy-aware fixed network infrastructures," *IEEE Comm. Surveys & Tutorials*, vol. 13, no. 2, pp. 223-244, July 2011.

[2] FTTH Council Europe, "FTTH Business Guide," Second Edition, 2011.

[3] F. Saliou et al., "Reach extension strategies for passive optical networks," *J. Opt. Commun. Networking*, vol. 1, no. 4, pp.C51-C60, August 2009.

[4] F. Saliou , P. Chanclou , N. Genay, F. Laurent , F. Bourgart , B. Charbonnier, "Energy efficiency scenarios for long reach PON central offices," Proc. *Optical Fiber Communication Conf. (OFC)*, Los Angeles, CA, March 2011, paper OThB2.

[5] C. Lange, D. Kosiankowski, R. Hülsermann, R. Weidmann, A. Gladisch, "Energy footprint of telecommunication networks," Proc. *Eur. Conf. Opt. Commun. (ECOC)*, Torino, Italy, September 2010, paper Mo.1.D.2.

[6] D. Gardan, A. Zaganiaris, A. Madani, R. Madigou, and D. Machon, "Techno-economics of advanced optical subscriber networks," Proc. *Global Telecommunications Conference (GLOBECOM)*, Dallas, TX , November 1989.

[7] http://www.zhone.com/products.

[8] K. Grobe, M. Roppelt, A .Autenrieth, J.-P. Elbers, M. Eiselt, "Cost and energy consumption analysis of advanced WDM-PONs," *IEEE Communications Magazine*, vol. 49, no. 2, pp. s25-s32, February 2011.

[9] EU Code of Conduct on energy consumption of broadband communication equipment, http://re.jrc.ec. europa.eu/energyefficiency/html/standby_initiative.htm

[10] J. Baliga, R. Ayre, W. V. Sorin, K. Hinton, R. S. Tucker, "Energy consumption in access networks," Proc. *Optical Fiber Communication Conf. (OFC)*, San Diego, CA, February 2008, paper OThT6.

[11] Y. Zhang, P. Chowdhury, M. Tornatore, and B. Mukherjee, "Energy efficiency in telecom optical networks," *IEEE Comm. Surveys & Tutorials*, vol. 12, no. 4, pp. 441 - 458, July 2010.

[12] J. Baliga, R. Ayre, K. Hinton, W. V. Sorin, and R. S. Tucker, "Energy consumption in optical IP networks," *J. Lightw. Technol.*,, vol. 27, no. 13, pp. 2391-2403, July 2009.

[13] C. Lange and A. Gladisch, "On the energy consumption of FTTH access networks," Proc. *Optical Fiber Communication Conf. (OFC)*, San Diego, CA, March 2009, paper JThA79.

[14] C. Lange, D. Kosiankowski, R. Weidmann, and A.Gladisch, "Energy consumption of telecommunication networks and related improvement options," *IEEE J. of Selected in Quantum Electronic*, vol. 17, no. 2, pp. 285 - 295, Auguest 2010.

[15] A. Lovric, S. Aleksić, J. Lazaro, G. M. Tosi Beleffi, F. Bonada, J. Prat, and A. Teixeira, "Influence of broadcast traffic on energy efficiency of long-reach SARDANA access network," Proc. *Optical Fiber Communication Conf. (OFC)*, Los Angeles, CA, March 2011, paper OThB5.

[16] http://www.ict-oase.eu/public/files/OASE_WP4_D4_1_29th_October_2010_v1_0.pdf.

[17] Cisco visual networking Index: forecast and methodology, 2009-2014, Cisco Systems, San Jose, CA, 2009, http://www.cisco.com/en/US/solutions/collateral/ns341/ns525/ns537/ns705/ns87 white aper_c11- 481360_ns827_Networking_Solutions_White _Paper.html

[18] B. Tarnai "Requirements and traffic dimensioning for system concepts and architecture, joint workshop OASE and ACCORDANCE FP7 projects," BROADNETS 2010.

[19] S. Smolorz, H. Rohde, E. Gottwald, D. Smith, A. Poustie, "Demonstration of a coherent UDWDM PON with real-time processing," Proc. *Optical Fiber Communication Conf. (OFC)*, Los Angeles, CA, March 2011, paper PDPD4.

CHAPTER 3 SPECTRALLY-EFFICIENT OPTICAL ACCESS NETWORKS

Summary

Coherent Ultra-Dense Wavelength Division Multiplexing (UDWDM) together with multi-level modulation formats allow high wavelength count with high aggregated capacity and easier network upgrade for flexible bandwidth Passive Optical Networks (PONs). In addition, Nyquist pulse shaping is a key technology to achieve full usage of the available spectrum, optimizing the number of users, network capacity, reach and flexibility in PON. In order to apply efficient Nyquist schemes in PON, we need to consider its potentials and properties as well as limitation, complexity and requirements needed to obtain the high spectral efficiency objectives. To discuss the latter topics, this chapter presents different technical aspects of UDWDM-PON using Nyquist pulse shaping. Furthermore, it also presents the application of coherent self-homodyne detection for the implementation of laser-less optical network units in UDWDM-PONs. Finally, fully bidirectional schemes, based on this technology, are experimentally demonstrated.

3.1 Introduction

The increased demand for broadband services in Optical Access Networks (OAN) has pushed engineers and scientists around the world to develop new technologies to better exploit the bandwidth capabilities of Passive Optical Networks (PONs). Most of the research works focuses on how to maximize the number of users, capacity, reach, and flexibility at minimal cost, complexity, and occupied bandwidth (e.g., from 1538 nm up to 1551 nm). Recently, particular attention has been given to Orthogonal Frequency-Division Multiplexing/Multiple Access (OFDM/OFDMA) and Ultra-Dense Wavelength-Division Multiplexing (UDWDM) [1-3] technologies as solutions for enhancing spectral efficiency, capacity, and flexibility of Future Optical Access Networks (F-OANs). Furthermore, these technologies are the enablers of a flexible OAN, capable of supporting users with different bandwidth demands, i.e., from residential to business customers and possibly mobile back/front hauling applications.

Both UDWDM and OFDM technologies share similar concepts such as providing very high wavelength channel granularities, i.e., allocating narrow optical bands per user (e.g., 5 GHz) for several users (e.g., 1000 users) in the same Optical Distribution Network (ODN). The referred technologies can be enhanced by resorting to coherent detection along with advanced modulation formats in the network transceivers. The latter, consequently, will improve receiver sensitivity, wavelength tuning range, and provide means of simple data rate upgrade without changing optoelectronic components and simply by updating Digital Signal Processing (DSP) techniques in the transceivers. Hence, the DSP resources required in both optical line terminal and Optical Network Unit (ONU) sides play a major role for both network operation and flexibility in high-capacity PONs. For example, the work in [4] demonstrated symmetric 1 Gb/s per user for 1000 users using dense WDM with OFDMA sub-band allocation in a total wavelength spectrum of 16 nm. A total capacity of 1.92 Tb/s (40 × 48 Gb/s spaced by 50 GHz) has been demonstrated with ONUs electronics operating at 5 GHz and requiring two laser sources, i.e., one for coherent detection of downstream data and the other for upstream data transmission. In the case of UDWDM, with very high channel count but at the same time very narrow channel separation (or spacing), e.g. 3 GHz, high channel granularity is achieved [5]. However, it can be quite challenging to upgrade to

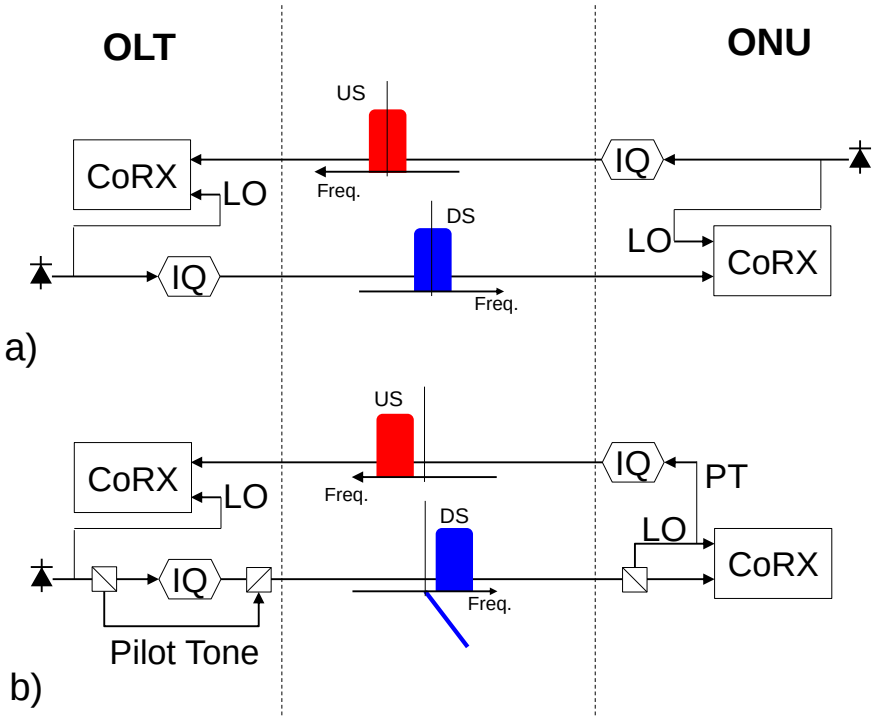

Figure 3.1 (a) Heterodyne detection. (b) Self-homodyne detection.

higher bit rates per channel/user when resorting to narrow channel spacing and reduced symbol rates. One possible solution relies on Nyquist pulse shaping to compress the signal bandwidth along with high-order modulation to increase the bit rate up to 10 Gb/s per user/ wavelength without calling upon polarization multiplexing schemes. Also, in UDWDM-PON systems, due to heterodyning [5], as shown in Fig. 3.1 (a) only one laser source is required in the ONU, i.e., the laser source can be split between upstream and downstream transmissions. In addition, the electronics in the ONU may operate at the symbol rate as very simple DSP is required for recovering the data information. For instance, if 2.5 Gbaud 16-ary Quadrature Amplitude Modulation (16QAM) (10 Gb/s) with Nyquist pulse shaping is employed, sampling at 2.5 GSa/s (one sample per symbol) is sufficient for performing all the DSP functionalities needed in the receiver: clock recovery, phase estimation, and frequency offset estimation. Extra DSP blocks such as Fast Fourier Transform (FFT)/Inverse FFT (IFFT), cyclic prefix, channel estimation, and symbol synchronization are not needed as in the case of receiving OFDM signaling. In fact, the Coherent Receiver (CoRX) includes a Local Oscillator (LO) with narrow linewidth (due to low symbol rate) tuned to the signal carrier frequency and DSP for carrier frequency offset compensation and Carrier Phase Recovery (CPR) [6]. Although that may lead to the use of potentially costly LO and some

complexity in the DSP at the Optical Line Terminal (OLT) and ONUs, with Self-Homodyne Detection (SHD) schemes, this cost can be mitigated. In SHD systems, the modulated signal is multiplexed with an unmodulated Pilot Tone (PT) originating from the same light source prior to transmission, as represented in Fig 3.1 (b). Both signals are transported along the network and demultiplexed at the receiver. There, the PT is used for coherent homodyne detection of the signal instead of a LO, as would be the case of heterodyne detection. Since the signal and PT originate from the same light source and assuming that they have similar propagation delays along the link, phase coherence is preserved.

Nyquist pulse shaping has been extensively investigated as a solution to improve spectral efficiency, thus achieving full usage of the available spectrum [7-9]. More recently, optical Nyquist filtering for 10 Gb/s on-off keying in OFDMA based PONs has been proposed to extend reach and split ratio [10]. Nyquist pulses enhance the mitigation of back-reflections in bidirectional transmission, when the two directions are paired and interleaved, and compensation of nonlinear crosstalk [11]. Moreover, using frequency up/down-shifting of Nyquist pulse shaped from optical carrier, one can transmit the information in Downstream (DS) and Upstream (US), respectively, with full bandwidth allocation and with the same laser frequency in both directions, which is useful for easy maintenance of UDWDM networks. In addition, this brings benefits in terms of reduction of Rayleigh Back-Scattering (RBS), since this impairment affects mainly the carrier, which has a frequency spacing in respect to the modulated information and can therefore be mitigated by proper filtering in the receiver. Therefore, when Nyquist pulse shaping combined with high-order modulation formats such as 16QAM, which attains a good compromise between Signal-to-Noise Ratio (SNR) and Analog to Digital Converter (ADC)/Digital to Analog Converter (DAC) amplitude resolution [12], they may also achieve higher bit rates per user with low speed electronics.

In the first section of this chapter, we present (i) by means of numerical simulations some techniques to optimize the feeder power (mitigation of crosstalk and interchannel nonlinearities) using Nyquist shaped signaling in UDWDM systems and (ii) experimentally analyze the bidirectional performance of coherent UDWDM based PON networks in terms of sensitivity and nonlinear tolerance. The network at hand transports 1 or 16 UDWDM channel groups employing 16QAM with Nyquist pulse shaping. Using DSP techniques in

the ONUs, transmission over 40 km of Standard Single-Mode Fiber (SSMF) is successfully demonstrated considering different channel granularity conditions, i.e., symbol rate R_S (5 Gb/s or 10 Gb/s per channel), channel spacing Δf, and number of channels N_{CH} per UDWDM.

In the second part of this chapter, we elaborate the fully coherent bidirectional PON system concept and demonstrate a coherent SHD-PON approach that enables transmission and fully coherent reception of both the US and DS Nyquist bands using a single laser at the OLT, thus laser-free ONU. The experimental results are presented for a coherent UDWDM with 4 GHz channel spacing in both directions with a total of 20 Gb/s per channel. Finally, a fully loaded bidirectional ultra-high capacity coherent PON (2 × 1008 × 8.3 Gb/s) is demonstrated.

3.2 Nyquist Shaped UDWDM-PON (papers J1-J2, C4-C5)

In this section we present the benefits of Nyquist shaping when compared to Non-Return-Zero (NRZ) in terms of mitigation of crosstalk arising from back-reflections in bidirectional transmission, Four-Wave Mixing (FWM) and possibly Cross-Phase Modulation (XPM) in UDWDM based networks.

3.2.1 Mitigation of Back-Reflections

The problem of back-reflections arises from the same wavelength channel propagating in the opposite direction via RBS due to either bidirectional transmission or due to faulty components in the network. These back reflections can be mitigated using the appropriate pulse shaping for compressing the spectrum as demonstrated in [11]. Here, we simulate a total of 16 UDWDM channels at 10 Gb/s-16QAM equally spaced by 3.125 GHz and into two groups split for downstream and upstream. The two groups are interleaved in a way that in each group the effective channel spacing is 6.25 GHz, as demonstrated in Fig. 3.2. The crosstalk at coherent receiver due to back reflections is emulated by changing the relative power between nearest neighbor channels from 2 dB (Fig. 3.2 (a)-(c)) up to 20 dB (Fig. 3.2 (b)-(d)) considering both NRZ and Nyquist pulse shaping depicted in Fig. 3.2 (a) and (b) and Fig. 3.2 (c) and (d), respectively. We define Nyquist as *sinc* pulses with a zero roll-off factor. At the transmitter side, Nyquist filtering is carried out digitally via a matrix multiplication of an array of delayed *sinc* pulses (size 16384 × 512) and the incoming vector of 16QAM

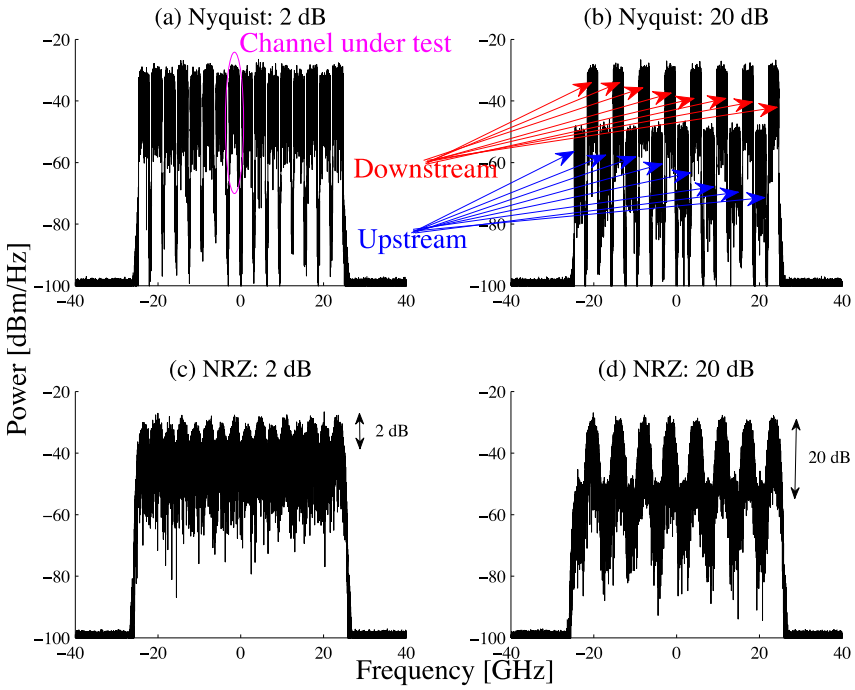

Figure 3.2 Nyquist versus NRZ pulse shaping for mitigating crosstalk in bidirectional 10 Gb/s-16QAM channels at 3.125 GHz. The relative power between nearest neighbor channels (a) Nyquist: 2 dB. (b) Nyquist: 20 dB. (c) NRZ: 2 dB. (d) NRZ: 20 dB.

symbols (512 symbols). The array of *sinc* pulses has an oversampling factor of 32 and a filter length corresponding to 512 symbols, i.e., 16384+1 coefficients. It is worth pointing out that this filter has a prohibitive DSP resource as both filter length and oversampling factor have to be optimized to be suitable for real-time implementations [7-9]. The 2.5 Gb/s NRZ signals are generated with the same properties, i.e., 512 bits sampled at 32 samples per bit. With an oversampling factor of 32 samples, there is 80 GHz (32 × 2.5 Gbaud) available for simulating all the 16 WDM channels spaced by 3.125 GHz.

The crosstalk is evaluated in the channel under test (eighth center channel) highlighted by the magenta circle in Fig. 3.2 (a) after multiplexing and demultiplexing. To obtain over 8000 simulated symbols or 32000 simulated bits, the simulations are carried out independently 16× (16 × 512 = 8192). In each simulation, the root-mean-square Error Vector Magnitude (EVM) is calculated in percent for the coherently detected 16QAM symbols with respect to the reference transmitted symbols, i.e., EVM_{RMS} [%] = EVM_{RMS}×100. We use an optical transmitter consisting of an IQ Modulator (IQM) plus laser source with 100 kHz linewidth. The optical receiver is comprised of 100 kHz-local oscillator, optical hybrid, and balanced

detection akin to the ones used in [13] to simulate the UDWDM-PONs. Nyquist filtering is carried out in the electrical domain via a super Gaussian filter with 3-dB bandwidth around 1.125 × R_S symbol rate. After Nyquist filtering and resampling, the signal from 32 samples down to 1 sample per symbol, DSP techniques such as retiming and carrier phase estimation are performed. On the transmitter side, optical filtering effects due to multiplexing operations are emulated by a 3.25 GHz second order super Gaussian filter.

Fig. 3.3 shows the EVM of the channel under test considering both Nyquist pulse shaping (red circles) and NRZ pulse shaping (blue squares) at 10 Gb/s-16QAM for different crosstalk levels. As observed in Fig. 3.3, after multiplexing and demultiplexing via coherent detection, Nyquist shaping is more robust than the NRZ shaping for a fixed symbol rate and channel spacing. At least 4 dB EVM reduction (highlighted by the inset constellations in Fig. 3.3), or equivalently 4 dB SNR improvement, is attained when Nyquist pulses are employed in UDWDM-PONs. This filtering technique, besides improving spectral efficiency, provides extra benefits in terms of crosstalk mitigation when compared to legacy NRZ pulse shaping. These benefits certainly ease the implementation of the bidirectional concept in UDWDM systems.

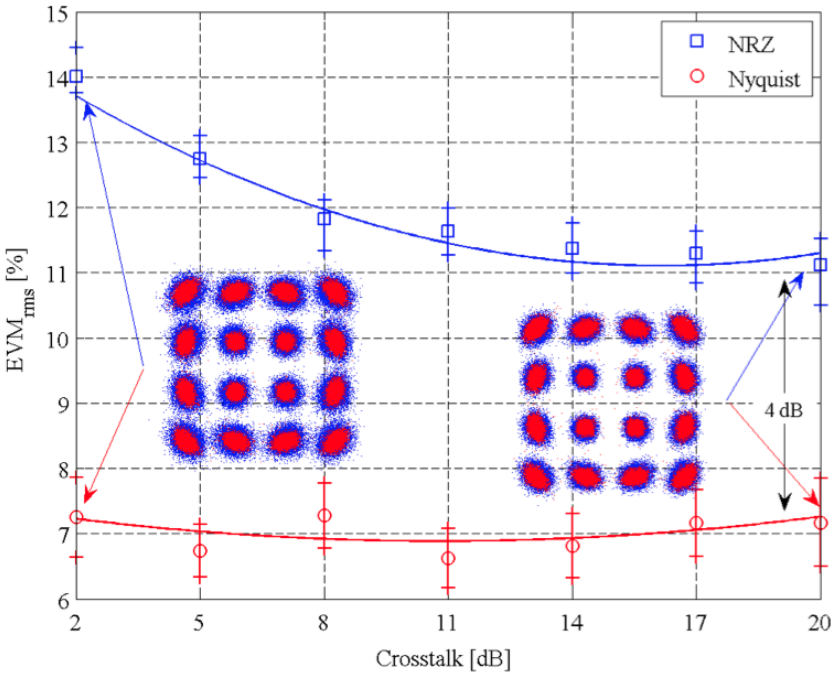

Figure 3.3 EVM (eighth downstream channel) for different crosstalk levels.
NRZ: blue squares. Nyquist: red circles. Vertical bars: 95% confidence interval.

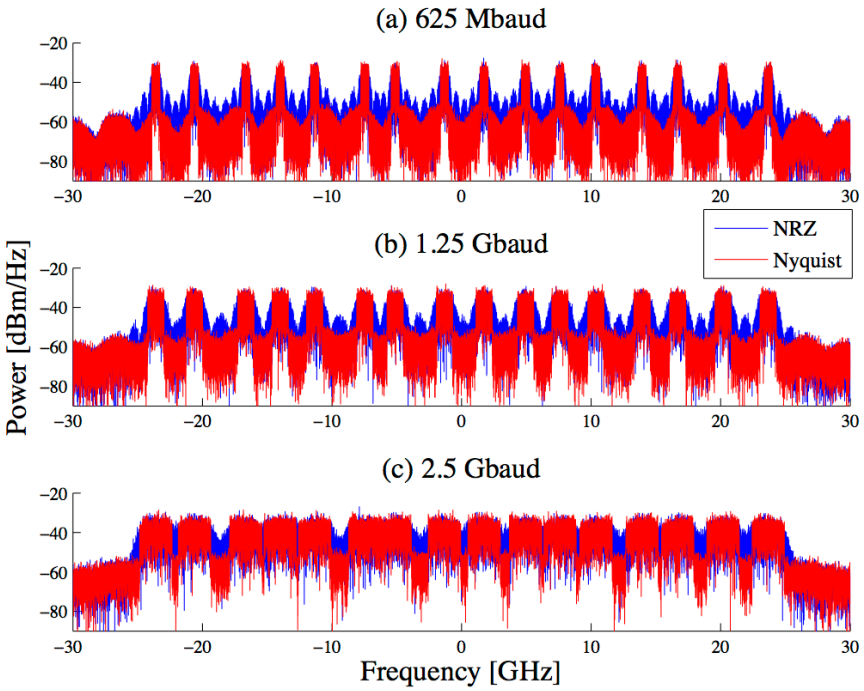

Figure 3.4 Nyquist versus NRZ pulse shaping for mitigating inter-channel nonlinearities in 16×16QAM channels at 3.125 GHz. (a) 2.5 Gb/s. (b) 5 Gb/s. (c) 10 Gb/s.

3.2.1.1 Mitigation of FWM

Both FWM and XPM are relevant in UDWDM systems when channel separations of the order of 3 GHz are employed [13]. FWM can be mitigated using unequally spaced channels as shown in [14]. Unequally spaced channels can be efficiently obtained using small frequency tuning without penalizing spectral efficiency [15]. In this study, we show that FWM can be further mitigated if the spectral profile of UDWDM channels is compressed using Nyquist pulse shaping for instance. The methodology used in this section is demonstrated in Fig. 3.4. 16 equally spaced channels (16QAM) at 3.125 GHz are generated, according to the previous section, and transmitted over 25 km of SSMF (0.2 dB/km, 16.5 ps/nm/km, 1.35 $(W.km)^{-1}$). The optical power per channel at the input of the fiber is set to −3 dBm per channel so that the system's performance is mostly limited by fiber nonlinear effects. Symbol rates at 625 Mbaud (2.5 Gb/s, Fig. 3.4(a)), 1.25 Gbaud (5 Gb/s, Fig. 3.4 (b)), and 2.5 Gbaud (10 Gb/s, Fig. 3.4 (c)) are used in order to investigate the interplay between signal bandwidth and FWM mitigation for a fixed channel spacing. Both Nyquist (red) and NRZ (blue) pulse shaping techniques, as shown in Fig. 3.4, are used in the transmitted channels. To achieve unequally spaced channels, the transmitted channel frequencies are

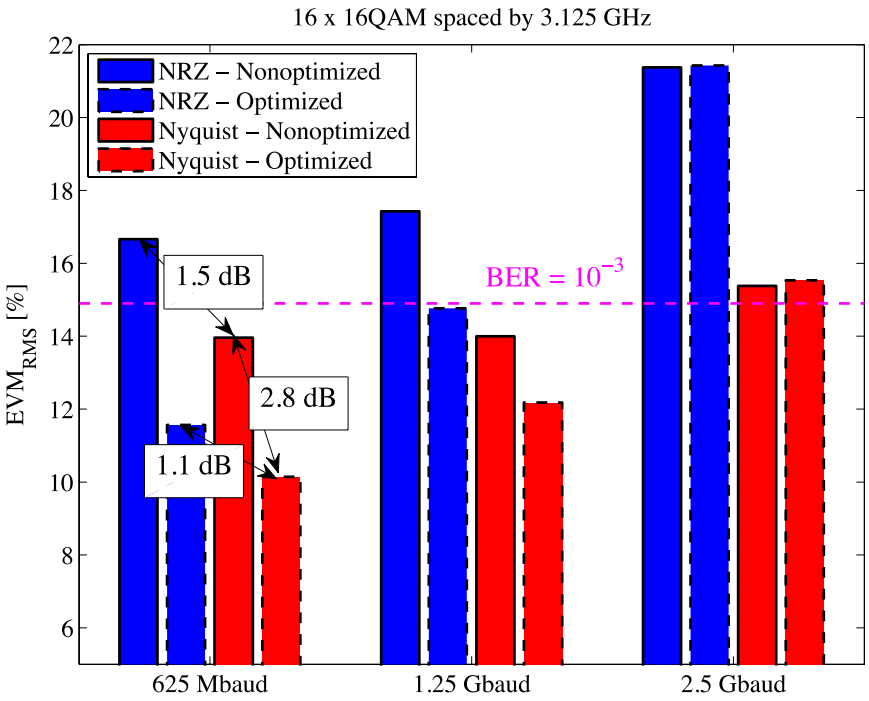

Figure 3.5 EVM (center channel) for different symbol rates with (solid line edges) and without (dash line edges) optimized channel frequencies via MGA. NRZ: blue bars. Nyquist: red bars.

optimized off-line (maximum tuning range ≤ |650 MHz |) using a Multi-objective Genetic Algorithm (MGA) [15].

The results in Fig. 3.5 show the EVM of the center channel under test for Nyquist (red bars) and NRZ (blue bars) pulse shaping techniques with (solid line edges) and without (dash line edges) using optimized channel frequencies via an MGA. If we directly compare Nyquist in red to NRZ in blue, we can observe that Nyquist pulse shaping always provides lower EVM. The lower EVM stems from reduced nonlinear effects via FWM and XPM, and also reduced crosstalk from neighbor channels as discussed before. Furthermore, lower symbol rates enhance the ability of the receiver to filter out the FWM components when optimized channel frequencies and coherent detection are used. As the symbol rate increases, the benefit of MGA optimized channel frequencies for mitigating FWM is decreased due to the narrow guard band between the channels. Essentially, higher guard bands make it easier to filter FWM products out of band. If the frequency tuning range is excessive for the 2.5 Gbaud case, it might happen that unequally spaced channels may induce extra linear crosstalk if the channel spacing is of the same order as the signal bandwidth. A 1.5 dB EVM reduction is achieved if Nyquist pulses instead of NRZ pulses are used for 625 Mbaud without optimized

channel frequencies (solid line edges). This improvement may suggest that Nyquist pulses induce lesser phase distortion via XPM when compared to NRZ pulses. Further studies will be carried out to identify which nonlinear effect (FWM or XPM) is more relevant in this case. If optimized channel frequencies along with Nyquist pulses are employed in the transmitter, an extra 2.8 dB EVM reduction (or 2.8 dB SNR improvement) is achieved when compared to the non-optimized situation (dash line edges). This performance improvement results from the lower frequency overlap between the baseband signal and FWM components that can be more easily removed by the appropriate low pass filters in the coherent receiver, as demonstrated in Fig. 3.4 (a). A 1.1 dB penalty is observed if NRZ pulses (broader bandwidth compared to *sinc* pulses) are employed along with optimized channels for 625 Mbaud.

3.2.2 Terabit Nyquist Shaped UDWDM Coherent PON with Upstream and Downstream over a 12.8 nm Band (papers J1 and C4)

This section describes the lab setup, whose instrumentation picture is depicted in Fig. 3.6, implemented for experimentally characterizing the Terabit+ UDWDM-PON transporting Nyquist 16QAM channels with coherent detection. The experimental setup depicted in Fig. 3.6 is used to study the bidirectional transmission characteristics of coherent UDWDM-PON employing Nyquist 16QAM, operating at 5 Gb/s or 10 Gb/s per channel. First, a bank of 15 distributed feedback laser plus an External Cavity Laser (ECL) (channel under test) is multiplexed using a 100 GHz arrayed waveguide grating. 16QAM signaling with Nyquist pulse shaping is digitally implemented with zero roll-off factor *sinc* pulses in a 12 GSa/s Arbitrary Waveform Generator (AWG) (Tektronix 7122C). The Nyquist filter impulse response is shown in Fig. 3.7, whereby the digital filter length corresponds to 212 symbol periods with a total of 16384+1 (4 × oversampling) and 32768+1 (8 × oversampling) filter coefficients for 2.5 Gbaud and 1.25 Gbaud, respectively. A pre-emphasis filter implemented as a Gaussian filter with 2.55 GHz bandwidth is used to mitigate the limited AWG bandwidth (~3 GHz) and resolution (10 bits) as well as crosstalk between UDWDM channels. The baseband signal is defined in a temporal window with 16384 (4096 × 4) and 32768 (4096 × 8) samples for R_S = 1.25 Gbaud (eight samples per symbol) and R_S = 2.5 Gbaud (four samples per symbol), respectively. The electrical 16QAM signals then drive the IQM to

modulate the bank of lasers. The UDWDM channel group is generated using a Mach-Zehnder Modulator (MZM) driven by two radio frequency signals (phase relation ≈ 3π/2) with Δf = 2.5 GHz (N_{CH} = 16 channels), 3.125 GHz (N_{CH} = 14 channels), and 5 GHz (N_{CH} = 12 channels) to set the channel spacing as demonstrated in the measured optical spectra in Fig. 3.8 (a). The appropriate number of channels was selected by limiting the inter- channel power variation to 3 dB, as shown in Fig. 3.8 (b). The UDWDM channel group under test is generated by an ECL source (<100 kHz linewidth) at 1550 nm; see Fig. 3.8 (b). Each UDWDM channel group is amplified and further filtered by a Wave Shaper (WS) (Finisar 4000S) tuned to ~60 GHz bandwidth. The upstream signal (following the red arrow) is a Δf/2 frequency offset copy of the transmitted optical signal in the downstream direction (following the blue arrow) as demonstrated in the inset measured spectrum in Fig. 3.6.

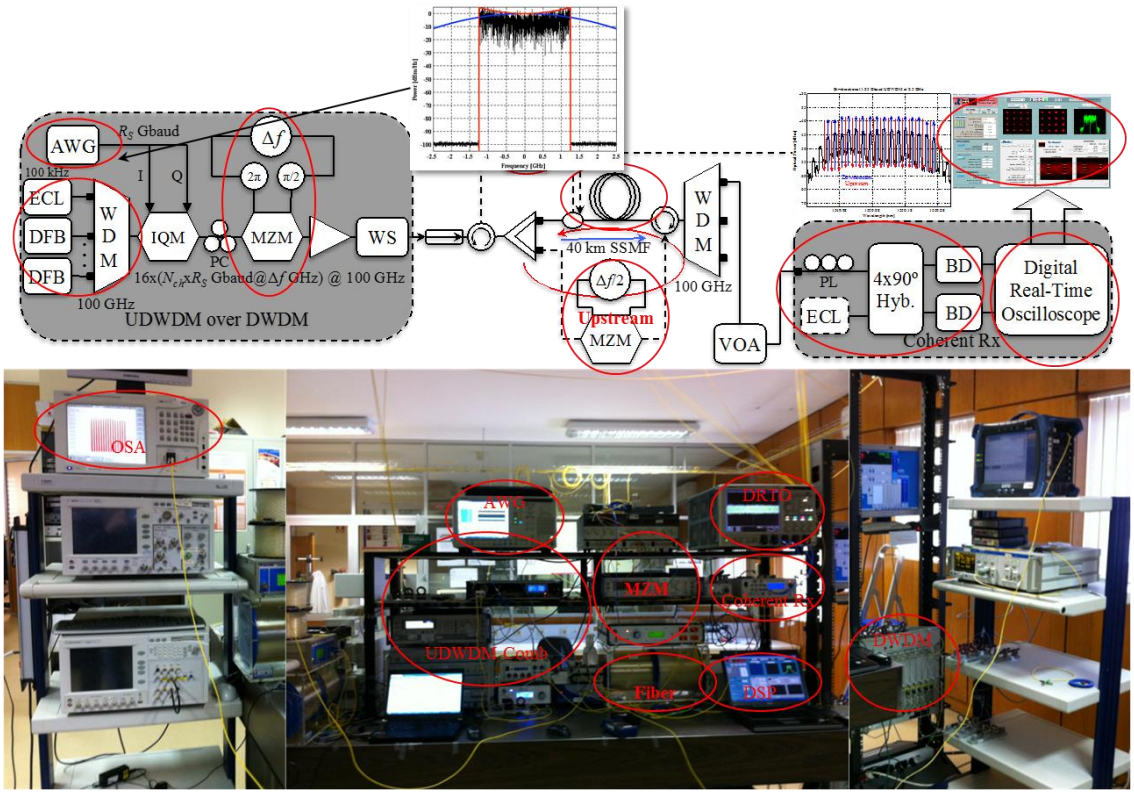

Figure 3.6 Experimental setup and laboratory infrastructure for bidirectional transmission. R_S: symbol rate, N_{CH}: number of channels, Δf: channel spacing in each channel group. OSA: Optical Spectrum Analyzer. AWG: Arbitrary Waveform Generator. MZM: Mack-Zehnder Modulator. IQM: IQ Modulator. VOA: Variable Optical Attenuator. WS: Wave Shaper. BD: Balanced Detectors.

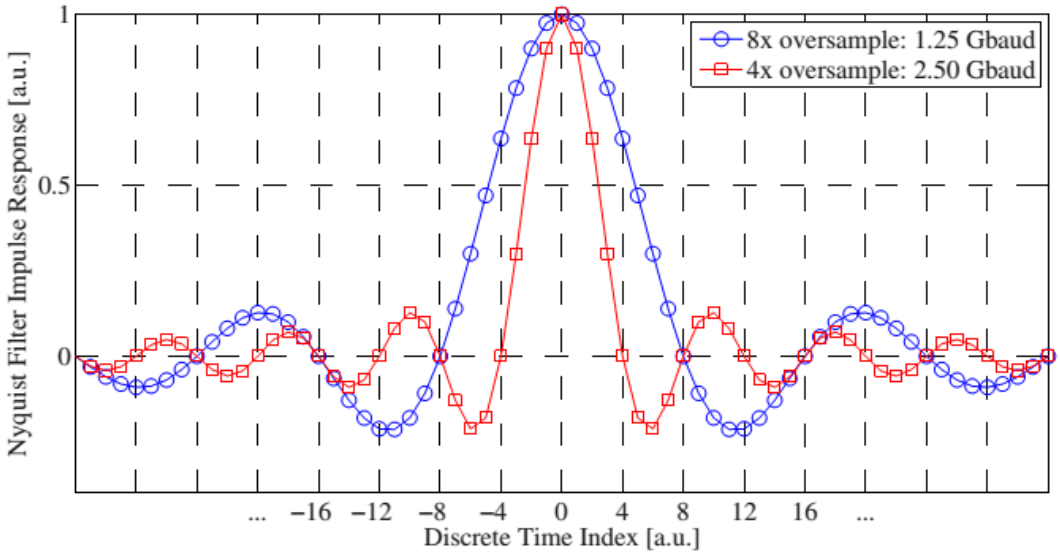

Figure 3.7 Nyquist filter impulse response.

The total optical signal, whose optical spectrum is shown in Fig. 3.9 with a total bandwidth of 12.8 nm, is transmitted over 40 km of SSMF. The total loss budget of the optical link is around 10 dB. After de-multiplexing all the 16 channel groups, the received 16QAM signals are coherently detected with the local oscillator (<100 kHz-linewidth ECL at 1550 nm) tuned to the center channel under test (worst case fiber nonlinear performance [13]) using a $4 \times 90^{\circ}$ optical hybrid. The optical signal is converted to the electrical domain using a pair of Balanced Detectors (BD). The resulting electrical signal is converted to a digital form using a 100 GSa/s real-time oscilloscope with analogue bandwidth around 20 GHz (Tektronix MS072004C). Since the scope bandwidth is much broader than the signal bandwidth (1.25 GHz and 2.5 GHz), seven channels and five channels in the UDWDM channel group under test are processed for 2.5 GHz/3.125 GHz (1.25 Gbaud) and 5 GHz (2.5 Gbaud) channels spacing, respectively. The digital signal is processed off-line as shown in the inset DSP diagram as follows: normalization, retiming, and Nyquist filtering implemented as a super Gaussian filter with bandwidth defined by R_S and down-sampling to 1 sample per symbol. We point out that neither chromatic dispersion compensation nor digital back-propagation is employed for signal equalization. For both 1.25 Gbaud and 2.5 Gbaud signaling, the temporal effects due to chromatic dispersion is negligible for SSMF up to 100 km [13]. After applying Viterbi and Viterbi algorithm to recover the phase and frequency, the network performance is measured in terms of root-mean-squared EVM_{RMS},

estimated for 1048 recovered symbols and averaged over 16 independent measurements to establish a 95% confidence interval.

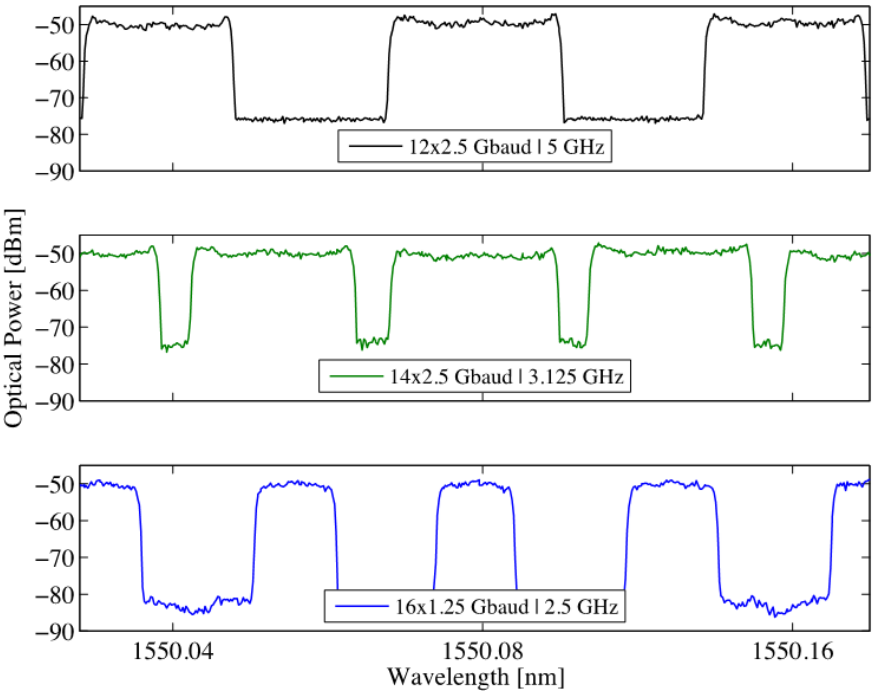

(a)

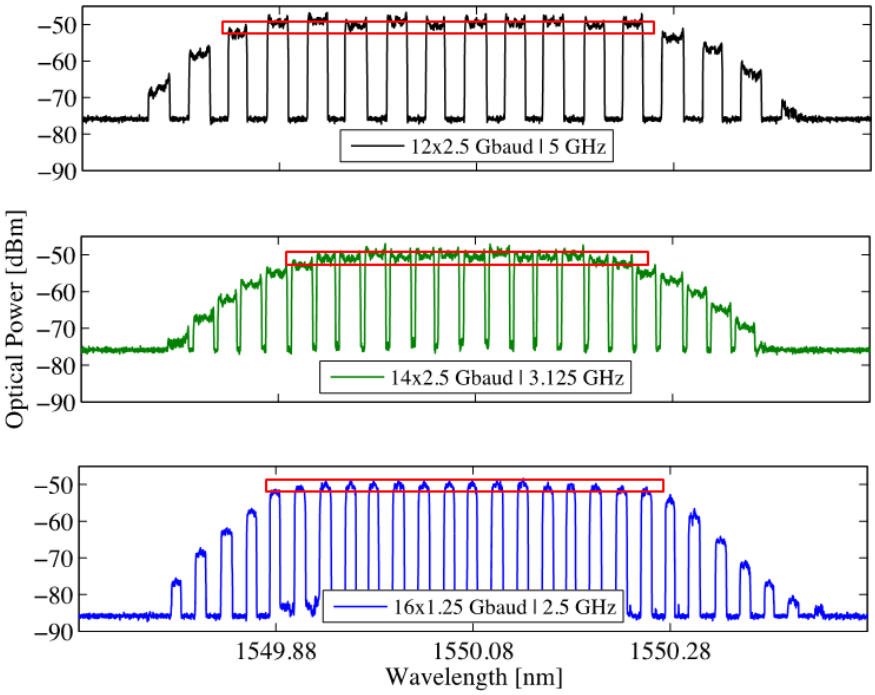

(b)

Figure 3.8 Measured optical spectra for different UDWDM configurations. (a) UDWDM using Nyquist, (b) different UDWDM channel group configurations.

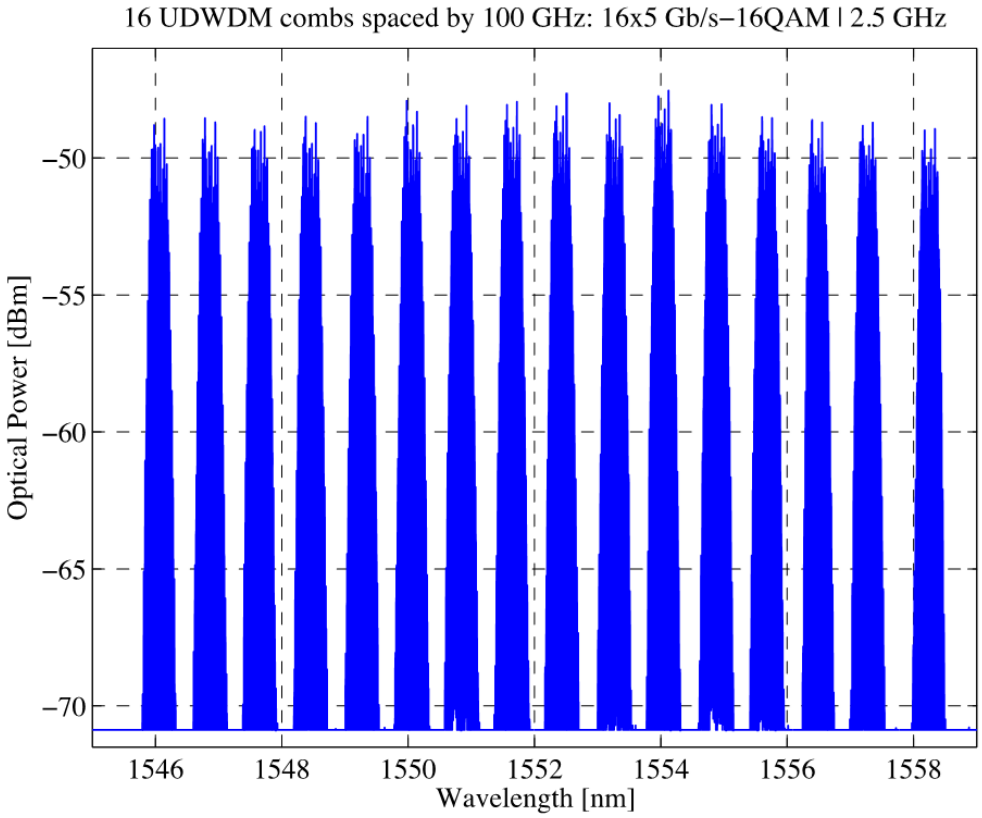

Figure 3.9 Overall spectrum (UDWDM over DWDM) spanning over 12.8 nm in the 100 GHz grid.

In this section, EVM is calculated in dB (EVM_{RMS}[dB]=20log10 (EVM_{RMS}[%]/100)), from which, one can relate to SNR per symbol in dB as SNR[dB]= 20log10(100/(EVM_{RMS}[%]) [16]. In addition to EVM, Bit Error Ratio (BER) estimates by direct error counting from 16 windows with 4096 symbols (65536 16QAM symbols) are also measured.

3.2.2.1 Experimental Results

Fig. 3.10 and Fig. 3.12 depict the network performance in terms of EVM [Figs. 3.10 (a) and 3.12 (a)] and BER [Figs. 3.10 (b) and 3.12 (b)] measurements of the center 16QAM channel in the downstream direction. The performance in Back-to-Back (BTB) (solid lines + filled markers) defines the best sensitivity at BER = 3.8×10^{-3} (corresponding to 7% Forward Error Correction (FEC) overhead limit [17, 18]), whereas the system nonlinear tolerance is characterized after transmission over 40 km of SSMF (dashed lines + open markers).

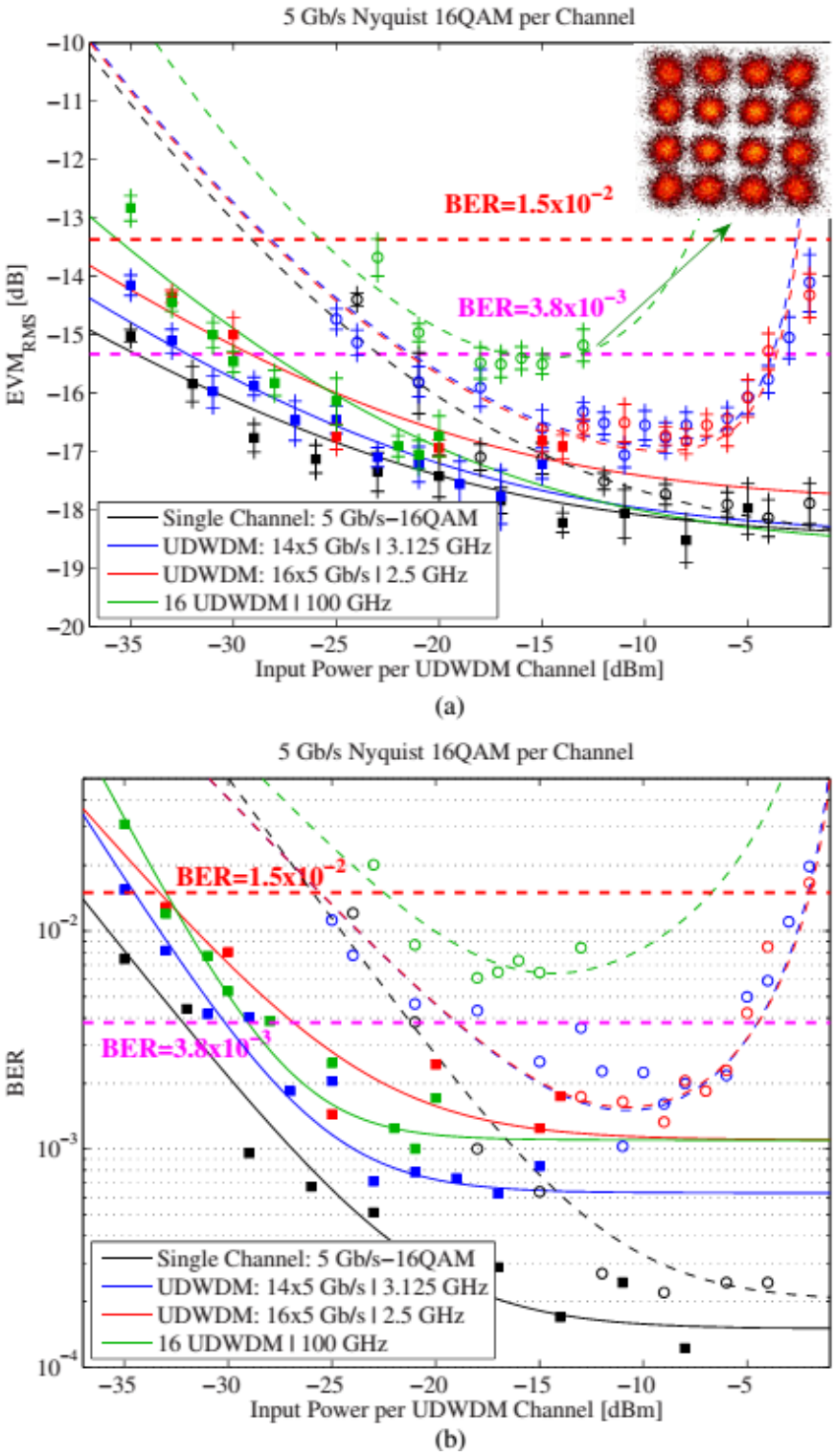

Figure 3.10 Experimental results for 5 Gb/s-16QAM: (a) EVM. (b) BER. Solid lines + filled markers: BTB performance. Dashed lines + open markers: 40 km of SSMF. Vertical bars: confidence interval.

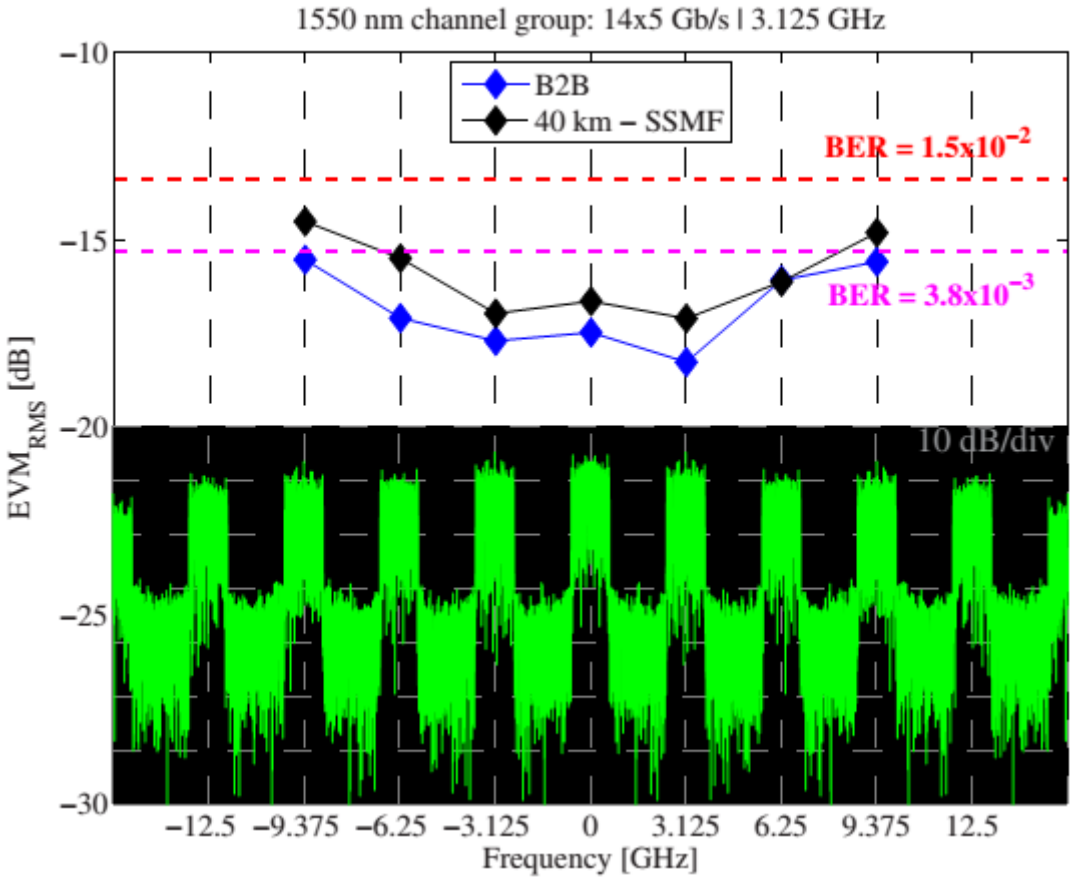

Figure 3.11 UDWDM channel group after transmission at the optimum power: EVM per channel for 14 × 5 Gb/s-16QAM at 3.125 GHz. Inset shows electrical spectrum after coherent detection.

Fig. 3.11 and Fig. 3.13 show the performance for seven and five channels in the UDWDM channel group under test with $\Delta f = 3.125$ GHz and $\Delta f = 5$ GHz, respectively.

A. 5 Gb/s per channel, 1.28 Tb/s (16 × 16 × 5 Gb/s)

According to Fig. 3.10 (a), the best sensitivity around −35 dBm is achieved for single channel at 5 Gb/s. This sensitivity at BER=3.8×10^{-3} is degraded by 5 dB when considering the UDWDM channel group generation either at 3.125 GHz (14 channels) or 2.5 GHz (16 channels with the highest channel granularity) of channel spacing. For 16 UDWDM (16 × 16 = 256 channels), the performance in BTB is very similar to when the system has only one UDWDM channel group. As far as the transmission over SSMF is concerned, both EVM [Fig. 3.10 (a)] and BER [Fig. 3.10 (b)] results obtained from the measurements indicate that the optimum power is around −10 dBm per channel when a sole UDWDM channel group is transmitted. A 5 dB penalty in the nonlinear tolerance (−15 dBm per UDWDM channel as

in constellation in Fig. 3.10 (a)) is observed when the network is upgraded to 16 channel groups spaced by 100 GHz, as depicted by the green lines of Fig. 3.10. The quality of the remaining channels in the UDWDM channel group under test, at the optimum optical power per channel, is analyzed in Fig. 3.11 in terms of EVM per channel. Fig. 3.11 also shows the inset electrical spectrum after coherent detection. The channels in the edge of the spectrum present worse EVM than the center channels, which is caused mostly by the reduced SNR and filtering effects due to the analogue bandwidth of the real-time scope. In principle, they would present better results when coherently detected by a separate ONU receiver.

B. 10 Gb/s per channel, 1.92 Tb/s (16 × 12 × 10 Gb/s)

Regarding the operation at 10 Gb/s per channel as shown in Fig. 3.12 (a), sensitivity of −32 dBm is achieved for single-channel operation. Similarly, there is an extra penalty of 5 dB when the number of channels are increased using UDWDM channel group generation (12 channels spaced by 5 GHz). After transmission over 40 km of SSMF, the optimum power per channel was about −11 dBm using only one channel group, as observed in EVM and BER results in Fig. 3.12 (a) and (b), respectively. This channel group is also characterized in Fig. 3.13 in terms of EVM measurements of the five most center channels that are available for processing after coherent reception. The electrical spectrum is also depicted in Fig. 3.13. When using 16 channel groups (192 channels), the best measured performance was at −14 dBm per UDWDM channel, whose constellation is shown in Fig. 3.12 (a). Due to the narrow bandwidth and limited resolution of the AWG used throughout the experiments, the best EVM results of −18.3 dB (or SNR ≈ 18.3 dB) and −17.4 dB (SNR ≈ 17.4 dB) were achieved for 5 Gb/s and 10 Gb/s per channel, respectively, as shown in Figs. 3.10 (a) and 3.12 (a). By converting these EVM results to BER values following the relations in [16], one can find theoretical BER floors at BER 5 Gb/s ≈ 1.5×10^{-4} and BER 10 Gb/s ≈ 7×10^{-4} akin to the ones shown in Figs. 3.12 (b) and 3.10 (b), respectively. Moreover, an operational power margin of >17 dB and >12 dB for the case of measured EVM and BER (1.5×10^{-2}), respectively, is achieved when considering a 20.5% overhead soft decision FEC [17, 18] for both considered total network capacities of 1.28 Tb/s (16 × 16 × 5 Gb/s) and 1.92 Tb/s (16 × 12 × 10 Gb/s) in total bandwidth of only 12.8 nm.

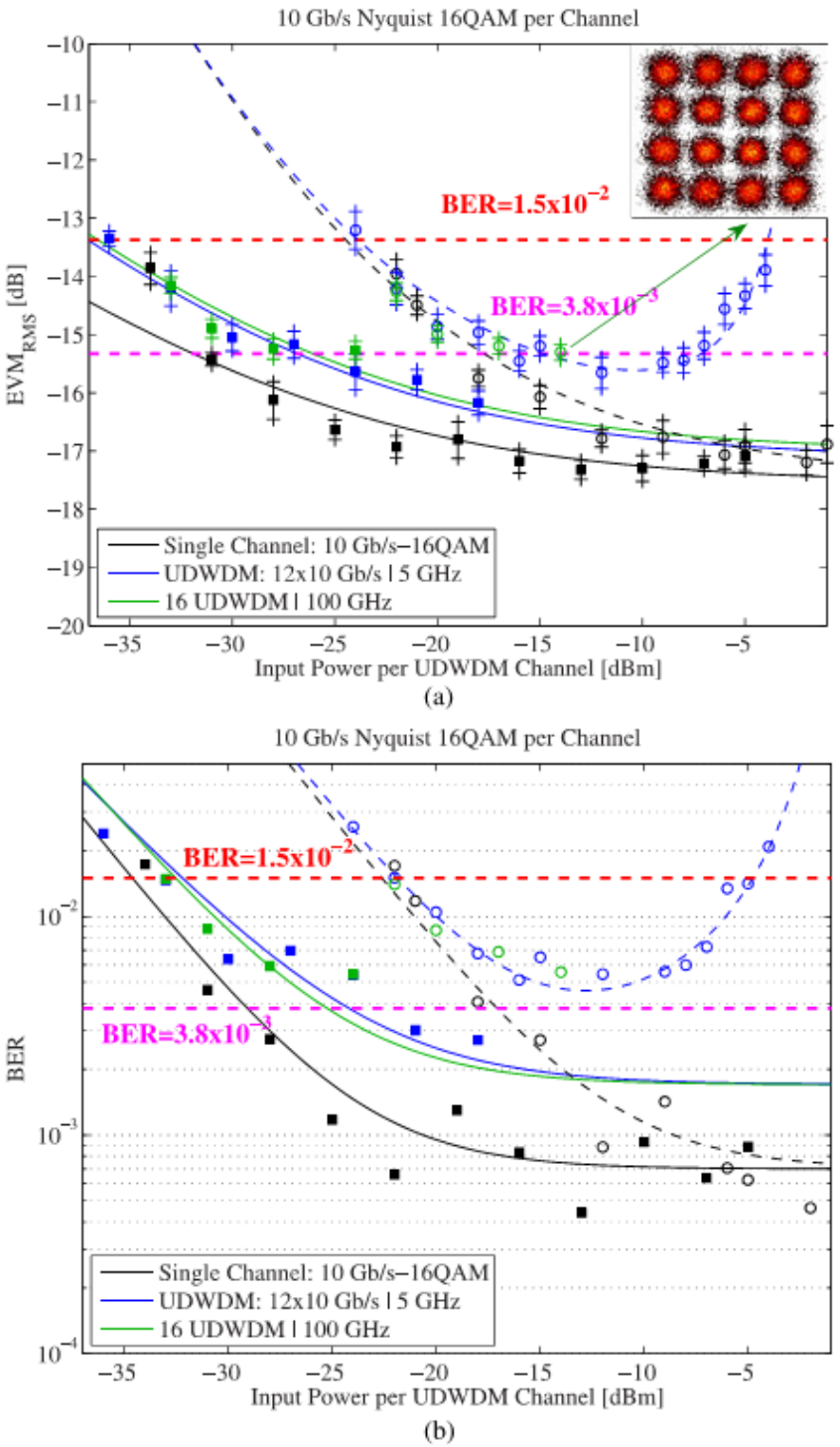

Figure 3.12 Experimental results for 10 Gb/s-16QAM: (a) EVM. (b) BER. Solid lines + filled markers: BTB performance. Dashed lines + open markers: 40 km of SSMF. Vertical bars: confidence interval.

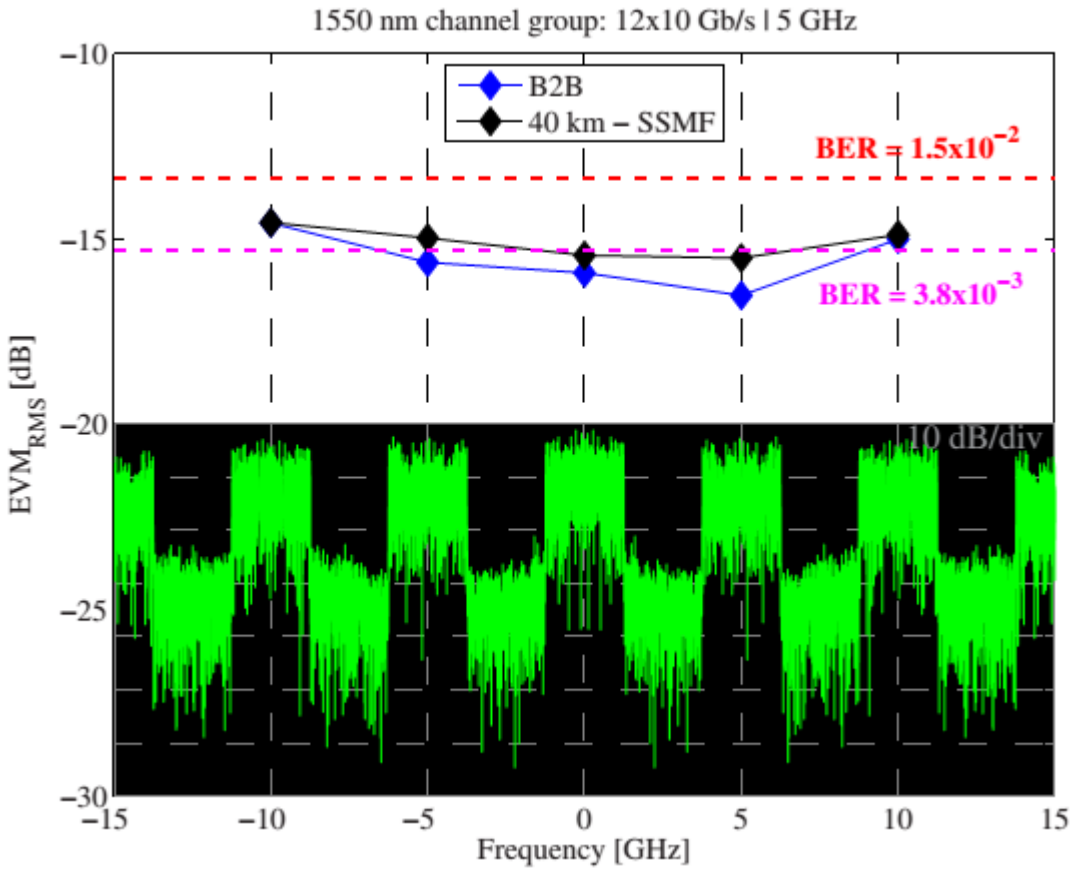

Figure 3.13 UDWDM channel group after transmission at the optimum power: EVM per channel for 12 × 10 Gb/s-16QAM at 5 GHz. Inset shows electrical spectrum after coherent detection.

Nyquist pulse shaping achieves full usage of the available spectrum. Combined with 16QAM format, which attains a good compromise between SNR and ADC/DAC amplitude resolution, Nyquist shaping allows using lower order modulations without significant hardware change. Additionally, UDWDM enables the bidirectional concept to work at reduced laser count, simple management, and flexibility. These three techniques simultaneously provide network scalability, flexibility, and efficiency, keeping the required ODN transparency and optical filter-free ONUs.

3.3 Fully Coherent Self-Homodyne Bidirectional Enhanced Performance PON (papers J3-J4, C6-C7)

To meet the ONU cost requirements in coherent UDWDM-PON, the need for very accurate tunable laser and complex DSP have to be addressed. Recently, the combination of WDM-PON with multiple access techniques such as OFDM [1, 19, 20] and Subcarrier Multiplexing

(SCM) [21, 22] have been demonstrated. Particularly, “colorless” and “laserless” ONUs are proposed in [20-22] to reduce capital and operating expenditures. Therefore, to achieve cost-effectiveness coherent PON, it is also important to carefully select the utilized technologies such as coherent detection techniques, laser-free ONUs and Burst Mode (BM) operation. In previous section, we have presented a Nyquist shaped UDWDM-PON that delivering 10 Gb/s bidirectional data rate achieving very high spectral occupation and reduced RBS. This technology, with paired-channel technology in [5] has shown its capability to meet the huge demand for capacity in heterogeneous networks and datacenters, bringing the benefits of high sensitivity and dynamic bandwidth allocation. However, for this architecture, the requirements of laser linewidth and phase noise cancellation have to be taken into account. One path towards the mitigation of these phenomena is to use SHD and signal frequency upshifting from DC. SHD enables laser linewidth cancelation, reducing laser phase noise requirements and simplifying the DSP.

In this section, we elaborate the fully coherent bidirectional PON system concept using SHD and focus on crosstalk mitigation of this system with its spectral architectures to increase the capacity of optical access networks. The proposed architecture of self-homodyne PON system is introduced. Fully loaded bidirectional demonstration over 30 km of fiber and the experimental setup to study performance analysis and the characterization of the UDWDM system are demonstrated. We extend the network capacity using UDWDM with 4 GHz channel spacing in both directions (2×10 Gb/s), enabled by Nyquist pulse shaping, partial spectral overlap and digital frequency shifting to reduce RBS. Also, we demonstrate 1008 symmetric bidirectional channels, for a combined throughput exceeding 20 Tb/s to further extending the maximum number of users and network flexibility. Finally, we address compatibility with Time-Division Multiple Access (TDMA) schemes, using BM upstream transmission method. In the following, we describe these phases for every protocol of this category.

3.3.1 Self-Homodyne System Concept

To achieve such a highly aggregated coherent PON system, two options may be followed. One option is a single high bandwidth front end generating/processing unit using one wave-length, one modulator and one receiver that requires high electrical bandwidth devices in

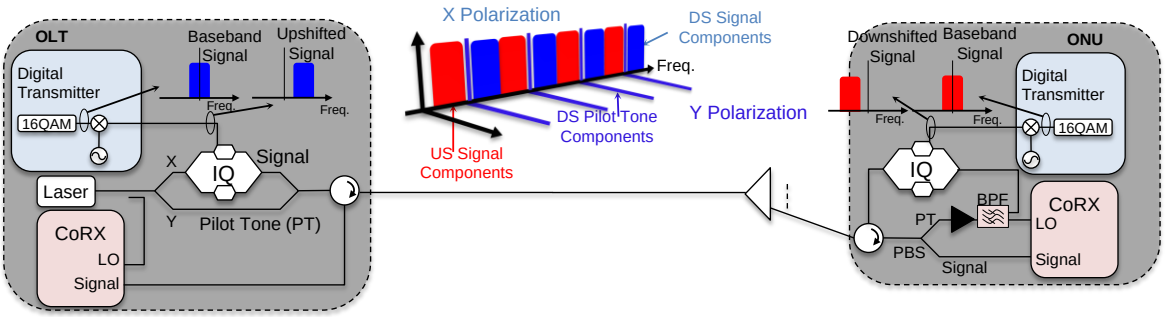

Figure 3.14 Self-homodyne detection fully coherent PON using digital frequency shifted signals.

transmitter and receiver sides [23, 24]. The other option is to use several lasers integrated in the same wafer with the same number of modulators and receivers, partitioning in this way the required electrical bandwidth by each component. The proposed PON architecture follows the second method using a set of innovative features, including Nyquist pulse shaping, SHD and digital frequency shifting. Figure 3.14 illustrates the principle behind an SHD PON using polarization multiplexed PTs to enable transmission and fully coherent reception of both the US and DS signals using a set of lasers at the OLT, with laserless ONU. For each DS channel, the light from a laser source is split between a modulated signal and an unmodulated PT. Both are polarization multiplexed before transmission through the network and again polarization demultiplexed at the receiver by a PBS. There, the PT is filtered with a high Q Band Pass Filter (BPF) and used at the CoRX to detect the signal, avoiding the need for an external, free-running LO. Also, this signal is used as the carrier for the US signal. The proposed SHD-PON scheme requires a single laser per TWDM wavelength at the OLT for generation and homodyne detection of US and DS data. It should be noted that unlike intradyne detection schemes, SHD requires narrow filtering at the ONU, in order to isolate the PT for the intended WDM channel. Furthermore, to meet the power budget required for NG-PON2 whilst maintaining enough PT power for coherent reception, it is necessary to amplify the PT at the ONU, as shown in Fig. 3.14. When considering these additional component costs, one should take into account that tunable filtering is already required for TWDM-PONs [25]. Also, the PT is a constant amplitude signal and may be amplified using low-complexity Semiconductor Optical Amplifiers (SOAs) with negligible performance impact. We note that the sensitivity of DS signals is affected by Amplified Spontaneous Emission (ASE) noise introduced by amplification of the PT at the receiver, as demonstrated in [26]. Recently, it has been shown that SOAs can achieve significantly lower noise figures

through appropriate optimization [27]. As such, the amplification stages could be performed using a SOA before BPF and IQ modulator. Hence, a cost comparison between the proposed approach and an equivalent intradyne detection-based ONU would arguably weight the cost of a filter and amplifier against that of a laser, which is restricted to demonstrating the novel concepts of SHD-PONs. Another relevant issue is that the proposed scheme requires sharing the same wavelength for US and DS and is therefore susceptible to spurious reflections and RBS. To counteract these impairments, we employ Nyquist pulse shaping, to minimize crosstalk between channels, and opposing Digital Frequency Shifting (DFS) in the US and DS directions, both enabled by IQ modulation. With DFS, the baseband signals are shifted to an intermediate frequency, Δf, coherently with the signal clock. The use of SHD enables recovering the baseband signals with conventional clock recovery mechanisms and static frequency multipliers, without intermediate frequency estimation mechanisms. Also, Δf can be chosen such that a small margin is left from the DC frequency, to allow dynamic Stimulated Raman Scattering (SRS) mitigation on other systems sharing the same fiber resource, such as video overlay that we will explain in the next chapter. Also, Δf is used in order to assure maximum bandwidth usage and minimum impact of crosstalk. In such a bidirectional PON system, Spectral Efficiency (SE) is given by [20]:

$$SE_{bidirection} = \frac{DS[b/s]+US[b/s]}{\{DS \bigcup US\}[Hz]} = \frac{10[Gb/s]+10[Gb/s]}{4GHz} = 5[b/s/Hz] \qquad (3.1)$$

3.3.2 Self-Homodyne Experimental Setup

Fig. 3.15 shows the proof-of-concept setup. At the OLT, the Continuous Wave (CW) from a 100 kHz linewidth ECL operating at 1556.55 nm was split to provide a LO for a phase-diverse CoRX and to serve as test signal for the DS/US links. The narrow linewidth laser source was required here as the DSP used in the US receiver was unable to handle signals with high phase noise. The test signal was multiplexed with 83 CW signals from Distributed Feedback lasers (DFBs) within a 50 GHz grid, using an arrayed waveguide grating. Power and polarization of each CW was manually adjusted using Variable Optical Attenuators (VOAs) and Polarization Controllers (PCs).

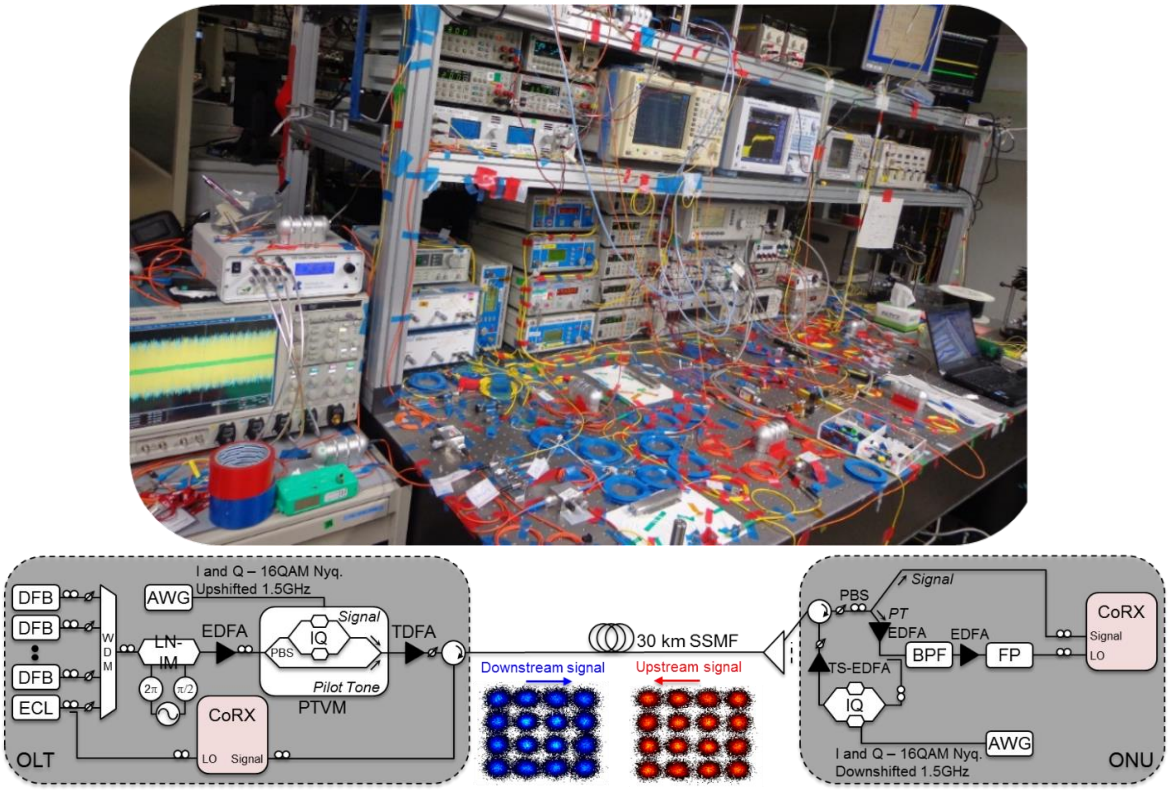

Figure 3.15 Experimental and laboratory infrastructure setup.

The resulting signal was injected in a MZM driven by 4 GHz RF signals to generate 84 frequency combs of 12 CW wavelengths using the technique proposed in [28]. The CWs within each comb had a spacing of 4 GHz and the spacing between adjacent combs was 6 GHz. This yielded a total of 1008 CW wavelengths, which were fed into a Pilot Tone Vector Modulator (PTVM) [29] after amplification and polarization control. In the PTVM, an integrated PBS divided the signal into two polarization components of which one was modulated by an integrated IQ modulator and recombined with the other on orthogonal polarizations. This technique emulated a 1008 UDWDM channel set with polarization-multiplexed PTs, populating a total bandwidth of 33 nm in the C-band. The PTVM was driven by a 10 GS/s AWG, producing a 2.5 Gbaud 16-QAM signal from a $2^{11}-1$ Pseudo-Random Binary Sequence (PRBS) with Nyquist pulse shaping (0.05 roll-off factor) and digital frequency upshift of 1.5 GHz. This combination provided a 250 MHz offset from DC. The full DS/US signal spectrum is shown in Figs. 3.16. As shows in this figure, a sample of the DS signal spectrum, combining both signal polarizations. From this spectrum, one may easily distinguish the signal and PT components on each channel. The launch power was set

by a wide-bandwidth tellurite-EDFA followed by a VOA and a circulator to separate US and DS signals. Transmission was performed on 30 km of SSMF. The PT power was set to be similar to the average signal power. This remained true at the input of the ONU. However, we note that the ratio between signal and PT power can be optimized to improve sensitivity of DS signals [26].

At the ONU, signal and PT components were separated by a PBS with a loss of 3 dB, preceded by manual polarization control. The signal component was sent to a phase-diverse CoRX. For convenience purposes, the PT component was sent through two stages of amplification (two EDFAs with noise figure of 6 dB) and filtering before the CoRX. The first stage consisted of an EDFA followed by a 0.2 nm custom BPF to limit the number of CWs at the input of the second stage. A 3 dB coupler was used to extract a sample of the PT comb for re-modulation prior to the BPF. The second stage consisted of an EDFA followed by a standard 3.5 GHz temperature-controlled high-Q Fabry-Perot (FP) filter with a free-spectral range of 50 GHz and a loss of 10 dB. A polarization controller was used at the FP filter input to adjust the PT polarization, however, it should be noted that, in an integrated receiver this PC would be unnecessary. The PT input power at the CoRX was adjusted to 2 dBm in all cases.

In this experiment, the total loss of the PT path in the ONU exceeded 21 dB, justifying the need for two amplification stages. A substantial simplification of the amplification and filtering stages could be achieved by using commercially available low-loss PBS and non-periodic narrow-BPF, followed by a high-gain SOA, to reach acceptable PT powers.

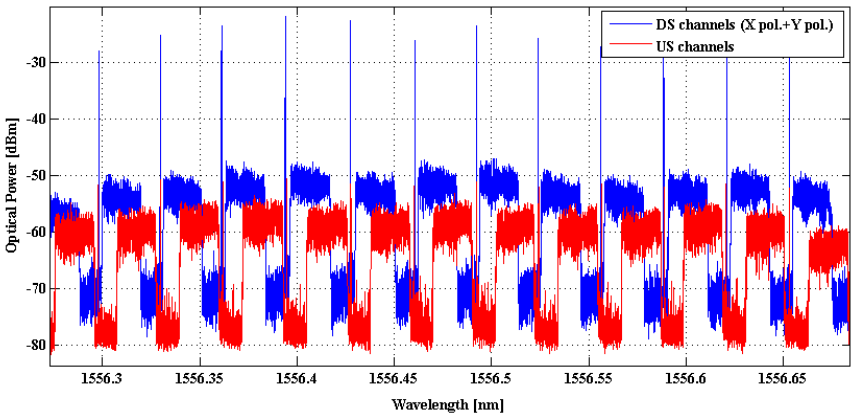

Figure 3.16 US/DS spectra.

However, we recognize that such technology may currently be unfeasible for PONs. Alternatively, redesigning a polarization-insensitive phase-diverse CoRX to handle polarization-multiplexed PT signals could improve the loss budget of the ONU. In this experiment, detection was performed using a single-polarization phase-diverse CoRX followed by a 50 GS/s real-time oscilloscope. DSP was implemented offline using MATLAB and included frequency downshifting and residual carrier phase recovery [30]. Insets of Fig. 3.15 shows a constellation of the received signal for an approximate BER of 10^{-3}. BER estimates were performed by direct error counting in 10 traces of 5×10^4 symbols. We assumed two maximum permissible BER limits of 3.8×10^{-3} for conventional FEC [17] with 7% overhead and 1.5×10^{-2} for soft-decision FEC with 20% overhead [18]. Note that the aforementioned FEC schemes have not been specifically designed for PON systems or burst-mode transmission. However, they remain indicative of the performance achievable with the proposed scheme. The US UDWDM signal was generated by modulating the PT comb at the PBS output with an IQ modulator driven by an independent 10 GS/s AWG. The latter produced a continuous 2.5 Gbaud 16-QAM signal with Nyquist pulse shaping (0.05 roll-off factor) and frequency downshift of 1.5 GHz. Fig. 3.16 also shows a sample of the US signal spectrum. Note the partial spectral overlap with the DS signal resulting from the narrow channel spacing. In BM operation, the AWG produced 820 ns frequency upshifted 16-QAM packets with a payload rate of 2.5 Gbaud and network load of 50%. Fig. 3.17 shows a sample trace of the US signal.

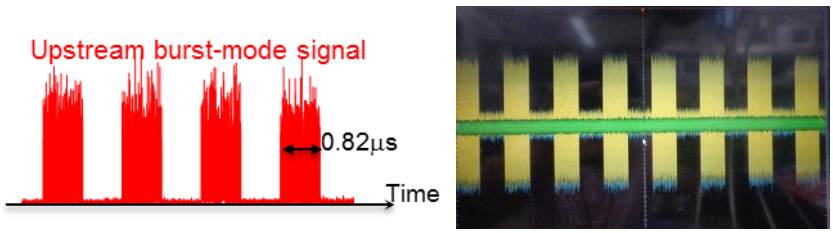

Figure 3.17 Trace of the US burst-mode signal.

A transient-suppressing EDFA [31] was used to compensate for the losses of the IQ modulator, which exceeded 15 dB. We note that in a real scenario, the PT extraction would be performed after the narrow BPF, with a single CW. As such, the amplification could be performed using an SOA placed before the IQ modulator and operating continuously or removed altogether, as the required launch power per channel in the fiber is less than −8 dBm. This setup emulates 1008 ONUs simultaneously transmitting US data, which may

be considered a worst-case scenario for fiber nonlinearities, particularly when using TDMA access schemes. Detection of the US signal at the OLT was performed using a single-polarization phase-diverse CoRX followed by a 50 GS/s real-time oscilloscope. The same DSP and BER estimation used by the ONU was implemented at the OLT. However, it was necessary to include frequency upshifting and QPSK partitioning CPR to compensate for phase noise incoherence between the signal and the LO. For BM operation, it was also necessary to implement burst detection based on power threshold. Fig. 3.16 shows a constellation of the received signal.

3.3.3 Experimental Results

Firstly, we evaluated the impact of fiber nonlinearities in the US and DS UDWDM channels separately (i.e., they do not coexist in the fiber) and compared with single channel signal. Fig. 3.18 presents the corresponding BERs of DS signals as a function of launch power per each DS channel.

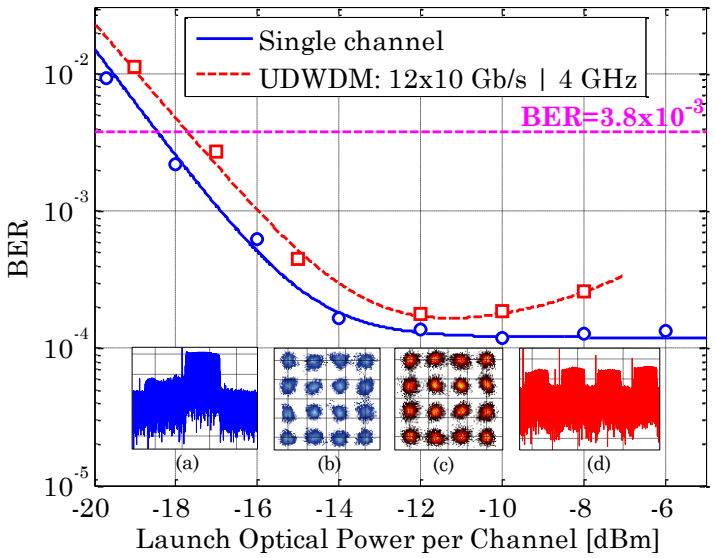

Figure 3.18 Dependence of the BER on the launch power per channel for DS signals in 30 km fiber. Insets: (a) single channel spectrum, (b) single channel constellation, (c) UDWDM channels constellation, (d) UDWDM channels spectrum. All results of insets were obtained after CoRX and with -8 dBm power in the input of fiber.

Due to nonlinear crosstalk, which affects multi-wavelength systems such as UDWDM, when the launch power increases, the DS signal performance starts to degrade relative to the single channel case, as can be seen by the aforementioned BER measurement. A launch power of

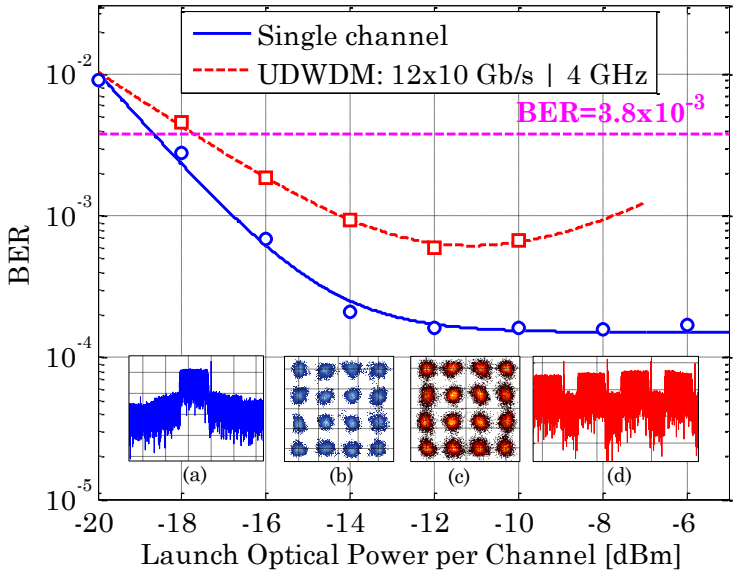

Figure 3.19 Dependence of the BER on the launch power per channel for US signals in 30 km fiber. Insets: (a) single channel spectrum, (b) single channel constellation, (c) UDWDM channels constellation, (d) UDWDM channels spectrum. All results of insets were obtained after CoRX and with -10 dBm power in the input of fiber.

-8 dBm is the best compromise between signal quality and ODN loss as we are using SHD in DS direction. If power decreases, the signal was disrupted because of low signal to noise ratio at the receiver. Then, we evaluated the US signal in the same situation with DS signals, as shown in Fig. 3.19. Inspection of that figure reveals that a launch power of -10 dBm (per channel) in the US minimizes the nonlinear crosstalk. However, the DS signal has significantly better performance than the US signal, as a result of the nonlinear resilience of SHD. Setting the launch power of -8 dBm and -10 dBm for DS and US, respectively, we observed that the impact of back reflection is minimized as can be seen in the spectrum of inset (d) in Fig. 3.18 and 3.19. Insets of Fig. 3.18 and 3.19 also show the constellations and spectrums of single and UDWDM signals in bidirectional operation.

To investigate the impact of RBS and crosstalk resulting from spectrum overlap of the DS and US signals, Fig. 3.20 and Fig. 3.21 show the corresponding BERs as a function of the US and DS launch power per channel, respectively, with 12 channels. As expected, we observe steady performance degradation in both directions, when the launch power of the opposite direction is increased. Nevertheless, the higher DS signal BER indicates additional degradation due to the superposition of the PT with the residual carrier of the US signal. We then considered the impact of fiber nonlinearities by measuring the dependency of the DS

and US signal BERs on the launched power/Ch in the same direction, observing optimum launch powers of −10 dBm for US and −8 dBm for DS.

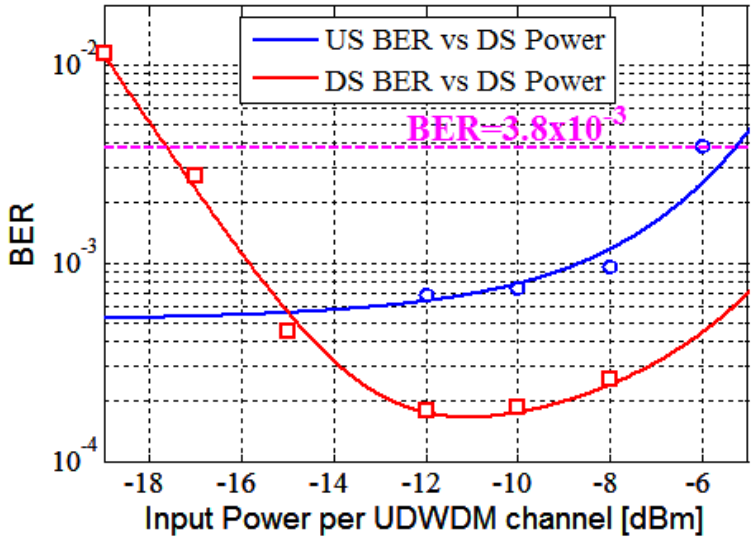

Figure 3.20 Dependence of the BER on the launch power per channel for the DS signals.

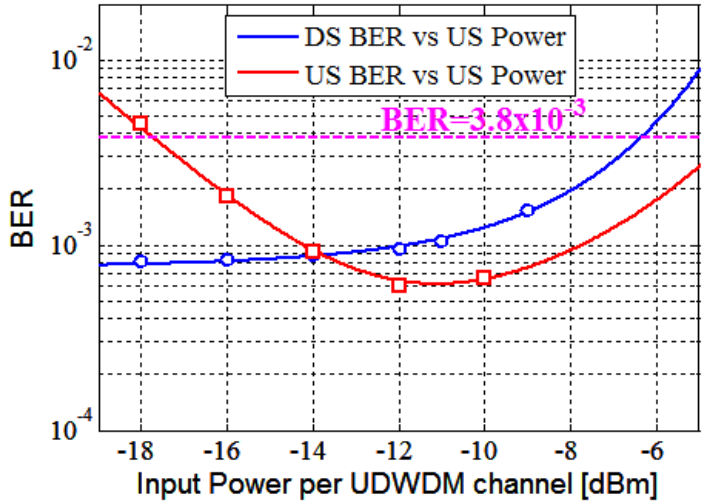

Figure 3.21 Dependence of the BER on the launch power per channel for the US signals.

In addition, Fig. 3.22 and Fig. 3.23 present the measured BERs as a function of the receiver input power per channel for both bidirectional single and 12 channels (center channel) cases in DS and US directions, respectively. It is shown that UDWDM induces a penalty around 2 dB for a FEC compatible BER of 3.8×10^{-3}, with respect to the single channel case. Sensitivity of -35 dBm and -34 dBm were achieved with 12 channels for DS and US signals, respectively, allowing a total ODN loss of 24 dB.

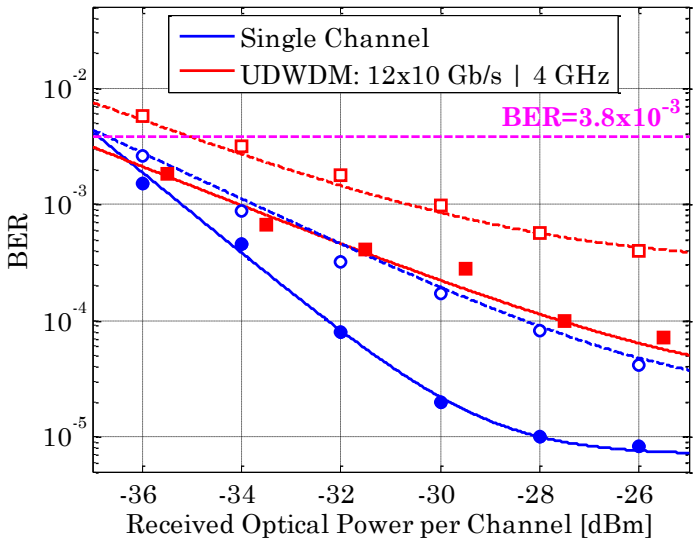

Figure 3.22 Sensitivity of DS signals. Solid lines + filled markers: BTB. Dashed lines + open markers: 30 km of SSMF.

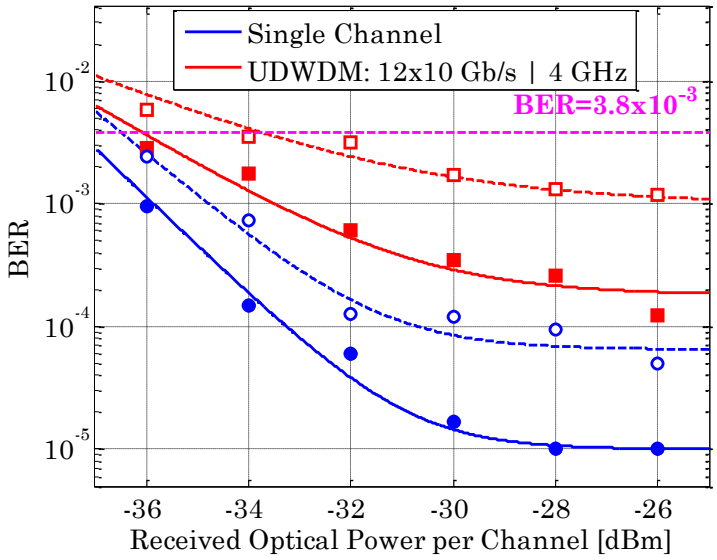

Figure 3.23 Sensitivity of US signals. Solid lines + filled markers: BTB. Dashed lines + open markers: 30 km of SSMF.

Figs. 3.24 and 3.25 show the measured BER as a function of the received signal power per channel for both the single and the 1008 channel cases in DS and US directions, respectively. In the DS direction, the amplification stages maintained the PT at a constant power at the CoRX input. The received signal power was modified by varying the transmitted power per channel. As such, the evolution of the performance includes the limitations of the receiver as well as the impact of fiber nonlinearities. For all cases, we considered only the performance of the test channel wavelength. Sensitivities of -33.5 dBm and -34 dBm were

achieved with 1008 channels for DS and US, respectively. Fig. 3.25 also shows the equivalent performance evaluation considering BM operation. We observed a 3 dB penalty with respect to continuous transmission sensitivity, mainly due to power transients in the ONU transmitter electronics.

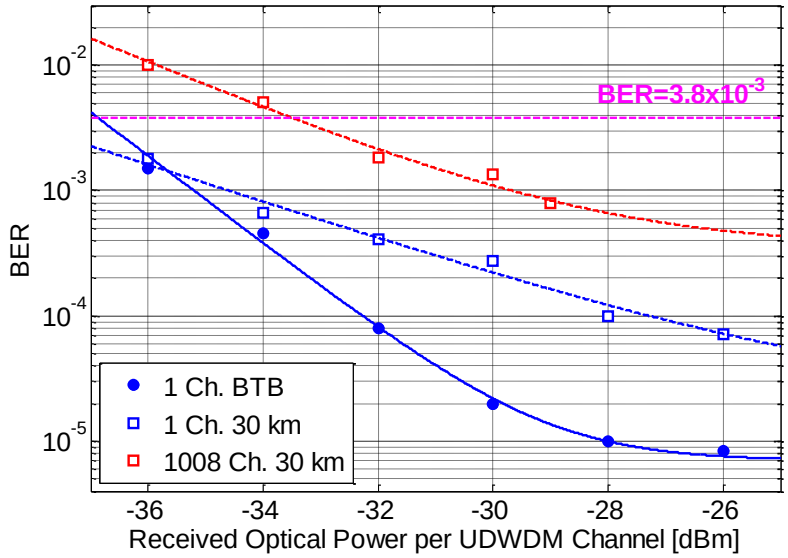

Figure 3.24 Sensitivity of the DS signals for single channel in back-to-back, and transmission and 1008 channels with transmission.

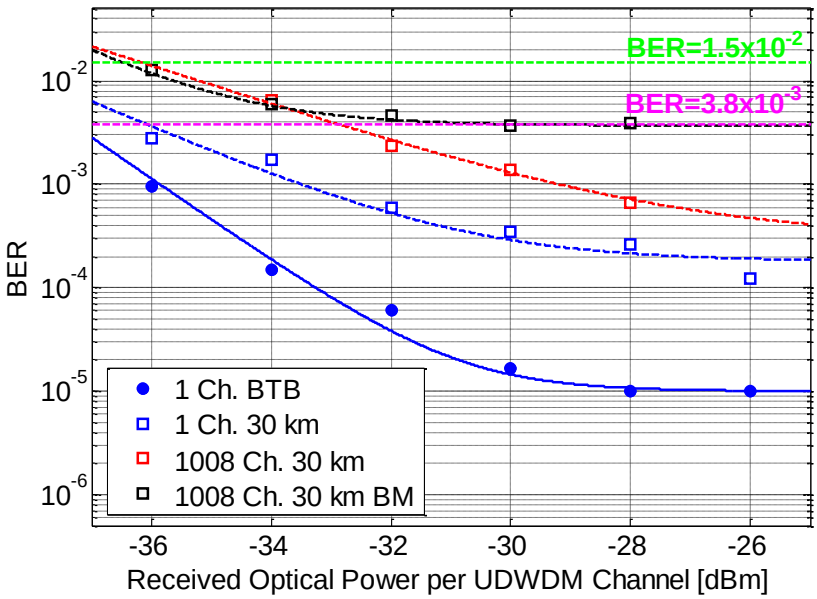

Figure 3.25 Sensitivity of the US signals for single channel in back-to-back and transmission as well as 1008 channels in continuous and BM transmission.

Finally, Fig. 3.26 depicts 4 consecutive BER measurements of 13 randomly selected continuous channels in the US and DS links with 1008 channels. With average receiver input

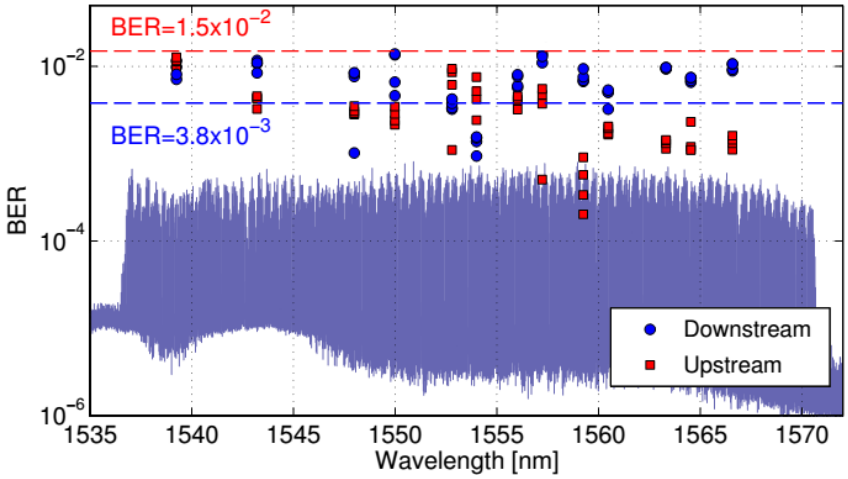

Figure 3.26 BER measurements of 13 random channels of the 1008 US and DS channels.

powers between −33 dBm and −36 dBm, we have achieved BER values below the FEC limit of 1.5×10^{-2} in both directions. Performance variations between channels result from the wavelength dependence of the amplifier noise, as shown by the spectrum shown in Fig. 3.26, as well as the response of the PTVM and other components in the experimental setup, which were originally tuned for the test channel wavelength. The presented results prove the concept of the proposed PON architecture. However, it is necessary to note the main limitations of our scheme. We achieved an ODN power budget of 24 dB emulating a 1008 users PON. The limited power budget results from excessive loss at the ONU receiver, including the need to filter and amplify the PT. Furthermore, the polarization of the US signal, which was left to vary arbitrarily in this work, can be optimized to reduce the impact of interference with the DS signal. The performance in the US direction was also affected by the need to amplify the PT comb signal at the ONU prior to transmission, thus introducing additional ASE noise in the signal. We can assume that in a real system, where a single PT is re-modulated, this limitation is significantly reduced. In addition, the impact of fiber nonlinearities in the US and DS signals may have been enhanced as a result of bit-pattern alignment, by having all 1008 channels synchronized [32]. Finally, we consider that the two main limitations of the proposed PON architecture are the need to align the DS signal polarization with the PBS at the ONU receiver and the need to filter and amplify the PT at the ONU receiver. These limitations may restrict the feasibility of the proposed architecture, unless the need for a large number of users and homodyne detection in both US and DS justifies the added costs.

3.4 Concluding Remarks

In the first part of this chapter, we experimentally and numerically investigated the transmission capabilities of coherent UDWDM-PON scenarios employing Nyquist shaped 16QAM modulated channels. We showed, by means of simulations, that Nyquist shaped UDWDM implemented with coherent detection enhances the ability of the receiver to mitigate crosstalk, arising from back-reflections and/or inter-channel FWM. Operating at either 5 Gb/s (16 × 5 Gb/s at 2.5 GHz channel spacing or 14 × 5 Gb/s at 3.125 GHz channel spacing) or 10 Gb/s per channel (12 × 10 Gb/s at 5 GHz channel spacing), bidirectional transmission over 40 km of SSMF has been successfully demonstrated via EVM and BER measurements. By exploiting 16 channel groups spanning over only 12.8 nm in the 100 GHz frequency grid, the network capacity has been increased to 1.28 Tb/s (5 Gb/s per user) and 1.92 Tb/s (10 Gb/s per user).

In the second part of this chapter, we have shown the proof-of-concept for a fully loaded coherent PON with 24 dB ODN budget, where a single wavelength per user generated at the OLT was sufficient for coherent homodyne detection and generation of US and DS data. This was achieved using self-coherent detection in the US direction and self-homodyne detection in the DS direction, with the latter based on polarization multiplexing a constant pilot tone with the DS signal. Coherent homodyne detection in both directions enabled the following technologies: (i) Nyquist-shaped 16-QAM signals at 2.5 Gbaud; (ii) UDWDM with channel spacing as low as 4 GHz, to reach 1008 channels over a 33 nm bandwidth; (iii) digital frequency up- and downshifting to minimize the impact of back-reflections. Burst mode operation in the US direction has also been shown, albeit with a penalty of 3 dB with respect to continuous transmission. It is shown that the main limitations of the proposed concept are: (i) the need to filter and amplify the pilot tone at the ONU receiver; and (ii) the need to align the polarization of the DS signal to separate the PT and the signal components.

References

[1] N. Cvijetic, "OFDM for next-generation optical access networks," *J. Lightwave Technol.*, vol. 30, no. 4, pp. 384-398, February 2012.

[2] S. Smolorz1, H. Rohde1, E. Gottwald, D. Smith, A. Poustie, "Demonstration of a Coherent UDWDM PON with Real-Time Processing," Proc. *Optical Fiber Communication Conf. (OFC)*, Los Angeles, CA, March 2011, paper PDPD4.

[3] E. Wong, "Next-generation broadband access networks and technologies, " *J. Lightwave Technol.*, vol. 30, no. 4, pp. 597-608, February 2012.

[4] N. Cvijetic, M.-F. Huang, E. Ip, Y. Shao, Y.-K. Huang, M. Cvijetic, and Ting Wang, "1.92Tb/s coherent DWDM-OFDMA-PON with no high-speed ONU-side electronics over 100 km SSMF and 1:64 passive split," *Opt. Exp.*, vol. 19, no. 24, pp. 24540-24545, November 2011.

[5] H. Rohde, S. Smolorz, S. Wey, E. Gottwald "Coherent optical access networks," Proc. *Optical Fiber Communication Conf. (OFC)*, Los Angeles, CA, March 2011, paper OTuB1.

[6] S. J. Savory, "Digital Coherent Optical Receivers: Algorithms and Subsystems," IEEE JSTQE vol. 16 no. 5, pp. 1164-1179, September 2010.

[7] R. Schmogrow, M. Winter, M. Meyer, D. Hillerkuss, S. Wolf, B. Baeuerle, A. Ludwig, B. Nebendahl, S. Ben-Ezra, J. Meyer, M. Dreschmann, M. Huebner, J. Becker, C. Koos, W. Freude, J. Leuthold., "Real-time Nyquist pulse generation beyond 100 Gbit/s and its relation to OFDM," *Opt. Exp.*, vol. 20, no. 1, pp. 317-337, December 2011.

[8] R. Schmogrow, D. Hillerkuss, S. Wolf, B. Bäuerle, M. Winter, P. Kleinow, B. Nebendahl, T. Dippon, P. C. Schindler, C. Koos, W. Freude, and J. Leuthold, "512QAM Nyquist sinc-pulse transmission at 54 Gbit/s in an optical bandwidth of 3 GHz," *Opt. Exp.*, vol. 20, no. 6, pp. 6439-6447, March 2012.

[9] B. Châtelain, Ch. Laperle, K.Roberts, M. Chagnon, X. Xu, A. Borowiec, F. Gagnon, and D.V. Plant, "A family of Nyquist pulses for coherent optical communications," *Opt. Exp.*, vol. 20, no. 8, pp. 8397-8416, March 2012.

[10] A. Tanaka, N. Cvijetic, and T. Wang, "First optical Nyquist filtering of 10G OOK for OFDMA λ-overlays on 40 km and 1:128 split PON," Proc. *Proc. OptoElectron. Commun. Conf. (OECC)*, Kyoto, Japan, July 2013, paper PD3-1.

[11] D. Lavery, M. Paskov and S. J. Savory, "Spectral shaping for mitigating backreflections in a bidirectional 10 Gbit/s coherent WDM-PON," Proc. *Optical Fiber Communication Conf. (OFC)*, Anaheim, CA, March 2013, paper OM2A6.

[12] J. D. Reis, D. M. Neves, and A. L. Teixeira, "Weighting nonlinearities on future high aggregate data rate PONs," *Opt. Exp.*, vol. 19, no. 27, pp. 26557-26567, December 2011.

[13] J. D. Reis, D. M. Neves, and A. L. Teixeira, "Analysis of nonlinearities on coherent ultra-dense WDM-PONs using Volterra series," *J. Lightw. Technol*., vol. 30, no. 2, pp. 234-241, January 2012.

[14] F. Forghieri, R.W. Tkach, A.R. Chraplyvy, D. Marcuse, "Reduction of four-wave mixing crosstalk in WDM systems using unequally spaced channels," *IEEE Photon. Technol. Lett.*,vol. 6, no. 6, pp. 754-756, June 1994.

[15] J. D. Reis, B. Neto, P. S. André, A. Teixeira., "WDM ring performance improvement by means of a nonlinear effects crosstalk minimization algorithm," Proc. *Optical Fiber Communication Conf. (OFC)*, San Diego, CA, USA, March 2009, paper JThA77.

[16] R. A. Shafik, M. S. Rahman, and A. R. Islam, "On the extended relationships among EVM, BER and SNR as performance metrics," Proc. *Int. Conf. Electr. Comput. Eng*., December 2006, pp. 408-411.

[17] Forward Error Correction for High Bit-Rate DWDM Submarine Systems, *ITU-T Rec. G.975.1*, February 2004.

[18] F. Chang, K. Onohara, and T. Mizuochi, "Forward error correction for 100 G transport networks," *IEEE Commun. Mag.*, vol. 48, no. 3, pp. S48-S55, March 2010.

[19] L. Mehedy, M. Bakaul, A. Nirmalathas, and E. Skafidas, "Scalable and spectrally efficient long-reach optical access networks employing frequency interleaved directly detected optical OFDM," *J. Opt. Commun. Netw.*, vol. 3, no. 11, pp. 881-890, November 2011.

[20] A. Agmon, M. Nazarathy, D. M. Marom, S. Ben-Ezra, A. Tolmachev, R. Killey, P. Bayvel, L. Meder, M. Hübner, W. Meredith, G. Vickers, P. C. Schindler, R. Schmogrow, D. Hillerkuss, W. Freude, C. Koos, and J. Leuthold, "OFDM/WDM PON with laserless, colorless 1 Gb/s ONUs based on Si-PIC and slow IC," *J. Opt. Commun. Netw.*, vol. 6, no. 3, pp. 225-237, March 2014.

[21] C. Kottke, K. Habel, M. Eiselt, H. Griesser and J. P. Elbers, "Coherent subcarrier-WDM-PON system with SSB modulation and wavelength reuse," Proc. *Optical Fiber Communication Conf. (OFC)*, Anaheim-CA, March 2013, paper OM2A3.

[22] J. M. Buset, Z.A. El-Sahn, D.V. Plant, "Experimental demonstration of a 10 Gb/s 16-QAM SCM-WDM-PON with bandwidth limited RSOA and IM/DD transceivers," Proc. *Eur. Conf. Opt. Commun. (ECOC)*, London, September 2013, paper Tu.3.F.5.

[23] H. Rohde, E. Gottwald, A. Teixeira, J. D. Reis, A. Shahpari, K. Pulverer, J. S. Wey, "Coherent ultra-dense WDM technology for next generation optical metro and access networks," *J. Lightwave Technol.*, vol. 32, no. 10, pp. 2041-2052, April 2014.

[24] Z. Dong, H.-C. Chien, Z. Jia, J.Zhang, L. Cheng, k. Chang, "A bandwidth-efficient coherent ultra-dense WDM-PON based on Nyquist independent-sideband modulation," Proc. *Eur. Conf. Opt. Commun. (ECOC)*, Cannes, September 2014, paper Th.2.6.5.

[25] 40-Gigabit-Capable Passive Optical Networks (NG-PON2): General Requirements, ITU-T Rec. G.989.1, November 2013.

[26] M. Sjödin, P. Johannisson, M. Karlsson, Z. Tong and P. Andrekson, "OSNR requirements for self-homodyne coherent systems," *IEEE Photon. Technol. Lett.*, vol. 22, no. 2, pp. 91-93, January 2010.

[27] K. Carney, R. Lennox, R. Maldonado-Basilio, S. Philippe, F. Surre, L. Bradley and P. Landais, "Method to improve the noise figure and saturation power in multi-contact semiconductor optical amplifiers: simulation and experiment," *Opt. Express*, vol. 21, no. 6, pp. 7180-7195, March 2013.

[28] T. Sakamoto, T. Kawanishi, and M. Izutsu, "Optimization of electro optic comb generation using conventional Mach-Zehnder modulator," Proc. I*nternational Topical Meeting on Microwave Photonics*, Victoria, BC, pp. 50-53, October 2007.

[29] T. Miyazaki, and F. Kubota, "PSK self-homodyne detection using a pilot carrier for multibit/symbol transmission with inverse-RZ signal," *IEEE Photon. Technol. Lett.*, vol. 27, no. 6, pp. 1334-1336, June 2005.

[30] J. M. D. Mendinueta, B. J. Puttnam, J. Sakaguchi, R. S. Luís, W. Klaus, Y. Awaji, N. Wada, A. Kanno and T.Kawanishi, "Investigation of receiver DSP carrier phase estimation rate for self-homodyne space-division multiplexing communication systems," Proc. *Optical Fiber Communication Conf. (OFC)*, Anaheim, CA, March 2013, paper JTh2A.48.

[31] Y. Awaji, H. Furukawa, N. Wada, E. Kong, P. Chan, and R. Man, "Burst-mode EDFA based on a mid-position gain flattening filter with an over pumping configuration for variable traffic conditions in a WDM environment," *Opt. Quantum Electron.*, vol. 40, no. 5-6, pp. 461-466, April 2008.

[32] L. Wickham, R. Essiambre, A. H. Gnauck, P. J. Winzer, and A. R. Chraplyvy, "Bit pattern length dependence of intrachannel nonlinearities in pseudolinear transmission," *IEEE Photon. Technol. Lett.*, vol. 16, no. 6, pp. 1591-1593, June 2004.

CHAPTER 4 CROSSTALK IN MULTI-SYSTEM NEXT GENERATION OPTICAL ACCESS NETWORKS

Summary

In the present Passive Optical Networks (PONs), bandwidth is like a high value real state. Service providers would like to make it available, as much as possible, to their users, since new services and technologies are arriving to the market. Therefore, the efficiency improvement of network resources in PONs when several technologies coexist in the same feeder fiber is the main issue which should be tackled. One of the challenges of UDWDM systems is the coexistence with deployed PON technologies and video overlay. To save optical spectrum, it is relevant to minimize the optical power of each system as well as the guard band between coexisted systems. This chapter considers several crosstalk impairments such as cross-phase modulation and stimulated Raman scattering in heterogeneous access scenarios. Numeric simulations of system limitation caused by fiber nonlinearities, as well as experimental results of UDWDM transmission in the presence of legacy systems are presented.

4.1 Introduction

Open Access is a vital requirement for today's Passive Optical Networks (PONs) that can allow multiple service providers to use the same fiber optic to the customers. Recently, several PON technologies such as Gigabit-capable PON (GPON), Wavelength-Division Multiplexing PON (WDM-PON), Time-Wavelength-Division Multiplexing PON (TWDM-PON) under the umbrella of the FSAN group have been considered [1, 2]. Coherent Ultra-Dense WDM (UDWDM) PONs, either based on Quadrature Phase-Shift Keying (QPSK) [3] or Nyquist pulse shaped 16-Quadrature Amplitude Modulation (16QAM) [4], have been demonstrated as promising candidates of Next-Generation Optical Access Networks (NG-OAN) deployments. The goal of each of these technologies is to reduce the complexity of delivering required high but flexible bandwidth demands. One of the challenges on NG-OAN solutions refers to the coexistence with already deployed PON technologies. To save the already populated wavelength spectrum, it is relevant to minimize the guard band to legacy technologies [5]. On the other hand, reducing the guard band comes at a price of higher interference between different technologies sharing the same Optical Distribution Network (ODN). This interference is mostly induced by fiber nonlinearities such as Four-Wave Mixing (FWM) and Cross-Phase Modulation (XPM) that limit the network's performance as the launched power increases [6-8]. Therefore, it is of great significance to optimize both launch power and guard band.

Video overlay (analogue or digital in Fig. 4.1), being one of the oldest technologies available in access networks, broadcasts a portion of the radio frequency spectrum (54 MHz to 1 GHz) at C-band (1550-1560 nm) to each customer. Consequently, transmitting video overlay with current PON technologies offers several benefits to operators and current PON customers at a reduced incremental cost. However, in fiber optic RF transmission links, the nonlinear Raman crosstalk introduced by other baseband modulated signals disturbs the lower frequencies of the RF-video signal due to Stimulated Raman Scattering (SRS) [9-11]. The dynamic SRS crosstalk from baseband signal to the RF video signal strongly depends on the Power Spectral Density (PSD) of the baseband signal [12, 13]. Several techniques have been proposed and demonstrated to cope with Raman crosstalk based on suppressing the lower frequency (below 200 MHz) contents of the baseband spectrum. For example, in [14],

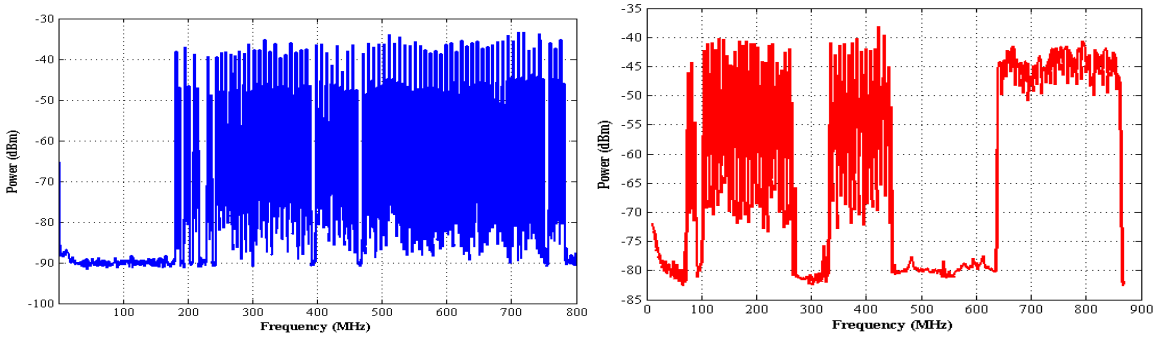

(a) (b)

Figure 4.1 RF- video signals: (a) analogue, (b) digital.

spectral shaping of the digital signal bit-stream with coding is proposed. Moreover, Miller code [15] and physical-layer RF filtering [12, 16] are used to suppress the signal spectrum. In addition, owing to the constant optical intensity of the signals in phase modulation formats such as QPSK the crosstalk reduction may be achieved [13, 17]. However, for UDWDM systems with pulse shaping, this reduction can be achieved by frequency shifting of the signal from the DC component. In the other side, video signal envisages high optical powers, around 16.5 dBm [2], in the feeder fiber that can create XPM in UDWDM channels or other technologies. Therefore, it is of great significance to optimize the Raman crosstalk of UDWDM signal on the video and mitigate XPM effects of video signal to not impair the quality of UDWDM wavelengths. The challenge for service providers is to manage these distortions in an efficient way.

In this chapter, we experimentally analyze the required guard band of coherent optical UDWDM networks transporting 16x1.25 Gb/s-QPSK at 3.125 GHz frequency grid to coexist with RF-video and 10G- Non-Return to Zero (NRZ) transmissions. Also, the coexistence of Nyquist pulse shaped UDWDM transporting 12x10 Gb/s-16QAM at 6.25 GHz frequency grid RF-video are experimentally investigated. Moreover, we present a simple tool (based on measurements) for estimating the carrier-to-Raman-crosstalk ratio of RF-video to easy optimize the launch power limits for arbitrary NG-OAN signals. We validate the model for single, multi-wavelength, multi-format prediction of the SRS crosstalk based on PSD of digital baseband signal. Also, we analyze the dynamic SRS of each system on video overlay and calculate the Carrier-to-Noise Ratio (CNR) of analogue and digital video signals. Finally, we compare carrier-to-Raman-crosstalk ratio of digital baseband and shifted Nyquist signals with 2.5 Gb/s and 10 Gb/s NRZ signals.

4.2 Crosstalk in UDWDM-QPSK Co-existence with Legacy Systems (papers J5, C11-C12)

In this section, we experimentally analyze the required guard band of heterogeneous network scenarios comprised by 16x1.25 Gb/s coherent QPSK spaced by 3.125 GHz coexisting either with video overlay or 10 Gb/s-NRZ systems, whose optical powers scale up to nearly 17 dBm.

The experimental setup depicted in Fig. 4.2 (a) is used to study the required guard band between coherent UDWDM-PON network scenario and video or 10 Gb/s NRZ transmission systems. The UDWDM comb is based on [18] and includes an External Cavity Laser (ECL) source (100 kHz linewidth) that is modulated using an IQ Modulator (IQM) fed with two 625 Mb/s-NRZ electrical signals encoding 2^9 Pseudo Random Binary Sequence (PRBS). The resulting optical 1.25 Gb/s-QPSK is injected to a Mach-Zehnder Modulator (MZM) driven by two 3.125 GHz radio frequency signals with phase relation around 3л/2. The QPSK channels, equally spaced by 3.125 GHz, are filtered by a Wave Shaper (WS) tuned to 50 GHz bandwidth. The optical power per channel is set to around -3 dBm using an Erbium Doped Fiber Amplifier (EDFA). The digital video transmitter (Televes) firstly receives the radio frequency signals from satellite transmission with 40 European channels between 104 MHz and 860 MHz. Then, the electrical video signal (encoding 256QAM) modulates a Distributed Feedback (DFB) laser with 10 MHz-linewidth. The 10 Gb/s-NRZ transmitter is based on an Electro-absorption Modulator integrated Laser (EML), which is fed by 2^{23}-1 PRBS. The extinction ratio of the 10G-NRZ channel is set to 10 dB. The optical powers of

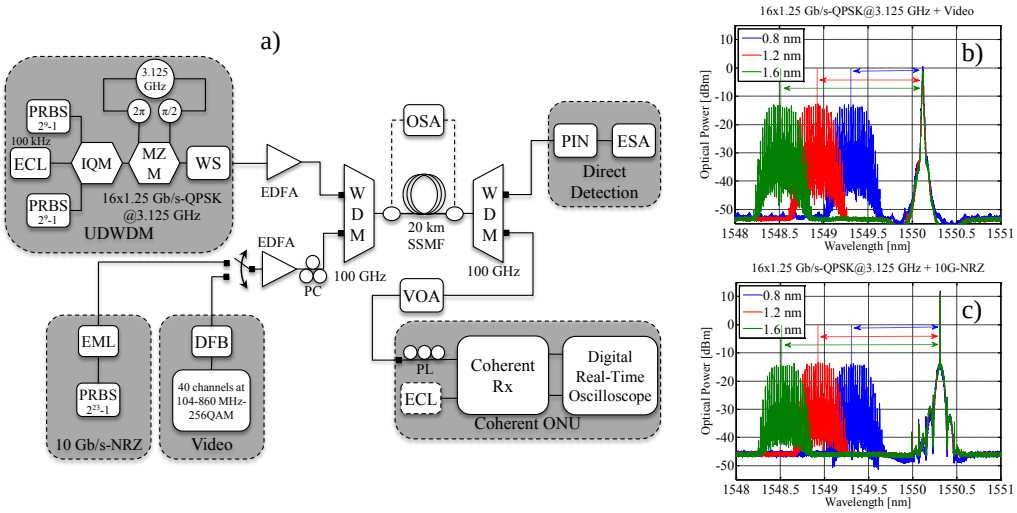

Figure 4.2 (a) Experimental setup of UDWDM coexistent with legacy PON systems. b) Coexistence with digital video. c) Coexistence with 10 G-NRZ.

both video and 10G-NRZ channels are set by an EDFA. The UDWDM comb is multiplexed either with the 10G-NRZ or video channel using a 100 GHz-WDM filter, as depicted in the measured optical spectra in Fig. 4.2 (b) and Fig. 4.2 (c). The total optical signal is transmitted over 20 km of SSMF. After demultiplexing, the 10G-NRZ and video channels reach the direct detection receiver with PIN photodetector plus Electrical Spectrum Analyzer (ESA). The 16x1.25 Gb/s-QPSK channels reach the coherent receiver shown in Fig. 4.2 (a). The received QPSK signals are mixed with the local oscillator (same laser used in the transmitter side) using a 4x90º optical hybrid. The optical signal is converted to the electrical domain using a pair of Balanced Detectors (BD). The resulting electrical signal is converted to a digital form using a 50 GSa/s real-time oscilloscope with analogue bandwidth around 20 GHz. The digital signal is normalized, filtered and down-sampled to 1 sample per symbol. After applying Viterbi and Viterbi algorithm to recover both phase and frequency, the root mean squared Error Vector Magnitude (EVM_{RMS}) is estimated for 512 recovered symbols with respect to the ideal transmitted QPSK symbols. The EVM is averaged over 16 independent measurements to establish 95% confidence interval.

Fig. 4.3 depicts the overall network's performance in terms of the EVM in dB measured in the center QPSK channel. Although the performance of both video and 10G-NRZ channels are not reported in this work, we checked that UDWDM comb does not impose significant interference in the aforementioned technologies if the QPSK power per channel is limited to -3 dBm. The results in Fig. 4.3 (a) and 4.3 (b) show that the EVM performance does not change significantly for input powers (video and 10G-NRZ) ranging from 0 dBm to 10 dBm. Indeed, the EVM is about 1 dB higher than the EVM of the reference homogeneous system comprised by only QPSK channels: -17.3 dB. In this power regime, the performance is mostly limited by FWM among the -3 dBm QPSK channels and an extra XPM penalty induced by the coexisting channel. As the input power increases higher than 10 dBm, the EVM performance rapidly reaches -9.8 dB (SNR≈9.8), represented by the magenta dash line corresponding to the theoretical BER=10^{-3} (Bit Error Ratio), at power around 16 dBm and 15 dBm for the video and 10G-NRZ channels, respectively. In that case, the EVM increases roughly with the square of the input power, i.e. EVM increases by 2 dB every 1 dB increase in the input power as confirmed in [6-8]. This performance degradation is due to inter-channel nonlinearities that induce both amplitude and phase noises in the recovered QPSK symbols.

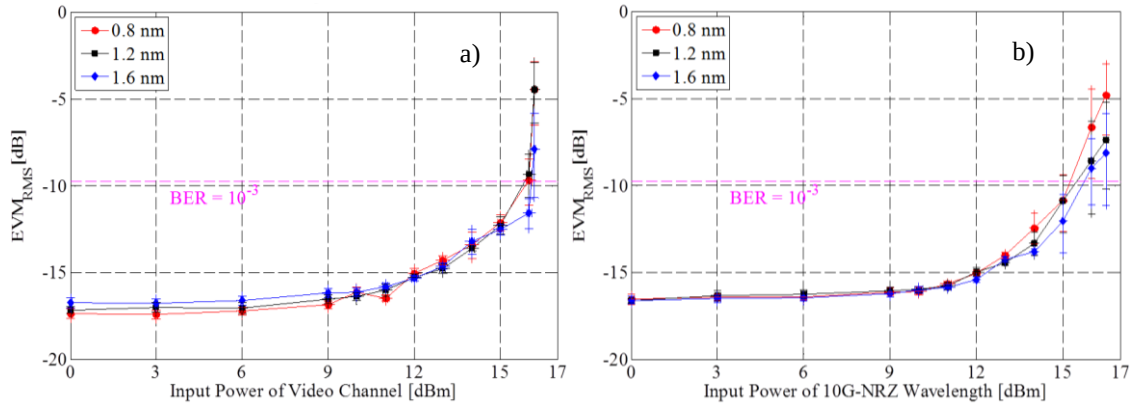

Figure 4.3 EVM in dB (center wavelength) after transmission over 20 km-SSMF versus input power of (a) video channel and (b) 10 G-NRZ channel for different.

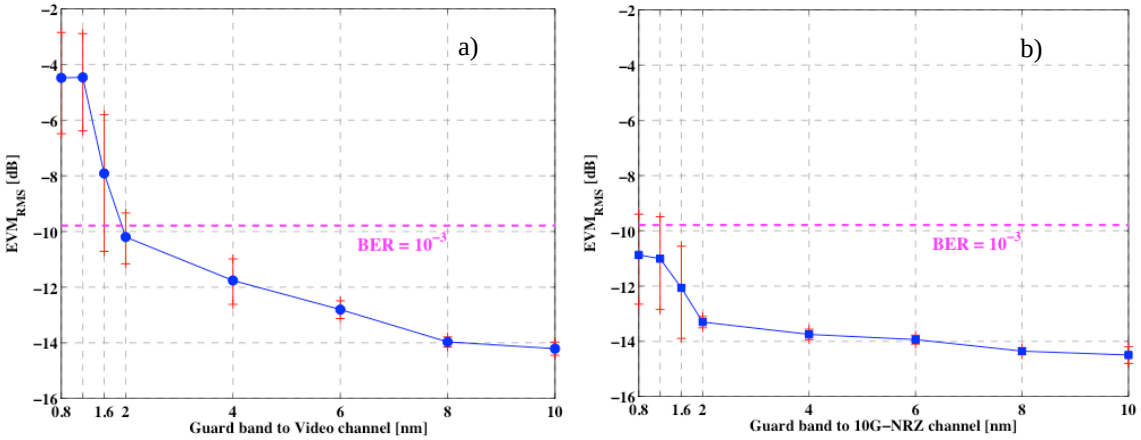

Figure 4.4 EVM (center wavelength) after transmission over 20 km-SSMF versus guard band for (a) video channel at 16.2 dBm and (b) 10 G-NRZ channel at 15 dBm.

The EVM dependence on guard band is only noticeable for input powers higher than 15 dBm. Such a high power is particularly relevant since some PON technologies, as some XG-PON transmitter classes for instance, may operate at power 16.5 dBm [2]. To understand this performance variation with guard band when the power is constant, Fig. 4.4 (a) and Fig. 4.4 (b) show the EVM in dB (center QPSK channel) versus the guard band up to 10 nm for input powers around 16.2 dBm for the video channel and 15 dBm for the 10 G-NRZ channel. In the case of 16.2 dBm video transmission in Fig. 4.4 (a), the performance is maintained below the EVM threshold when the guard band is higher than 4 nm. On the other hand, this guard band can be reduced to only 1.6 nm if 15 dBm 10 G-NRZ is transmitted along with the UDWDM comb as shown in Fig. 4.4 (b). Note that, after 8 nm guard band there is no penalty in EVM measurements for coexisting of UDWDM channels with video and XG-PON systems.

4.3 Crosstalk in Nyquist Pulse Shaped UDWDM-16QAM Co-existence with Video Overlay (paper C15)

In this section, taking advantage of Nyquist pulse shaped UDWDM (6.25 GHz ITU-T grid), we experimentally characterize a coherent bidirectional PON system over up to 20 km and 80 km SSMF. The system performance regarding the back reflection and XPM from analogue RF-video is evaluated. Optimized power per channel in both directions is obtained, and band separation is investigated. Video overlay with 48 users, requiring only 10 nm wavelength separation is successfully demonstrated with minimal penalty.

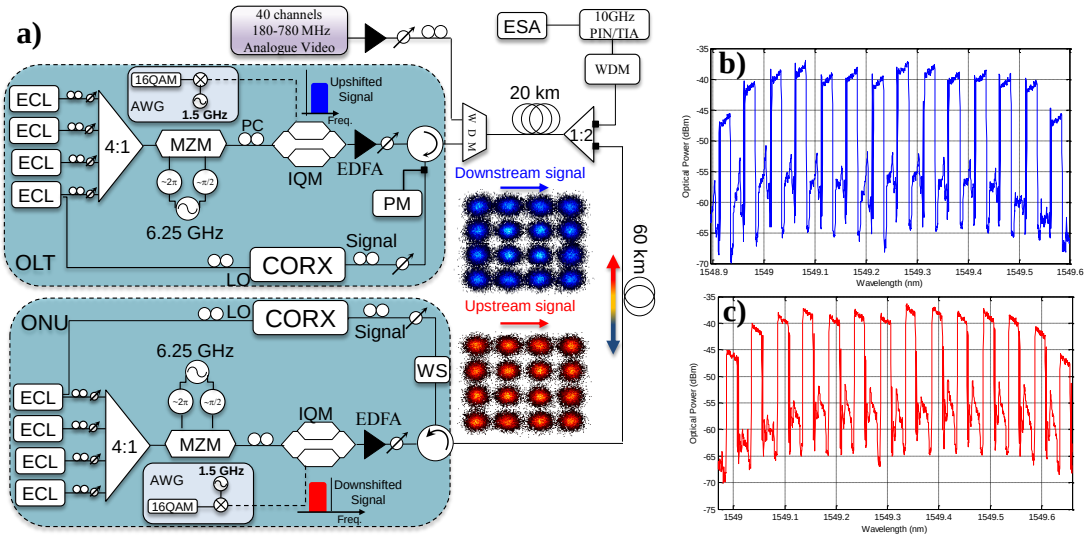

Figure 4.5 (a) Experimental setup for bidirectional transmission with up to 80 km fiber, UDWDM channels with digital frequency shifting, (b) DS and (c) US spectra.

Fig. 4.5 shows the experimental setup used to demonstrate the proposed PON architecture. At the OLT, the light from a 100 kHz linewidth ECL was split to provide a local oscillator (LO) for the receiver and to serve as source for the DS signal. The test signal was multiplexed with 4 dummy signals from ECLs within an 81.25 GHz grid, using a 4:1 coupler. The resulting signal was injected in a MZM driven by 6.25 GHz RF signals to generate 48 (4×12) tones. We note that, we used the optical comb in the proposed system due to unavailability of 48 lasers with the required spectral resolution. The wavelengths were fed into an IQ modulator, driven by a 12 GSa/s Arbitrary Waveform Generator (AWG), producing a 2.5 Gbaud 16QAM signal (2^{14}-1 PRBS) with Nyquist pulse shaping (roll-off factor 0.05). These signals were upshifted by 1.5 GHz, resulting in a 250 MHz offset from the carrier overall spectrum. The launch power for the 48 x 10 Gb/s group was set by an EDFA and a VOA prior to a circulator for bidirectional transmission over 20 km and 80 km fibers.

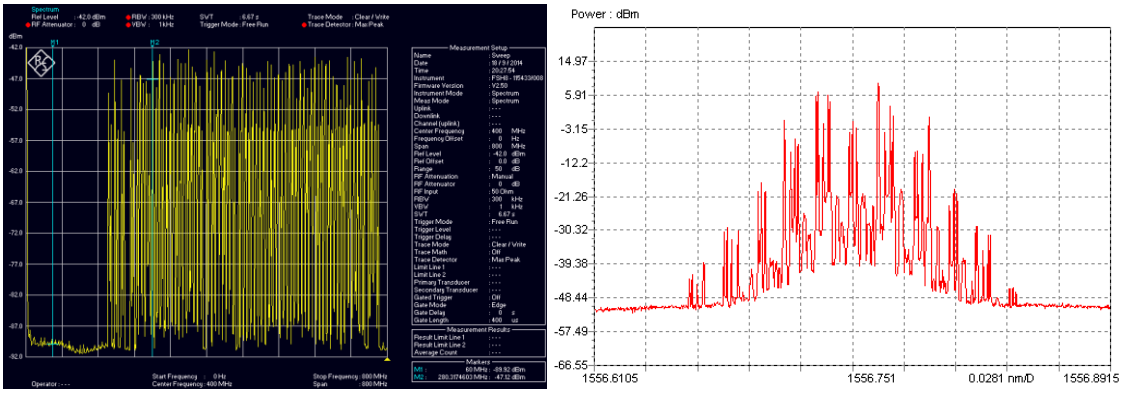

(a) (b)

Figure 4.6 (a) Electrical RF-video channels, (b) optical analogue video signal.

To demonstrate a heterogeneous coexistence scenario, the UDWDM comb was multiplexed with an analog RF-video channel with RF channels from 180 MHz to 780 MHz at 1556 nm via a WDM filter. After 20 km, the video signal was dropped by a coupler and a WDM filter. The signal on RF-video channel is detected directly by a 10 GHz PIN photodetector, and then the electrical signal was measured by an 8 GHz ESA with the Resolution Bandwidth (RBW) of 300 kHz and Video Bandwidth (VBW) of 1 kHz. To test the impact of video on UDWDM channels the 16QAM channels are coherently detected. Detection was performed using a coherent receiver followed by a 50 GSa/s real-time scope. DSP was implemented offline, by using MATLAB, which includes digital band pass filter, frequency downshifting and carrier phase recovery. BER estimates were performed by direct error counting in 10 traces of 4096 symbols. The US signals were generated by modulating the comb signals at the ONU with an IQ modulator driven by another 12 GSa/s AWG. The AWG produced a 2.5 Gbaud 16QAM signal with Nyquist pulse shaping (0.05 roll-off factor) with a frequency downshift of 1.5 GHz. Fig. 4.5 (b) and (c) show the DS and US signal spectra that was obtained by an Optical Spectrum Analyzer (OSA), for both US/DS directions, respectively. Also, the electrical RF-video channels obtained by ESA after PIN photodetector with -3 dBm optical input power is presented in Fig. 4.6. This figure also shows the optical video signal obtained by OSA at the input of fiber.

We started by evaluating the impact of RBS and fiber nonlinearities in the US and DS channels separately (e.g. they do not coexist in the fiber). Fig 4.7 (a) presents the sensitivity @ BER=3.8 x 10^{-3} of DS signals as a function of reflected power for 12 channels in 80 km fiber. At -30 dBm total reflected power measured by optical power meter corresponding to -6 dBm launched power in the fiber, we achieved 0.5 dB sensitivity penalty.

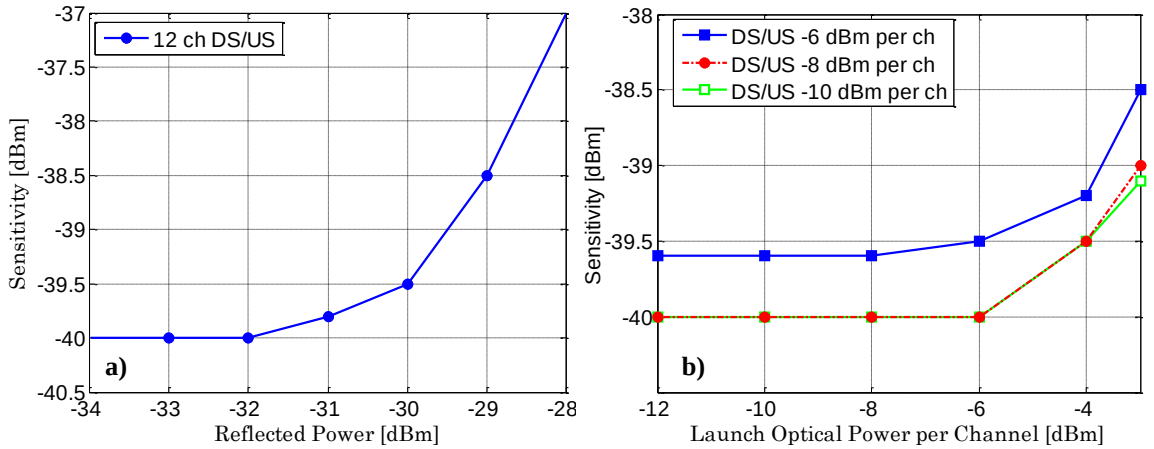

Figure 4.7 (a) Impact of back-reflection on receiver sensitivity @ BER=3.8 x 10^{-3}. (b) Impact of DS/US launch powers on receiver sensitivity.

We note that, all connectors used in this experiment are APC [20]. Then in Fig. 4.7 (b) the launched power of pivot channels in the US/DS was fixed to -6, -8 and -10 dBm and the power of opposite direction DS/US was changed. The optimum power was set to -8 dBm. If strict power budget requirements exist, -6 dBm power can also be used to achieve 33.5 dB power budget.

Then, we analyze the XPM impact of RF-video optical signal on UDWDM channels. Fig. 4.8 depicts the impact of XPM on DS and US channels due to the 16.2 dBm RF-video with respect to wavelength separation between video and central channel of UDWDM. After 10 nm, we did not observe major performance degradation due to XPM impact from video on the 12-48 channels after 20 km of fiber.

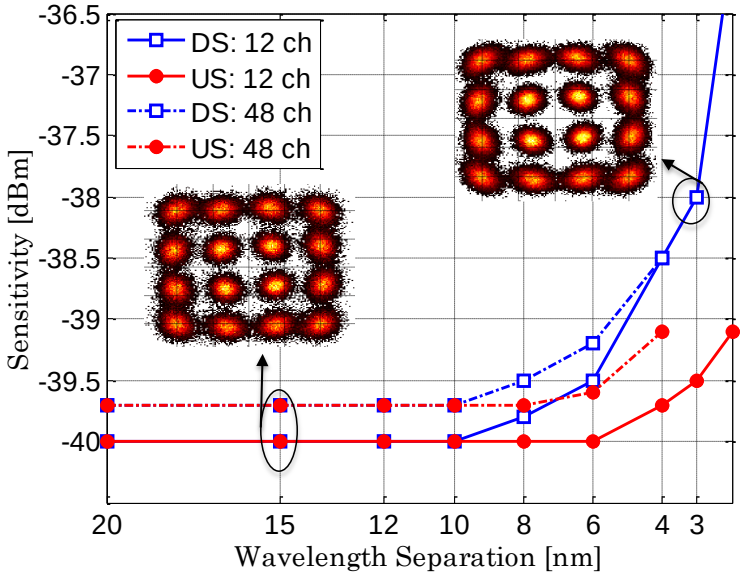

Figure 4.8 Impact of the 16.2 dBm analogue video @ 1556 nm on sensitivity of UDWDM central channel.

4.4 Multi system Next-Generation PONs impact on Video Overlay (papers J3, C13-C15)

As mentioned before, in fiber optic RF transmission links, both the electronics and optics disturb the input signal via various scattering phenomena, such as SRS. The main point of this section is to present a simple model for estimating the launch power limits for multi system NG-PONs signals for an acceptable level of RF. Authors in [9, 10] presented useful methods for measuring SRS in WDM systems using NRZ pulses whereas in [11] it is accounted the SRS effect of 1480 nm signal on a 1550 nm video. On the other hand, neither of the latter works is extended to model SRS caused by advanced digital modulation formats such as QPSK, QAM and OFDM, modulation formats commonly used in coherent multi-wavelength. Herein, we report an extension of SRS calculation from previous studies and experimentally validates it on a multi system next generation PON.

The power of the interfering crosstalk in video signal is related to the PSD of digital modulation signal [11]. The PSDs of NRZ and QPSK modulated signals with direct detection can be given by:

$$PSD(f)=\begin{cases}\dfrac{2}{R_s}R^2\left(\dfrac{\varepsilon-1}{\varepsilon+1}\right)^2\left(\dfrac{\sin(\pi f/R_s)}{\pi f/R_s}\right)^2 & for\ NRZ\\ \dfrac{1}{k^2R_s}\left(\dfrac{\sin(\pi f/kR_s)}{\pi f/kR_s}\right)^4 & for\ QPSK\end{cases} \tag{4.1}$$

where R is the responsivity of the analogue receiver, f is the RF frequency, Rs is the symbol rate and ε is the extinction ratio of NRZ baseband signal. Approximating the intensity variations of a QPSK signal under direct detection by a triangle pulse with 2/kT width and

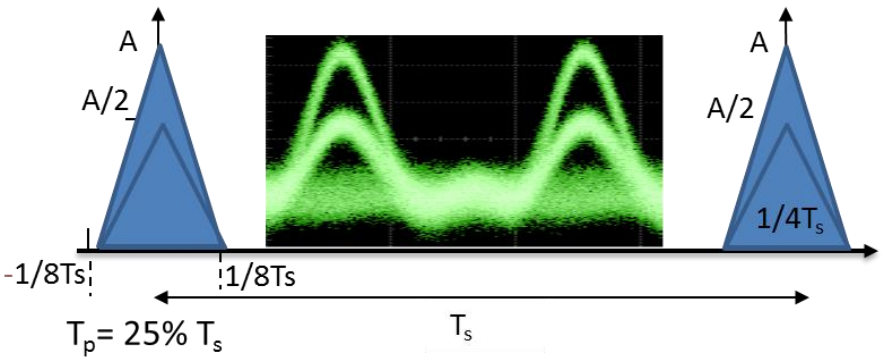

Figure 4.9 Intensity eye diagram of QPSK signal.

1 and 1/2 amplitude for π/2 and π phase conditions (Fig. 4.9), the PSD of QPSK (obtained by direct detection) could be represented by (4.1). In this case, *k* depends on the rise time of analogue receiver that, for the one in use in our experimental setup was calculated to be 8. As shown in Fig. 4.11 (a), the theoretical prediction of the PSD of QPSK only fits the first 200 MHz due to the fact that, after this point, statistics matters in the determination of the exact shape. The PSD of higher order modulation formats such as 16-QAM and OFDM are even more complex to model and therefore they can be used in our formulation by measuring with an ESA for both SRS and PSD evaluations. The relative intensity noise induced by crosstalk (RIN_{XT}) for multichannel hybrid WDM systems on video signals can be derived and expressed as a function of PSD and optical power per channel as:

$$RIN_{XT} = 10\log_{10}\left[\sum_{j=1}^{n}\left(PSD_j(f)\left(\frac{\rho_{SRS}P_{CH_j}}{A_{eff}}\right)^2 \cdot \frac{G_j\left(1-2e^{-\alpha L}\cos\left(2\pi d_j L f\right)+2e^{-\alpha L}\right)}{\alpha^2+\left(2\pi d_j L f\right)^2}\right)\right] \qquad (4.2)$$

where G_j and d_j are the Raman gain coefficient and the group velocity mismatch between the *j-th* WDM channel and video signal, respectively. A_{eff} is the effective area of fiber, ρ_{SRS} is the effective polarization overlap factor and P_{CHj} is the optical power per channel of the digital signal, α is the attenuation coefficient of the fiber and L is the fiber length. The CNR at the receiver is given by [11]:

$$CNR_{dB} = 10\log_{10}\left[\frac{\frac{1}{2}m^2(RP_{in})^2}{B_e\left[i_{th}^2+2qRP_{in}+(RIN+RIN_{XT})(RP_{in})^2\right]}\right] \qquad (4.3)$$

where R is the responsivity of the p-i-n diode, m the modulation index, B_e the bandwidth of video channel, i_{th} the thermal noise of receiver, P_{in} the power at the receiver. *RIN* is a typical Relative Intensity Noise at the receiver, which includes EDFA noise figure and RIN_{XT} is the induced crosstalk (dB/Hz) given by (4.2). Theoretical values of these parameters are shown in Table 4.1.

The experimental setup depicted in Fig. 4.10 is used to study the crosstalk between several digital signals and one video system. Firstly, a bank of 16 lasers ECL and DFB is multiplexed using a 100 GHz arrayed waveguide grating, that are modulated using an IQM driven by R_S= 625 Mbaud for 1.25 Gb/s QPSK from a 12 GSa/s AWG. The resulting optical

Table 4.1 Fiber parameters.

Symbol	Quantity	Value
α	Fiber loss	0.22 dB/km
A_{eff}	Mode effective area	80 μm²
D	Dispersion coefficient	16.5 ps/nm/km
n	Nonlinear refractive index	2.6×10^{-20} m²/W
G_i	SRS gain slope (triangle approximation)	5×10^{-15} m/W/THz
R	P-I-N diode Responsivity	0.88 A/W
m	Modulation index:	
	Analogue video	3.5 %
	Digital video	2.4 %
B_e	CATV channel bandwidth:	
	Analogue video	4 MHz
	Digital video	6 MHz
i_{th}	Thermal noise of receiver	6.5 pA/sqrt(Hz)
RIN	Typical Relative Intensity Noise at Rx includes EDFA	-153 dB/Hz
q	Electron charge	1.602×10^{-19}
ρ_{SRS}	Polarization overlap factor	~1

signal from the IQM is injected to a MZM driven by two radio frequency signals (phase relation ≈ 3π/2) with Δf = 3.125 GHz. The multi-channel system (UDWDM), is filtered by a wave shaper tuned to a 60 GHz bandwidth. The optical power per channel is varied using an EDFA. The video transmitter (digital video) at 1550 nm is set to 8 dBm by an EDFA. The 2.5 Gb/s and 10 Gb/s-NRZ transmitter is based on a MZM, which is fed with 2^{23}-1 PRBS.

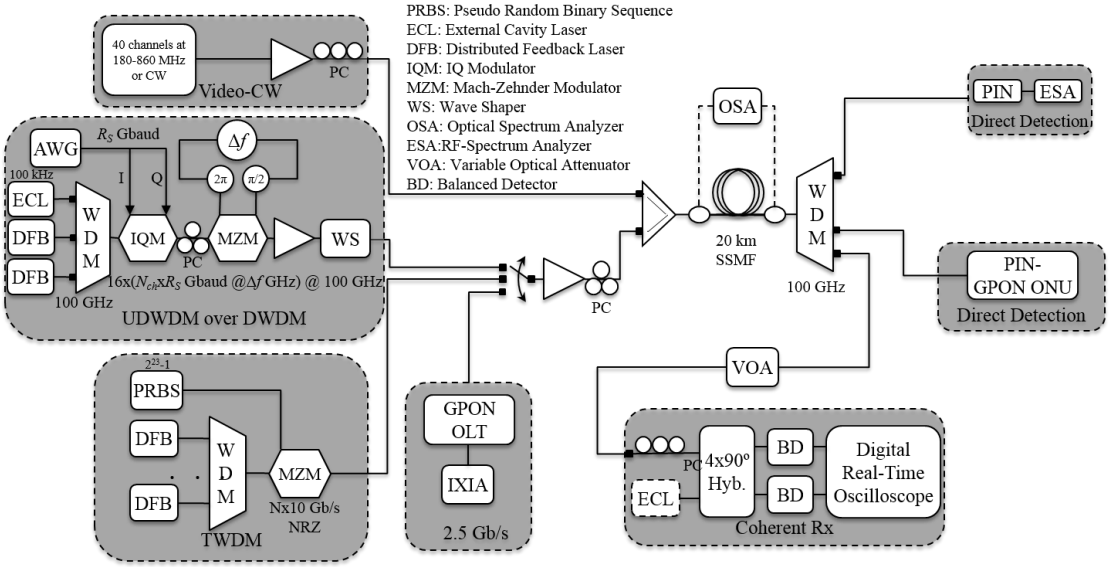

Figure 4.10 Experimental setup for modeling SRS crosstalk due to multi wavelength systems on analog video signal. R_S: symbol rate, N_{CH}: number of channels and Δf: channel spacing in each channel group.

The extinction ratio of the 10G-NRZ channel is set to 8.2 dB. The 2.5 Gb/s GPON transmitter is based on a GPON OLT, which is fed with IXIA-XM12. The optical power of GPON channels is set to 3 dBm. The digital baseband signals are multiplexed with the video channel using a 1:2 coupler. At the input of the coupler, we placed a polarization controller to maximize the SRS crosstalk ($\rho_{SRS} = 1$). The total optical signal is transmitted over 20 km of SSMF. After de-multiplexing, the 10G-NRZ and video channels (-3 dBm) reach the direct detection receiver comprised by PIN photodetector plus ESA. The RBW and VBW from ESA are set to 300 kHz and 1 kHz, respectively. The RBW and VBW play an important role when we calculate the RIN_{XT} in dB/Hz. After reaching the coherent receiver, the UDWDM channels are processed offline by coherent analyzer.

Fig. 4.11 (a) shows the PSD of 0 dBm power at the p-i-n for 2.5 and 10 Gb/s NRZ, and 1.25 Gb/s QPSK signals. As the RF output shows an increment of 2 dB for every 1 dB increase in the optical power, the 1.25 Gb/s QPSK signal has 3 dB lower SRS than 10 Gb/s NRZ with the same optical power . The crosstalk versus modulation frequency is depicted in Fig. 4.11 (b) for single and different multi-channel digital baseband signals. The experiments agree well with the model.

Fig. 4.12 (a) shows the CNR for the 55 MHz analogue video channel as a function of the optical power per channel of the interferer from different digital baseband and multi-channel signals. In this figure, 1530 nm is the lowest wavelength of the single or 1*st* channel in multi-wavelength scenario. After this validation, we have applied the model to a digital video scenario for information in Fig. 4.12 (b).

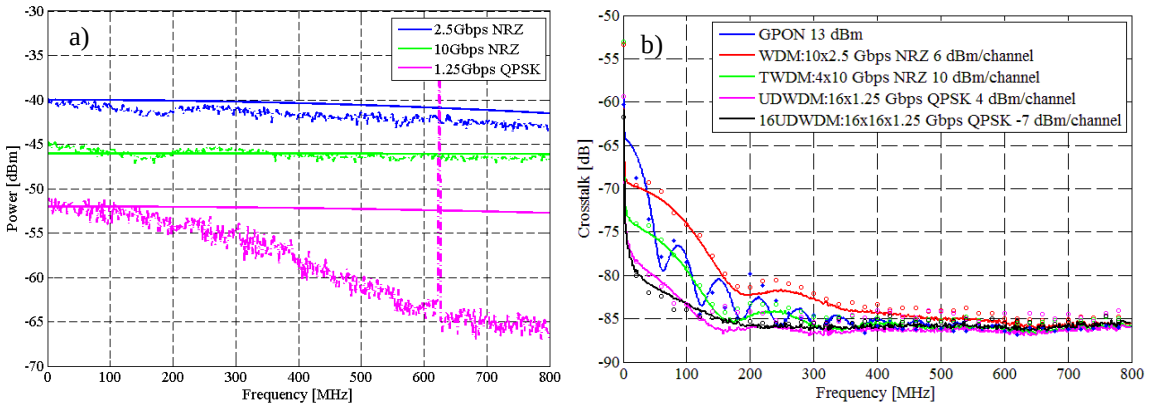

Figure 4.11 (a) PSD of 0 dBm power for 2.5-10 Gb/s NRZ and 1.25 Gb/s QPSK. (b) Theoretical (lines) versus measured (markers) SRS crosstalk for different PONs.

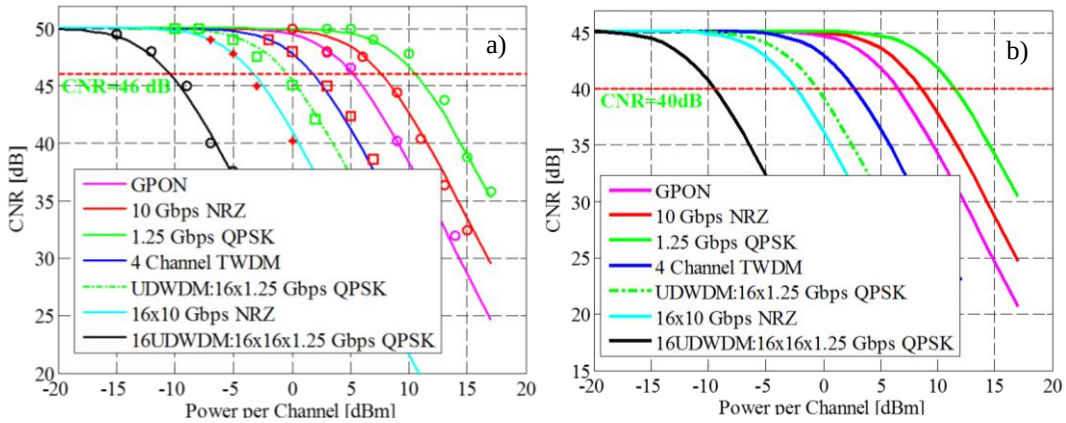

Figure 4.12 Theoretical versus measured (filled markers) of the 55 MHz CNR for (a) analogue video (b) digital video signals versus the optical power per channel of different digital baseband and multi-channel signals.

In order to fully explore the potential of the model a set of coexistence scenarios are considered: RF+ TWDM; RF+ TWDM+ GPON; RF+ TWDM+ XGPON; RF+ TWDM+ UDWDM or RF+ UDWDM. TWDM consists of 4 channels with 100 GHz channel spacing. UDWDM consists of 256 channels separated by 3.125 GHz. The CNR penalty is characterized as a function of the wavelength for the above mentioned coexistence scenarios when considering the 40 and 46 dB CNR requirements for the digital and analogue video, respectively. We observe the maximum power of TWDM+video or UWDM+video for all wavelengths.

It can be observed in Fig. 4.13 (a) and (b) that a good choice for the TWDM system with maximum power per channel, is the set of ~8 nm above 1590 nm. As shown in these figures, due to 6 dB lower power spectral density and high sensitivity of coherent detection in UDWDM scenario, we can put all 256 channels in 1530-1542 nm. The same type of conclusions can be taken for the remaining coexistence scenarios.

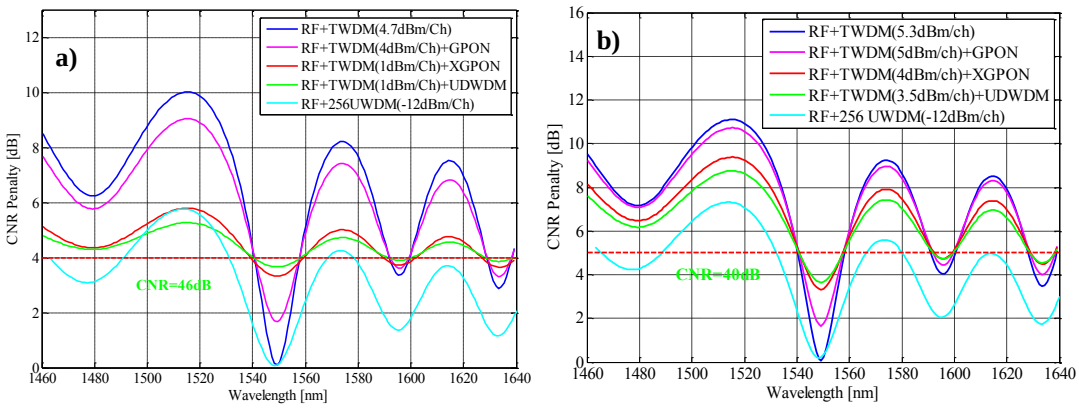

Figure 4.13 Coexistence scenario of TWDM-PON system: 3 dBm baseline GPON, 8 dBm XGPON@1580 nm and 256 channels UDWDM with -12 dBm/channel from 1530 nm. (a) Analogue. (b) Digital video with -3 dBm input received power.

4.4.1 SRS from Nyquist Shaped Signals on RF-Video

It has been shown in pervious chapter using frequency up/down-shifting from optical carrier, one can transmit the information in DS and US, respectively, with full bandwidth allocation and with the same laser frequency in both directions, which is useful for easy maintenance of UDWDM networks. In addition, it has been demonstrated that this brings benefits in terms of reduction of RBS, since this impairments affect mainly the carrier, which has a frequency spacing with respect to the modulated information and can therefore be mitigated by proper filtering in the receiver. Moreover, by suppressing or decreasing the lower frequencies of signals PSD, important in SRS on RF-video channels [12, 16], high number of users can transmitted in the same fiber with video overlay systems. To demonstrate this extra benefit of the proposed system regarding the dynamic SRS degradation, Fig. 4.14 shows the electrical PSD of baseband 2.5 Gb/s NRZ, 10 Gb/s NRZ, 2.5 Gbaud Nyquist 16QAM as well as the same Nyquist signal up-shifted by 1.5 GHz (250 MHz offset from DC). All of these PSDs were obtained by direct detection. As expected, we observe lower PSD (~4 dB) up to 250 MHz in the up-shifted signal compared to the non-shifted 16QAM signal. Baseband components result in internal beating of the signal with itself due to its Single Side Band (SSB) nature. Also, compared to 2.5 Gb/s NRZ (same equivalent symbol rate), we achieved 6 dB lower PSD in lower frequency and almost the same behavior with 10 Gb/s NRZ.

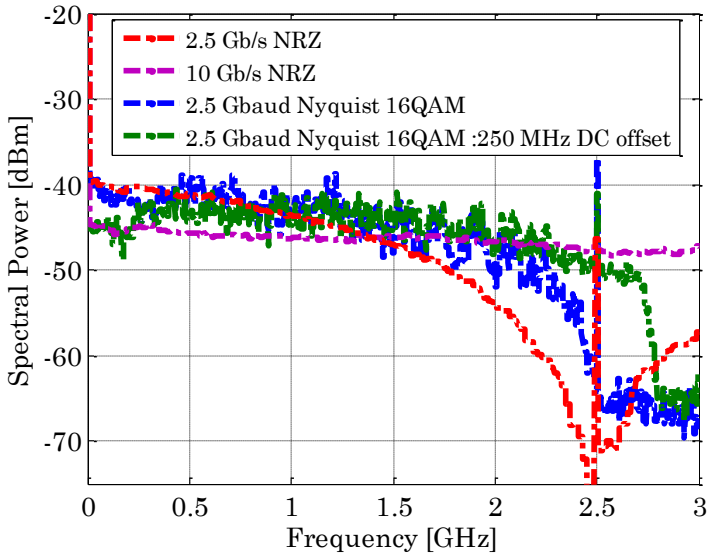

Figure 4.14 Measured PSD of single channel for 2.5 Gb/s NRZ, 10 Gb/s NRZ, 10 Gb/s Nyquist 16QAM and upshifted Nyquist 16QAM with -3 dBm in the input of the photodetector.

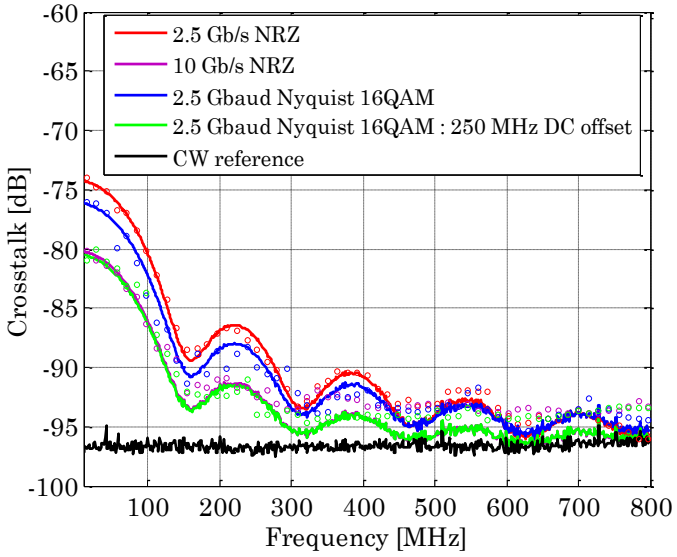

Figure 4.15 Theoretical (lines) versus measured (markers) SRS of 13 dBm single channel for 2.5 Gb/s NRZ, 10 Gb/s NRZ, 10 Gb/s Nyquist 16QAM and up-shifted Nyquist 16QAM at 1530 nm on CW signal at 1550 nm with 20 km SSMF.

Then, we measured the Raman crosstalk of our proposed system (depicted in Fig. 4.5 (a)) over 20 km of fiber transmission. The results of baseband Nyquist 16QAM, 2.5 and 10 Gb/s NRZ signals are also presented for comparison, which are shown in Fig. 4.15. In this measurement, all baseband signals had launch powers of 13 dBm. It can be observed that the SRS of the shifted signal in the lower frequencies (especially for the crosstalk at 50 MHz) is 4 dB and 6 dB lower than baseband 16 QAM signal and 2.5 Gb/s NRZ, respectively.

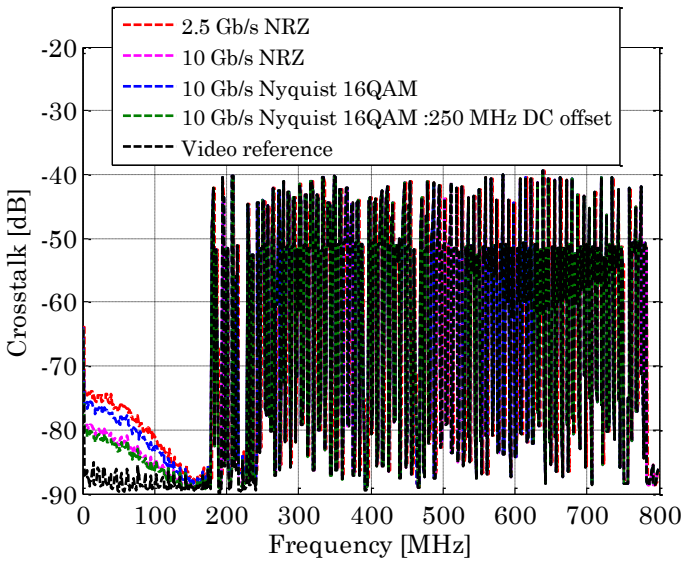

Figure 4.16 Theoretical SRS of 13 dBm single channel for 2.5 Gb/s NRZ, 10 Gb/s NRZ, 10 Gb/s Nyquist 16QAM and upshifted Nyquist 16QAM at 1530 nm on analogue video channels at 1550 nm with 20 km SSMF.

Moreover, we used the SRS model based on (4.2) for 20 nm wavelength spacing between single channel signal (1530 nm) with total power of 13 dBm and CW (1550 nm) with a 20 km fiber. Fig. 4.15 also shows the nonlinear Raman crosstalk of aforementioned systems which are well correlated with the experimental values of ~4 dB and ~6 dB. In addition, we implemented the SRS model to calculate the carrier-to-Raman crosstalk ratio of modulated signal on an analogue video. Figure 4.16 depicts the CNR degradation of video signals due to the nonlinear Raman crosstalk of the modulated signal. We used the same scenario of Fig. 4.5 (a). The main difference is that we changed CW to analogue video, with the parameters of Table 4.1. We measured the CNR of video and compare with theoretical value based on (4.3). As shown, the maximum CNR for this video reference is 50 dB. As we expected from the previous results of Fig. 4.16, the CNR of the proposed system is 4 dB and 6 dB higher than baseband 16QAM signal 2.5 Gb/s NRZ.

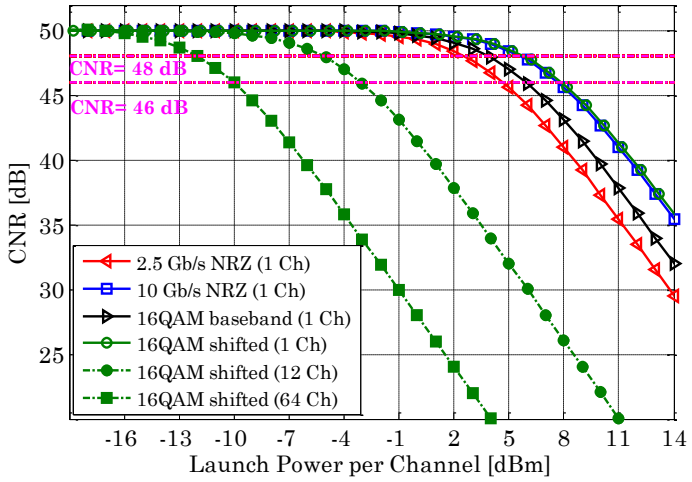

Figure 4.17 Theoretical CNR of the 55 MHz channel for analogue video signal versus the optical power per channel of different single and multi-channel signals for 20 km fiber.

Fig. 4.17 presents the theoretically calculated CNR at 55 MHz (the lowest frequency channel suffered the largest SRS-induced crosstalk) channel of analogue video signal as a function of the optical power of the modulated signal. These signals were tuned at 1530 nm (the lowest wavelength of the single or 1st channel in multi wavelength scenario) and video signal at 1550 nm. Fig. 4.17 shows a 2 dB penalty and a CNR of 46 dB as a threshold for 55 MHz channel. With -8 dBm power per channel and 12 channels there is less than 1 dB penalty for RF video at 55 MHz. For 64 channels/users (4 GHz channel spacing), we determined theoretically that -10 dBm is the maximum optical launch power that fits CNR at the threshold of 46 dB. The baseband Nyquist-shaped 16QAM and 2.5 Gb/s signals

require 2 dB and 3 dB lower power, respectively, for the same CNR in respect to shifted Nyquist-shaped 16QAM signal, as the RF output has an increment of 2 dB electrical power for every 1 dB optical power increment at the input of the fiber. The same conclusion can be achieved for digital video with the parameters in Table 4.1.

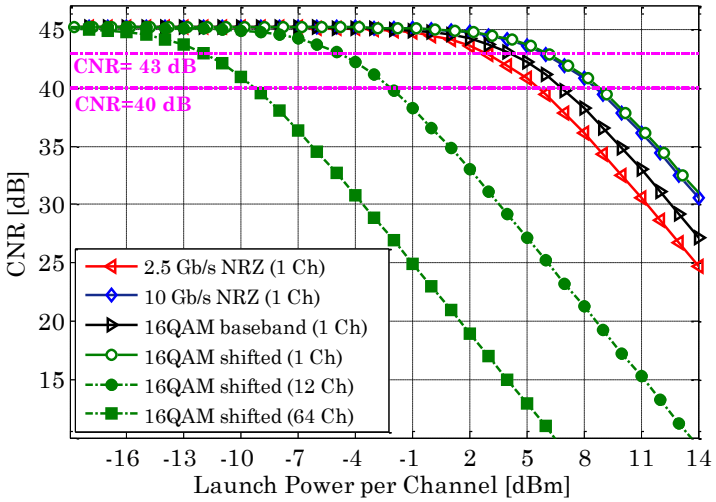

Figure 4.18 Theoretical CNR of the 55 MHz channels for digital video signal versus the optical power per channel of different single and multi-channel signals for 20 km fiber.

Fig. 4.18 depicts the CNR for the 55 MHz channel versus the power of modulated signals. RF channels in digital video are generally 6-10 dB lower in comparison to the peak value of analogue video [19] and as shown in Fig. 18, for -8 dBm power per channel still there is 4 dB more CNR than the required 40 dB CNR of digital video. Fig. 4.18 also shows the

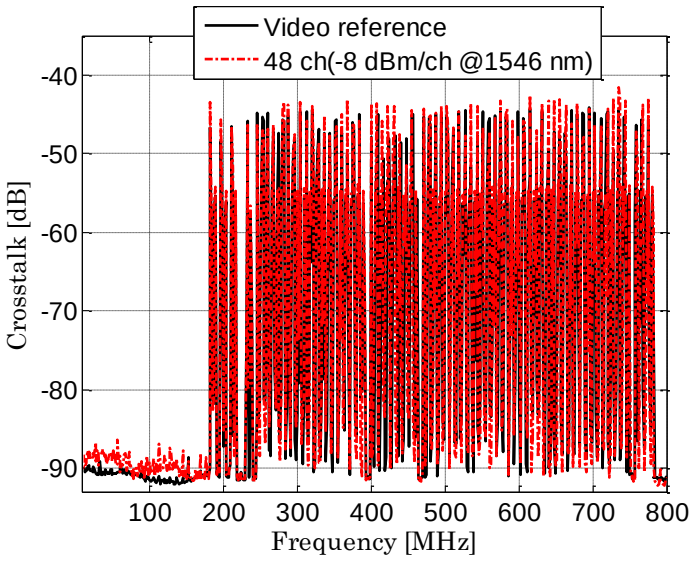

Figure 4.19 The nonlinear Raman crosstalk of 48 channels UDWDM @ 1546 nm with -8 dBm per channel on 8 dBm RF-video @ 1556 nm in 20 km fiber with -3 dBm received video power.

results for 64 channels/users. We can also see that -10 dBm is the maximum theoretically optical launch power, that puts the CNR above the 40 dB CNR threshold. However, past experiences with 256-QAM RF video has shown that 38 dB CNR is a safe threshold and therefore -8 dBm for 64 channels would be above the aforementioned threshold.

Fig. 4.19 shows the experimental nonlinear Raman crosstalk of 48 channels UDWDM at 1546 nm with -8 dBm per channel in 20 km fiber. As the required power per up-shifted DS channel in the fiber is lesser than -8 dBm and the signal presented reduced SRS, the overall number of channels in the proposed PON can be further upgraded to aggregate more users.

4.5 Concluding Remarks

In summary, we experimentally investigated the transmission capabilities of coherent UDWDM-PON scenarios (16 x 1.25 Gb/s coherent QPSK spaced by 3.125 GHz) in terms of the required guard band to video overlay and 10 Gb/s-NRZ technologies. We successfully transmitted over 20 km of SSMF UDWDM with coherent detection in the presence of video and 10G-NRZ channels separated by guard bands ranging from only 0.8 nm (100 GHz) to 1.6 nm (200 GHz). These results show that UDWDM-PON is a promising solution for NG-OAN deployments since it is robust enough to coexist with such legacy PON technologies. Also, we have validated a model for single, multi-wavelength, multi-format prediction of the SRS crosstalk based on PSD of digital baseband signal. We got good agreement with the measured results for several systems and numbers of wavelengths from the obtained formulation predictions for different video types, powers, wavelengths and types of systems coexistence were made, allowing the observation of the best operational zones for each of the systems. In addition, due to the lower PSD of up-shifted Nyquist pulse at low frequencies (<250 MHz), the proposed system had lower carrier-to-Raman crosstalk ratio than the baseband Nyquist signal as well as the comparable symbol rate NRZ equivalent. Furthermore, reduced impact of XPM and SRS with optimum guard band between RF-video and UDWDM channels resulted in spectral efficiency with high aggregated capacity.

References

[1] ITU-T recommendation G.989.1, “40-Gigabit-capable passive optical networks (NG-PON2): General requirements,” 2013.

[2] ITU-T recommendation G.989.2(draft), "40-Gigabit-capable passive optical networks: Physical media dependent layer specification," 2014.

[3] H. Rohde, E. Gottwald, A. Teixeira, J. D. Reis, A. Shahpari, K. Pulverer, J. S. Wey, "Coherent ultra-dense WDM technology for next generation optical metro and access networks," *J. Lightwave Technol.*, vol. 32, no. 10, pp. 2041-2052, April 2014.

[4] A. Shahpari, J. D. Reis, R. Ferreira, D. M. Neves, M. Lima and A. N. Teixeira, "Terabit+ (192×10Gb/s) Nyquist shaped UDWDM coherent PON with upstream and downstream over a 12.8 nm band," Proc. *Optical Fiber Communication Conf. (OFC),* Anaheim, CA, March 2013, paper PDP5B3.

[5] E. Wong, "Next-generation broadband access networks and technologies," J. Lightwave Technol., vol. 30, no. 4, pp. 597-608, February 2012.

[6] J. D. Reis, D. M. Neves and A. L. Teixera, "Analysis on nonlinearities on coherent ultra-dense WDM-PONs using Volterra series*," J. Lightw. Technol*., vol. 30, no. 2, pp. 234-241, Jane 2012.

[7] F. Vacondio, O. Rival, C. Simonneau, E. Grellier, A. Bononi, L. Lorcy, J.-C. Antona and S. Bigo, "On nonlinear distortions of highly dispersive optical coherent systems," *Optics Express*, vol. 20, no. 2, pp 1022-1032, January 2012.

[8] P. Poggiolini, A. Carena, V. Curri, G. Bosco and F. Forghieri, "Analytical modeling of nonlinear propagation in uncompensated optical transmission links," *IEEE Photon. Technol. Lett.* vol. 23, no. 11, 742-744, March 2011.

[9] M. R. Phillips and D. M. Ott, "Crosstalk due to optical Fiber nonlinearities in WDM CATV lightwave systems," J. Lightwave Technol., vol. 17, no. 10, pp. 1782-1792, October 1999.

[10] H. Kim, K. H. Han, and Y. C. Chung, "Performance limitation of hybrid WDM systems due to stimulated Raman scattering," IEEE Photon. Technol. Lett., vol. 13, no. 10, pp. 1118-112013, October 2001.

[11] F. Coppinger, L. Chen, and D. Piehler, "Nonlinear Raman crosstalk in a video overlay passive optical network," Proc. Optical Fiber Communication Conf. (OFC), Atlanta, GA, March 2003, paper TuR5.

[12] D. Piehler, "Minimising nonlinear Raman crosstalk in future network overlays on legacy passive optical networks," IEEE Electronics Lett., vol. 50, no. 9, pp. 687-688, April 2014.

[13] A. Shahpari, J. D. Reis, S. Ziaie, R. Ferreira, M. J. Lima, A. N. Pinto and A. Teixeira, "Multi system next-generation PONs impact on video overlay," Proc. Eur. Conf. Opt. Commun. (ECOC), London, September 2013, paper Tu.3.F.3.

[14] B. Colella, F. J. Effenberger, C. Shimer, and F. Tian, "Raman crosstalk control in passive optical networks," Proc. Optical Fiber Communication Conf. (OFC), Anaheim, CA, March 2006, paper NWD6.

[15] N. Cheng, M. Zhou, K. Litvin, F. Effenberger, "Delay modulation for TWDM-PONs," Proc. Optical Fiber Commun. Conf. (OFC), San Francisco, CA, March 2014, paper W1D.3.

[16] A. Tanaka, N. Cvijetic, and T. Wang, "Beyond 5 dB nonlinear Raman crosstalk reduction via PSD control of 10 Gb/s OOK in RF-video coexistence scenarios for next-generation PON," Proc. Optical Fiber Communication Conf. (OFC), San Francisco, CA, March 2014, paper M3I.3.

[17] H. Kim, H. C. Ji, and J. H. Lee, "Nonlinear optical crosstalk in analogue phase-modulated wavelength division-multiplexed systems," Proc. Optical Fiber Communication Conf. (OFC), San Diego, CA, February 2008, paper JThA69.

[18] T. Sakamoto, T. Kawanishi, and M. Izutsu, "Optimization of electro optic comb generation using conventional Mach-Zehnder modulator," Proc. *International Topical Meeting on Microwave Photonics*, Victoria, BC, pp. 50-53, October 2007.

[19] F. Villarruel, and L. Ray, "1550 video overlay: the new old reliable," Scientific Atlanta White paper, 2007.

CHAPTER 5 HIGH CAPACITY CONVERGENCE OPTICAL ACCESS NETWORKS

Summary

Mobility and ubiquitous coverage are two crucial pillars for future metro/access networks. Free-space optical communications can offer the highest capacity with license-free wireless spectrum and fast installation. PONs with Free-Space Optics (FSO) should couple very efficiently, since they work in the same wavelengths with a transparent link and can support both flexibility in wireless systems and high-capacity in fiber. Coherent detection with advanced modulation formats can fully utilize the bandwidth and increase the transmission capacity of FSO links. This chapter considers several optical wireless systems used in metro and access networks.

5.1 Introduction

The world of communications is developing toward connecting everyone and everything in every place. In the near future, the Internet of Things (Internet of Everything) vision forecasts that more than 30 billion devices will be wirelessly connected to the internet [1]. Radio Frequency (RF) theoretically goes almost everywhere. However, narrow available spectrum, interferences with other channels, and power consumption for high bit rates become the bottleneck of networking technology. Free-Space Optics (FSO) communication techniques have all the ingredients for low initial Capital Expenditure (CapEx), a wide-license free wireless domain, essential high-level data protection and security, good flexibility and immunity to Electromagnetic Interference (EMI) [2, 3].

The interest is currently growing around this technology in several application domains, for instance, the first/last mile in dense urban areas, network access for isolated premises, high-speed (Local Area Networks) LAN-to-LAN, terrestrial applications, transitional and temporary network connection, and undersea and space communication [4-6]. Therefore, telecommunication vendors and operators are starting to increase commercialization and the deployment of FSO in today's communication infrastructures.

Simultaneously on the research side, several studies and achievements have been reported, as summarized in Fig. 5.1 [7-9] (this figure includes the contribution in [J6]). In particular, it can be noted that 2011/2012 started a new panoply of application domains connected with

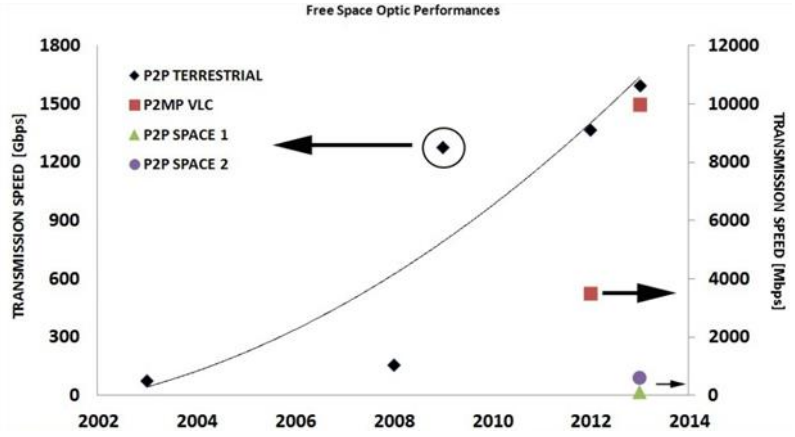

Figure 5.1 Summary of FSO research performance demonstrations.
Square dots represent recent records in VLCs where PtMP connections are implemented; space 1 (triangle) and space 2 (circle) stand, respectively, for space-to-earth and moon-to-earth PtP.

space communications and Visible Light Communications (VLCs). In the VLC world, in particular, standard Light-Emitting Diodes (LEDs) or light bulbs are used for FSO Point-to-Multipoint (PtMP) broadband transmissions.

Recently, a great attention has been given to merge Wavelength-Division Multiplexing (WDM) with FSO [10-14]. Although turbulence and variable attenuation in FSO links are still the main impairment, these have been intensively studied in the last years [15], paving the way to commercial deployment. In several FSO terrestrial links, 4x40 Gb/s with amplitude modulation and direct detection [10], 8x10 Gb/s with amplitude modulation and direct detection [11], 16x10 Gb/s with amplitude modulation and direct detection [12], 1x100 Gb/s Polarization Multiplexed Quadrature Phase Shift Keying (DP-QPSK) and coherent detection [13] and 32x40 Gb/s with amplitude modulation and direct detection [14], were successfully demonstrated.

Adoption of Dense WDM (DWDM) transmission in FSO systems was proposed in [16-17]. In [16], the authors introduced a DWDM transparent FSO system for in/outdoor applications at high bit rates. The procedure of transparent Optical Wireless Communication (OWC) tolerates the implementation of DWDM transmission in FSO systems, boosts the capacity of the OW channel, exploits the full capacity of optical fiber, and introduces DWDM into the access networks. In [16], an ultra-high-speed OWC channel using a Single-Mode Fiber (SMF) to a SMF with no steering mirrors in bidirectional DWDM is demonstrated and for the first time the multiple-user access capability by wavelength reuse is presented. In addition, the authors investigated the full system performance by eight channels in both transmission directions, each at 10 Gb/s, multiplexed and transmitted over a 10-m free-space channel, which could be increased within the available power link budget. In [18] we have pushed the limits even further by investigating the capability of ultra-DWDM (UDWDM) transmission of hybrid fiber-free-space Passive Optical Network (PON) and increasing the spectral density, aggregated capacity, and total throughput. UDWDM 10 Gb/s Nyquist-shaped 16-ary Quadrature Amplitude Modulation (16QAM), 10 Gb/s Radio over Fiber (RoF) Orthogonal Frequency-Division Multiplexing (OFDM), and 8.75 Gb/s baseband OFDM signals per user were transmitted through a maximum 40 km passive optical network, which includes a 6-m free-space optics link with acceptable performance.

In this chapter, firstly we present a fully transparent ultra-broadband OW coherent system demonstration obtained using only two passive heads, composed of GRIN fiber pigtailed lenses, simplifying and making it passive all over the entire FSO link (avoiding complex transmitter alignments or large area photodiodes). The adoption of DP-QPSK and wavelength multiplexing techniques allowed us to demonstrate the transmission of 640 Gb/s (16x40 Gb/s) and 1.6 Terabit/s (16x100 Gb/s) setting the highest capacity demonstrated, to our knowledge, for an OW system.

In the next section, taking advantage from experience in [18], we propose and experimentally demonstrate a coherent bidirectional PON system with FSO to increase the capacity of optical access networks. Reduced impact of Rayleigh Back-Scattering (RBS) is achieved due to Nyquist pulse shaping and digital frequency-shifting. A successful transmission of bidirectional 12×10 Gb/s UDWDM over 80 km fiber followed by 56 m PtMP FSO is experimentally demonstrated. In the end, we experimentally characterize a fully bidirectional hybrid Optical Distribution Network (ODN) for the first time, over up to 80 km SSMF plus two FSO links (of 60 m outdoor FSO and 20 m indoor FSO simultaneously).

5.2 1.6 Terabit/s OWC for Next Generation Convergent Urban Infrastructures (papers J6, C16-C17)

Atmospheric conditions are responsible for optical wireless communications degradation mainly due to scintillations and attenuation. Fog, rain, snow as well as randomly distributed cells formed through the medium due to thermal turbulences play a major role in FSO design [19-21]. Under such conditions, spectral efficiency and power efficiency have to be carefully considered in FSO communication applications. A mix of multi-level phase modulation schemes, polarization multiplexing and coherent detection can be a concrete answer to boost the today OWs performance.

The experimental setup used for the results obtained is shown in Fig. 5.2. The laser source array, from number 1 to 16, allow us to scale the system in terms of capacity by multiplexing and then simultaneous modulation with an IQ modulator of 25 GHz bandwidth in QPSK, thus achieving a 20 and 50 Gb/s per wavelength QPSK signal. The signal is separated into two polarizations, 255 symbols delayed for de-correlation purposes, using an Optical Delay

Line (ODL), and then multiplexed in polarization again to have a dual polarization 40 Gb/s and 100 Gb/s DP-QPSK signal per wavelength. The two driving electrical signals (2^9 -1), are generated by a pulse pattern generator from SHF 12100B. The described transmitter allows the generation of up to 16 channels of 40 Gb/s or 100 Gb/s by turning on and off the lasers.

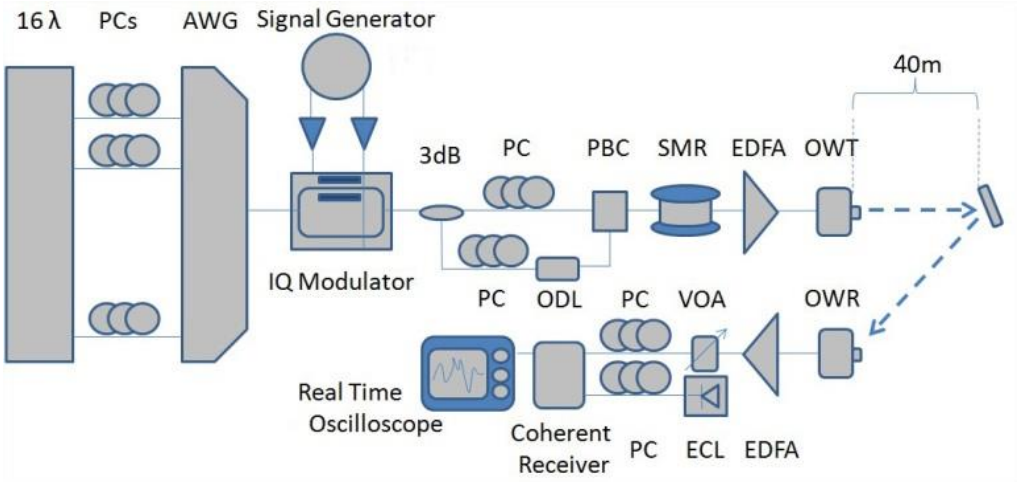

Figure 5.2 Outdoor FSO 1.6 Tb/s experimental setup.
PC: polarization controller; PBC: Polarization Beam Combiner; EDFA: Erbium Doped Fiber Amplifier; OWT-R: Optical Wireless Transmitter-Receiver; ECL: External Cavity Laser; VOA: Variable Optical Attenuator; ODL: Optical Delay.

An erbium Doped Fiber Amplifier (EDFA) is used as booster; the fiber is a single mode (step reduced type ITU-T G652) with 40 km length. At the receiver side a pre amplifier (EDFA) is used to control the power in conjunction with a Variable Optical Attenuator (VOA) in order to proceed with the required sensitivity analysis and measurements. The receiver is a typical coherent DP receiver directly connected to a real time oscilloscope and an optical tap connected to an optical complex spectrum analyzer for spectral monitoring. The FSO Transmission part (OWT) is composed by a GRIN lens, mounted on an x/y/z alignment system and fiber pigtailed, followed by two lenses (L1 - L2) used to collimate the beam. The FSO Receiving side (OWR) is made by a collimating lens (L3) and a GRIN lens. The effective aperture of the L1-L2 telescopic system is 2 cm. The GRIN lens is a flat surface lens characterized by a gradual, parabolic, variation of its refractive index. As the human eye, the GRIN lens permits to simplify mounting and alignment procedures and at the same time; thanks to the fiber pigtailing, it allows achieving a low divergence output beam, resulting in system performance improvement [16].The OWT and OWR were located at the

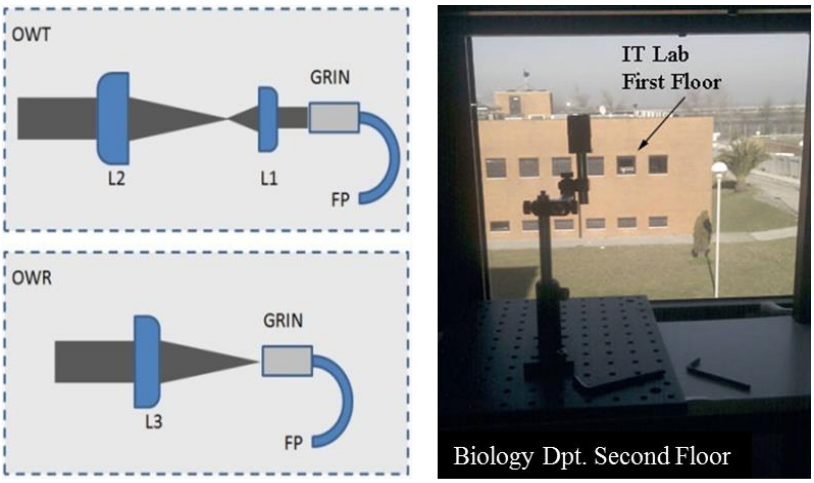

(a) (b)

Figure 5.3 (a) Schematics of optical wireless transmitter and receiver, (b) particular of biology department where a mirror was placed to perform the two ways transmission.

first floor of Institute of Telecommunication (IT) building. At the second floor of the Biology Department building (Biology Dpt.) a mirror was aligned to perform the two way experiments. The length of the entire wireless system was estimated in 80 m, with a quota difference of 4 meters between the building floors and a total loss equal to 55 dB. In order to achieve bidirectional tracking, the system was first aligned with a beacon beam (at 514 nm) using a laser diode. Afterwards, for better tuning, a second beacon beam (at 850 nm) was directly injected into the system via the fiber pigtailed GRIN lens (OWT side).

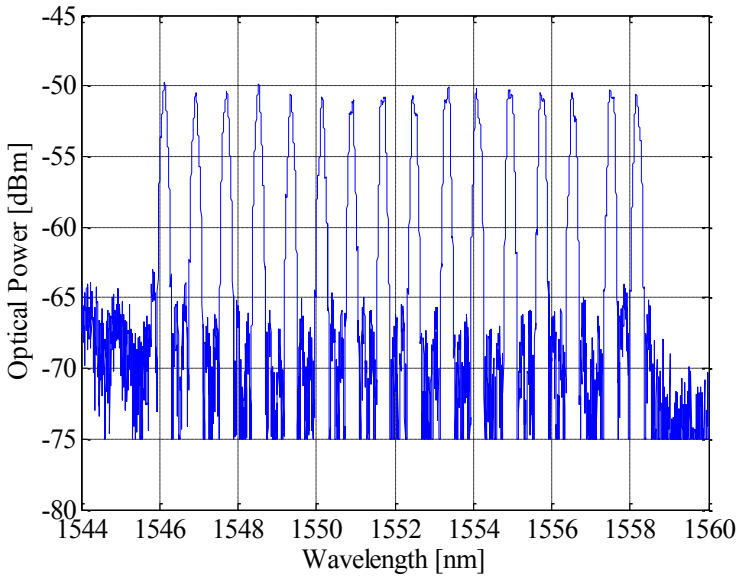

Figure 5.4 Optical channel comb, each channel modulated at 100 Gb/s DP-QPSK.

Two mirrors, one in the Biology department laboratory (see Fig. 5.3) and one, not reported for simplicity, located at the IT lab, were aligned accordingly in order to achieve the minimum losses over the entire system path. Two experiments were performed, 16x40 Gb/s and 16x100 Gb/s modulated combs were injected into the OWT, reflected by the mirror at Biology department laboratory and collected at the OWR. In Fig. 5.4 the optical spectrum and the X and Y polarization components of the signal are reported for the 1.6 Tb/s system configuration. As it can be seen, the channel equalization is high (<2 dB).

The experimental test took place in Aveiro, a city located on the Portuguese Atlantic ocean coast, where our OW field trial was set up in February 2013.

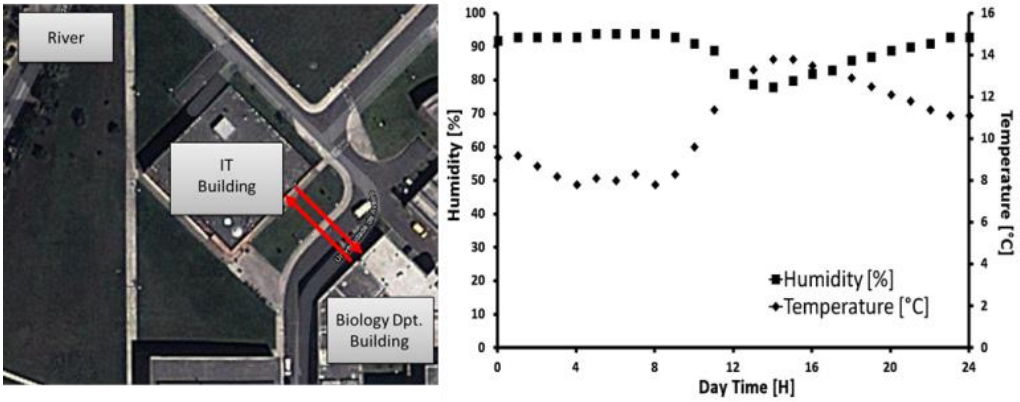

(a) (b)

Figure 5.5 (a) Satellite picture (courtesy from Google maps web system) of Aveiro University Campus site where the optical Terabit/s wireless system has been tested. (b) Temperature and humidity registered by the university weather station during the measurements.

The weather conditions experienced during the daylight measurements are reported in Fig. 5.5. As previously mentioned, the WDM signal, formed by 16 optical carriers spaced by 100 GHz, was launched between two different buildings located inside the University campus (see Fig. 5.5). A single mode step reduced (ITU-T G.652) fiber coil, 40 km long, was placed before the optical wireless path in order to simulate not only a simple building to building ultra-broadband interconnection but also a downstream telecommunications transmission in an urban environment. This type of scenario may result, besides the conditions referred previously, in fail recovery condition. In Fig. 5.6 and Fig 5.7 we report the experimental results in terms of Bit Error Rate (BER). As it can be observed, achieved results demonstrate that FSO enables very high capacity interconnections (640 Gb/s and 1.6 Tb/s). At 40 Gb/s, all the 16 channels (640 Gb/s total capacity) reach an error free

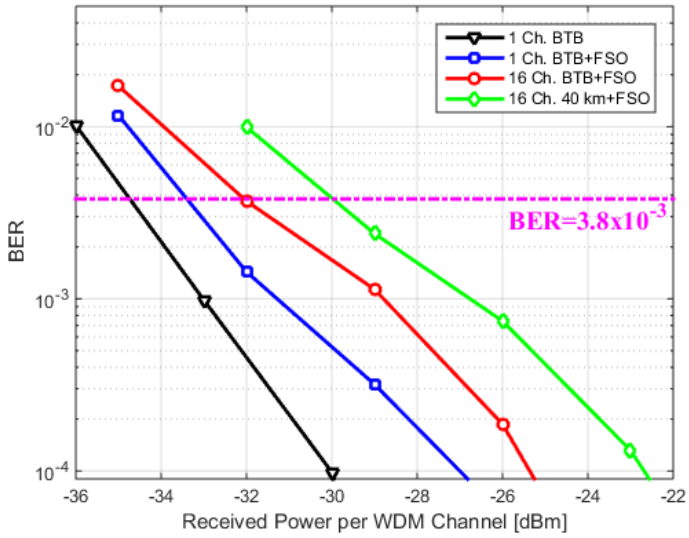

Figure 5.6 Experimental BER results: 40 Gb/s DP-QPSK transmission, single channel BTB, BTB plus 80 m FSO, 16 channels over 80 m FSO and over 40 km SMF plus 80 m FSO.

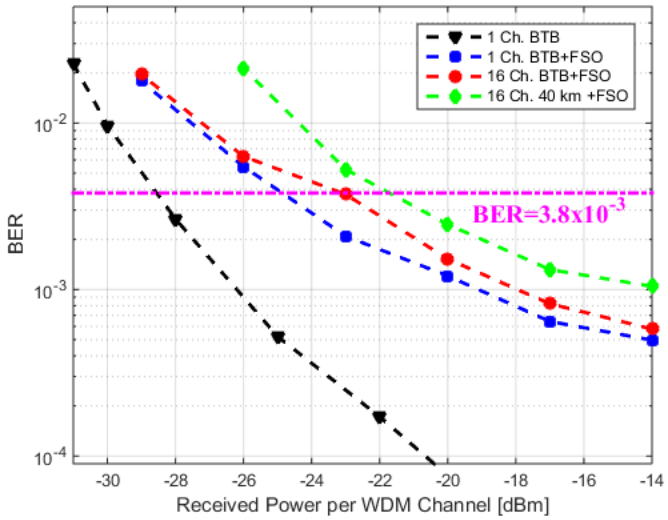

Figure 5.7 Experimental BER results: 100 Gb/s DP-QPSK transmission, single channel BTB, BTB plus 80 m FSO, 16 channels over 80 m FSO and over 40 km SMF plus 80 m FSO.

condition in both BTB and propagation after 80 m of FSO path, even considering that non equalized EDFAs have been used at both transmitting and receiving sides. The use of Forward Error Correction (FEC) is required for recovering error free conditions in the case of 16x100 Gb/s (1.6 Tb/s). Here, the effects of the wave front distortion at the GRIN receiver due to transmission combined with the extreme high data rate, determine a performance decrease. In order to lower such effects, the use of a diversity scheme at the receiver side is under study. The weather conditions experienced during the daylight measurements, (see Fig. 5.5), did not induced any kind of extra penalty but more investigations are needed in order to test the system with different turbulence conditions.

5.3 Hybrid Advanced Modulation Bidirectional PON with Free Space Optics (papers J7, C18-C21)

The presented results in [18] proved the concept of heterogeneous fiber/FSO UDWDM-PON architectures that would be attractive for future indoor FSO communications in order to serve high number of users with high data rates, high spectral efficiency over space and time regardless their modulation formats. In addition, this system could enhance more value-added services to next-generation broadband optical access networks in terms of transmitted data security and medical immunity.

Here, we propose and experimentally demonstrate a 12x10 Gb/s bidirectional hybrid SSMF and FSO PHY PON recurring to 6.25 GHz grid, Nyquist shaping and frequency-shifting. We extend the network reach to 80 km with 30.5 dB Optical Distribution Network (ODN) power budget. Furthermore, we analyze the heterogeneous networks scenario to characterize the required guard-band for coexistence with a TWDM-PON system.

5.3.1 System Concepts

As explained in section 3.3.1, to achieve such a highly aggregated coherent PON system, two paths can be followed. A single high bandwidth frontend generating/processing a set of wavelengths, or recurring to several lasers integrated in the same wafer with the same number of receivers, partitioning in this way the required electrical bandwidth by each component. Considering any of the above mentioned solutions, in order to be able to use the same carrier (as shown in Fig. 5.8) to transmit the upstream and downstream with low RBS,

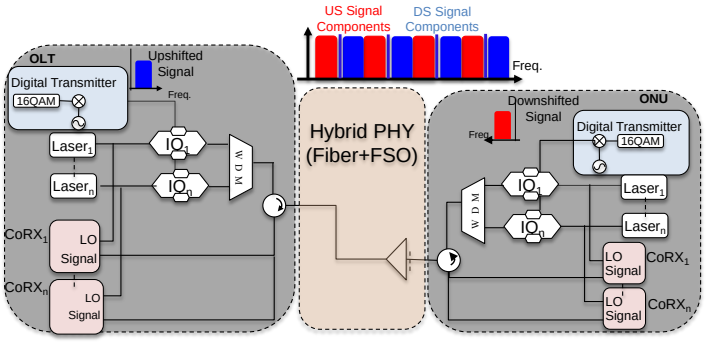

Figure 5.8 Block diagram of proposed architecture.

each of the channels should be up-shifted in frequency. This frequency shift should be sufficient to allow reduction of the impacts of RBS along with Stimulated Raman Scattering (SRS) at the base band and eventually on other coexisting channels [22]. These upshifted channels may be multiplexed optically after signal modulation. The multiplexed optical channels must provide the required aggregated bit rate. In the upstream, downshifting is used in order to assure maximum bandwidth usage and minimum impact of RBS.

The proposed architecture that can be used in PON and datacenters, is presented in Fig. 5.8. The original signal may be recovered in the digital domain after coherent detection using a constant frequency shift, without the need for intermediate frequency estimation.

5.3.2 Experimental Setup

Figure 5.9 shows the experimental setup used for the experiments. At the OLT, the light from a 100 kHz linewidth External Cavity Laser (ECL) at 1549.32 nm was split to provide a Local Oscillator (LO) for the receiver and to serve as source for the DS signal. The resulting carrier was injected in a Mach-Zehnder Modulator (MZM) driven by 6.25 GHz RF signals to generate comb of 12 equally spaced tones. Due to unavailability of lasers with the required spectral resolution, in this work we have opted to simulate the proposed system with a comb based on [23]. The latter were fed into an IQ modulator, driven by a 12 GSa/s arbitrary waveform generator, producing a 2.5 Gbaud 16QAM signal (2^{11}-1 PRBS) with Nyquist pulse shaping (roll-off factor 0.05). These signals were upshifted by 1.5 GHz, resulting in a 250 MHz offset overall spectrum offset from the carrier. The launch power for the 12 x 10 Gb/s group was set by an EDFA prior to a circulator for bidirectional transmission through 40 km or 80 km of SSMF. To achieve heterogeneous coexistence scenario the UDWDM comb was multiplexed with a 4 x 10 Gb/s NRZ channel via a 100 GHz WDM filter simulating a TWDM signal (the DS band for TWDM was shifted from the recommendation [24] due to lab limitations, however the resultant impact is approximately the same). This latter group was composed of an integrated laser Mach-Zehnder (ILMZ) and three lasers modulated by a single MZM with different PRBS of length 2^{31}-1, modulated in NRZ format, each with 8 dB extinction ratio, see Fig. 5.9 (a: I and II) for spectra. To test the potential use of FSO technology as part of the system, a 56 m outdoor FSO (Fig.5.9 (b)) link based on passive heads (collimator, beam splitter, lenses, two mirrors) was inserted in the last span with the extra loss compensation partially by an EDFA. The beam splitter provides

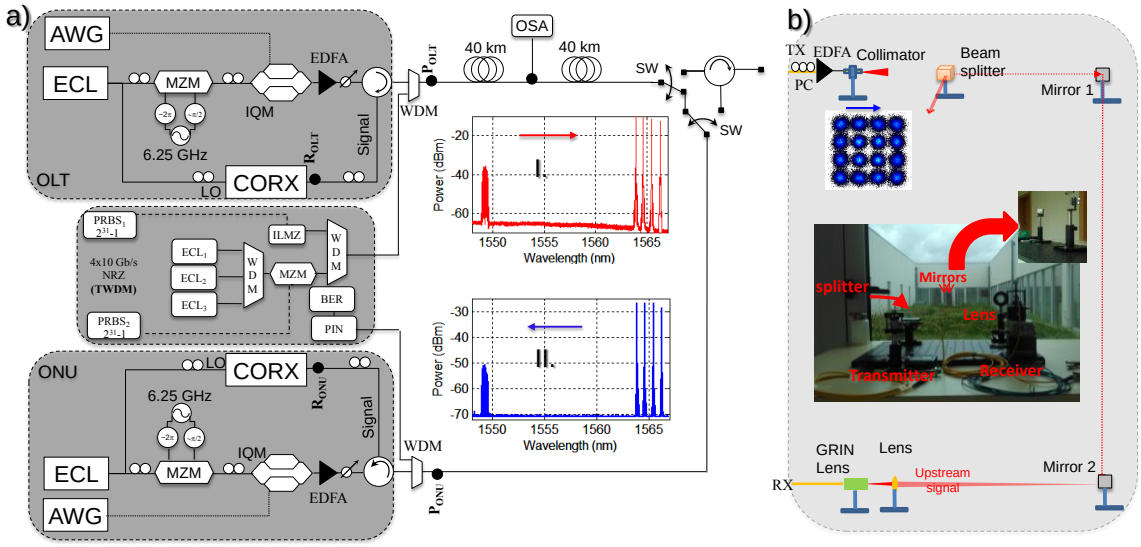

Figure 5.9 Experimental setup for bidirectional transmission with up to 80 km fiber. Insets: coexistence spectrum wavelength shifted TWDM with 12x10 Gb/s UDWDM at I. the fiber input II. After the FSO link. (b) Outdoor FSO setup with the picture in inset.

FSO polarization dependent splitting, through a Polarization Controller (PC), which sets the state of polarization in order drive light into distinct paths, with similar amount of power in each of them. The free-space communications link was established in completely transparent way using passive heads. The optical beam on SSMF fiber output was collimated by a reflection collimator, yielding a beam of 4 mm diameter and 0.02 degrees of full angle beam divergence. Near the collimator output, a beam splitter was used in order to evaluate the optical beam before sending it to the atmosphere. Above one meter the ground lawn, the aligned optical beam was propagated by a total distance of 56 m, subject to open environment weather conditions. As shown in Fig. 5.9 (b), the beam was reflected by two plane mirrors and finally was focused at 20 cm through a lens and collected by a GRIN Lens to the fiber. The FSO communication link was subject to the weather conditions of clear sky, wind speed of 3 m/s, temperature of 16º, relative humidity of 85%, yielding a loss of 29 dB between the input of the collimator and the output of the Grin-lens, having been this loss compensated by an EDFA.

We started by setting the DS signal through the 80 km fiber passing through a circulator to the FSO link and is received in the ONU. The mentioned circulator assures bi-directionality in the fiber span. The optical signal spectrum (UDWDM plus TWDM) after FSO is presented in Fig. 5.9 (a).

After demux, the 10 Gb/s signals were directly detected whereas the 16QAM channels were coherently detected. Detection was performed using a Coherent Receiver (CoRX) followed by a 50 GSa/s real-time scope. DSP was implemented offline, by using MATLAB, and included frequency downshifting, carrier phase recovery and frequency estimation. BER evaluation was performed by direct error counting in 10 traces of 4096 symbols. The US UDWDM signal was generated by modulating the comb signals at the ONU with an IQ modulator driven by another 12 GSa/s AWG. The AWG produced a 2.5 Gbaud 16QAM signal with Nyquist pulse shaping (0.05 roll-off factor) with a frequency downshift of 1.5 GHz. In a second stage of our experiment, we performed a test with the US signal passing through the FSO link. The signal coming from the ONU is connected to the TX point of the FSO link and was received in the RX point of OLT after passing the 80 km fiber. After that, the US signal passes through the fiber span and was received in the OLT. The US and DS signals counter-propagated in the 80 km fiber span. The same DSP and BER estimation included in the ONU was implemented in the OLT but with frequency upshifting.

5.3.3 Results and Discussions

We began by evaluating the impact of fiber nonlinearities in the US and DS channels separately (e.g. they do not coexist in the fiber). Due to the short transmission distances Four-Wave Mixing (FWM) is the main nonlinear impairment subject to a non-negligible penalty that depends on the power of UDWDM channels [25]. Fig 5.10 (a) presents the corresponding BERs of DS signals as a function of launch power per each DS channel when the received signal at the coherent receiver (@R_{ONU}) is -33 dBm. As expected, when the launch power in input of fiber (@P_{OLT}) increases, the DS signal performance starts to degrade as can be seen by the BER measurement. Here, it was shown that optimum launch power is -8 dBm. As we can see in Fig. 5.10 (b), the US BER plotted against launched power follows the same trend. -8 dBm per US channels (@P_{ONU}) is the optimum optical launch power when -33 dBm is the received power at the OLT receiver. Insets of Fig. 5.10 show the constellation of DS and US signals, for -8 dBm and 0 dBm launch power per channel (12 channels). The 16 QAM constellation of 0 dBm is visibly degraded with respect to -8 dBm. We can clearly see that phase noise affects mostly the higher power symbols indicating that degradation is caused by power dependent impairments, such as XPM and FWM.

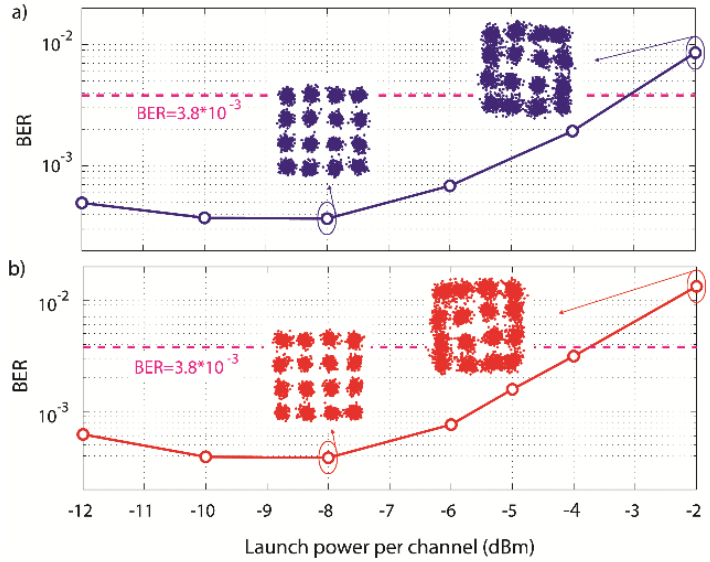

Figure 5.10 Dependence of the BER on the launch power per channel for (a) DS (b) US signals.

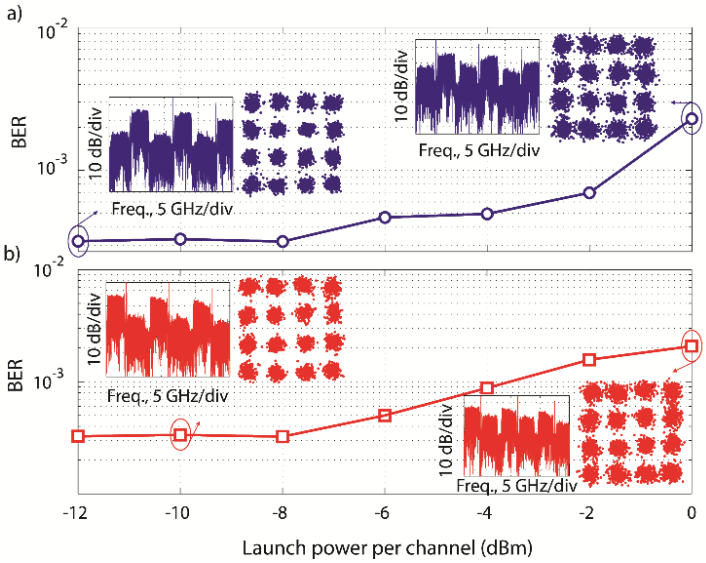

Figure 5.11 (a) DS BER @ R_{ONU}, (b) US BER @ R_{OLT} dependence on launch power per channels @ P_{ONU} /P_{OLT} respectively. Power of the pivot DS and US channels in the input of fiber is -8 dBm.

In bidirectional UDWDM-PON, reflections from one direction to other direction is an important issue. Optical power could be reflected into the receivers of opposite direction from circulator, fiber splices, connectors, splitters and mainly by RBS. The impact of back-reflection on the signals is presented in Fig. 5.11, fixing the power of the pivot channels in the US/DS to -8 dBm and varying the power in the DS/US counterpart. In Fig. 5.11 (a) we fixed the power of DS (@P_{OLT}) at -8 dBm and -33 dBm @R_{ONU} and increase the power of US (@P_{ONU}). We measured the performance of the DS channels at the ONU.

As the power of US direction increases, the degradation of the signal in the DS is increased due to back-reflection. Insets of Fig. 5.11 (a) shows the degradation in DS for launch powers in the US direction of -12 and 0 dBm. It should be noted that due to Nyquist pulse shaping and digital frequency shifting, the RBS impact was decreased considerably relatively to other schemes [26-28]. In Fig. 5.11 (a) we can see that the degradation in 0 dBm inset is uniform over all the symbols. Contrary to this is Fig. 5.10 where we can see clearly that degradation occurs mostly in the higher power symbols in the 0 dBm inset. This indicates that most of the degradation that we see in Fig. 5.11 (a) and (b) for the 0 dBm inset is not caused by nonlinearities such as XPM (FWM cannot occur since it requires phase matching condition which is not liable to exist in counter propagating signals), but by RBS and reflections from a set of optical devices.

In Fig. 5.11 (b) we fixed the power of US (@P_{ONU}) at -8 dBm and -33 dBm at R_{OLT} and increase the power of US @P_{ONU}. As expected, we observed the same trend as in Fig. 5.11 (a) and therefore we can achieve the same conclusions as we did it previously.

Fig. 5.12 shows the US and DS signal spectra that was obtained by an OSA, for both US/DS directions in output of mid span splitter. The BER results for the 12 channels versus frequency shifting of the LO are presented in Fig. 5.12 after optimizations of DS/US power with -33 dBm sensitivity in receivers of OLT and ONU and -8 dBm launched power in the input of fiber.

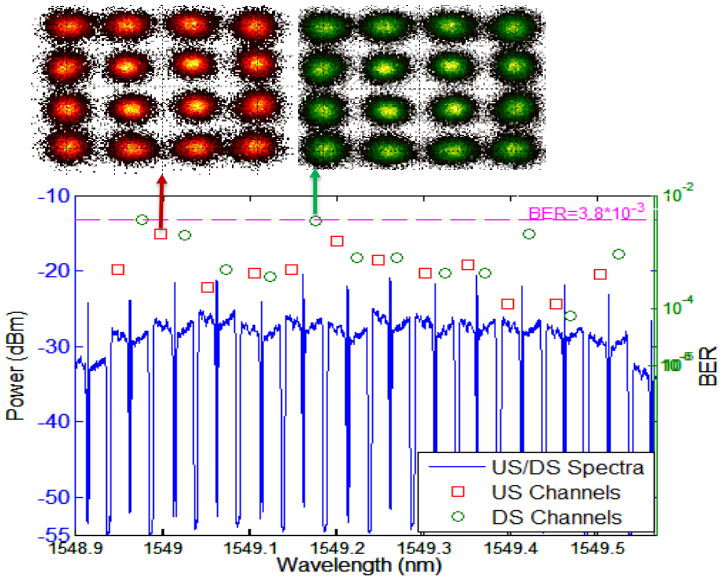

Figure 5.12 US/DS spectra and constellations with related BER after 80 km fiber.

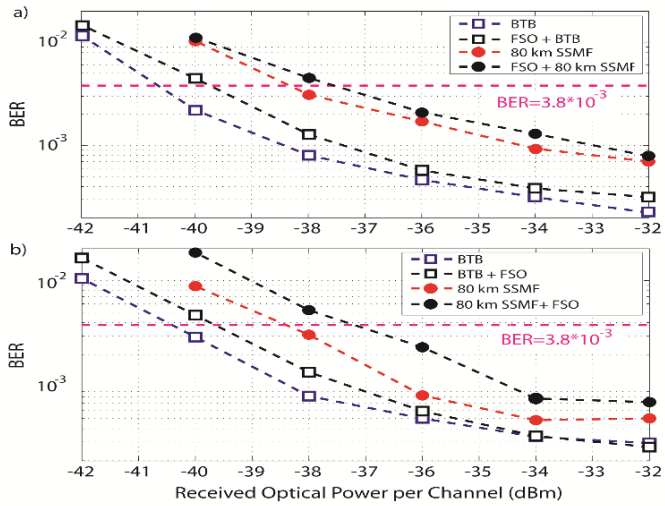

Figure 5.13 Measured BER for the central channel of the 12 (a) US, and (b) DS UDWDM channels.

Fig. 5.13 (a) and (b) present the measured BER as a function of the receiver input power per channel. We used the central channel of the spectrum shown in Fig. 5.12 as the reference for the results shown in Fig. 5.13. We evaluated the performance of the BTB, 80 km fiber and 80 km fiber plus FSO using -8 dBm as the input launch power.

It is shown that UDWDM channels in 80 km fiber have 2 dB penalty for a FEC-compatible BER of 3.8×10^{-3} [29] with respect to the BTB case. Sensitivities of -38.5 dBm were achieved for DS and US, allowing an ODN loss of 30.5 dB. Figs. 5.13 (a) and (b) also present 1 dB penalty for PtMP FSO results. We achieved an excellent receiver sensitivity of -37.5 dBm after 80 km fiber plus FSO. The achieved BER results with very small power penalty confirm the feasibility of the proposed hybrid bidirectional UWDM-PON with FSO.

5.3.4 Coexistence Scenario with TWDM-PON

Finally to test the coexistence of UDWM plus FSO with TWDM-PON channels we investigate the required frequency spacing between this two technologies in the spectrum domain. Fig. 5.14 depicts the UDWDM channels at shorter wavelengths with TWDM at longer wavelengths. Six frequency spacings were tested between the UDWDM and TWDM channels: 100 GHz (0.8 nm), 400 GHz (3.2 nm), 800 GHz (6.4 nm), 1200 GHz (9.6 nm), 1600 GHz (12.8 nm) and 2000 GHz (16 nm). As shown in Fig. 5.14 when the frequency spacing is 2 THz, a large launched power per TWDM channel window can be achieved. Fig. 5.14 also shows that below 11 dBm the FEC limit is not exceeded. Therefore to have

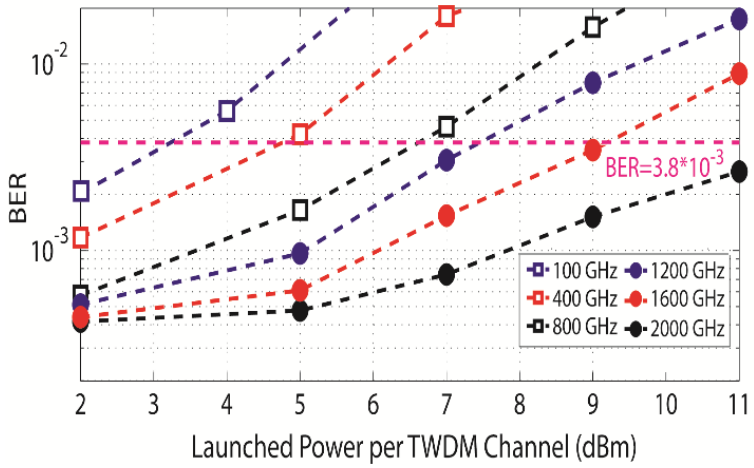

Figure 5.14 BER measurements (center wavelength of UDWDM channels) after transmission over 40 km-SSMF versus input power of each of the 4x10 Gb/s TWDM channels for different guard bands. Received optical power of UDWDM channels @ ONU is -35 dBm.

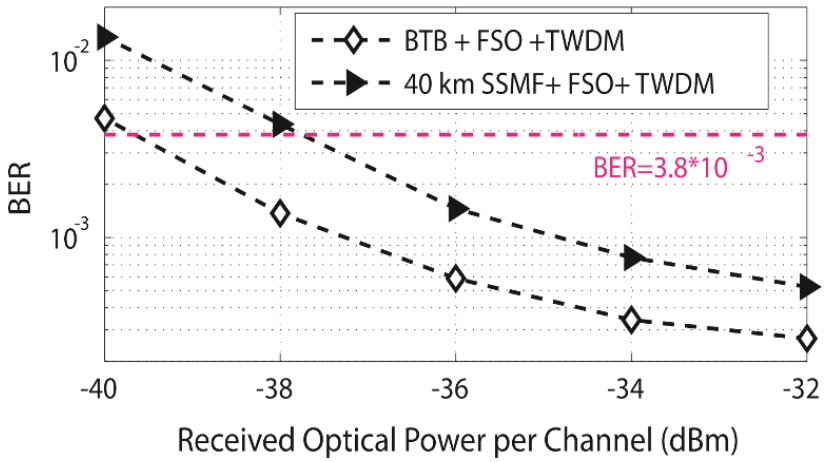

Figure 5.15 DS BER dependence of the UDWDM channels on received power in TWDM-PON coexistence scenario with 2 THz guard band after transmission over hybrid optical-wireless.

large power window and thus safe coexistence scenario it is recommended that UDWDM+ FSO with TWDM channels should have at least 2 THz frequency spacing. The overall network's performance in terms of the BER is evaluated in the center frequency from the aggregate 120 Gb/s (12x10 Gb/s which could represent a LR10 Ethernet link [30]) for 40 km fiber. As the input power increases for lower guard band, the BER performance is degraded due to inter-channel nonlinearities that induce both amplitude and phase noises in the recovered 16QAM symbols. The BER dependence on guard band is noticeable for lower guard band as TWDM power increases. TWDM envisages high powers even for the first ODN classes (e.g. N2 requires 5-9 dBm after the coexistence element [24]). Fig. 5.15 shows the measured BER as a function of the receiver input power per channel in both BTB and 40 km fiber plus FSO for 9 dBm per TWDM channels with 2 THz guard band.

5.4 Fully Bidirectional Hybrid ODN Advanced Modulation PON (paper C15)

In this section, taking advantage of Nyquist pulse shaped UDWDM (6.25 GHz ITU-T grid), we experimentally characterize a coherent bidirectional PON system over up to 80 km SSMF plus two FSO links (of 60 m outdoor FSO and 20 m indoor FSO, simultaneously). The system performance regarding the back reflection and power budget in hybrid ODN is evaluated.

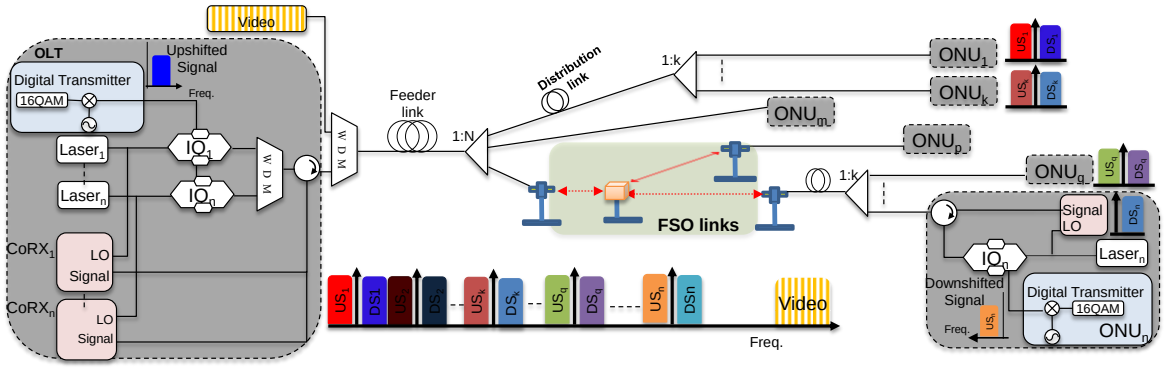

Figure 5.16 Proposed hybrid bidirectional coherent PON system with video overlay.

Fig. 5.16 depicts a diagram of proposed coherent PON system. In OLT transmitter, several lasers with the same number of receivers are used, and modulated with up shifted digital data. The DS signals may be combined by other system in fiber or hybrid ODN. In ONU, the DS signal is detected by coherent detection with same laser frequency in OLT and digital signal is down shifted and modulated by IQ modulator and to send to OLT. With this setup we are able to test all proposed impacts: RBS and hybrid ODN power budgets.

Fig. 5.17 shows the experimental setup used to demonstrate the proposed PON architecture that is equivalent to our previously proposed system (please refer to the section 5.3). To test the potential use of FSO technology as part of the system, a 1:2 FSO link, one 60 m outdoor FSO and one 20 m indoor FSO (inset of Fig. 5.17) links based on 3 collimators, polarization independence beam splitter and convex mirror, was inserted in the last span with the extra loss of ~9 dB in outdoor link and 11 dB in indoor link. We point out that each FSO link operates in bidirectional mode and with an optical switch we were able to characterize both video overlay and bidirectional outdoor/indoor links.

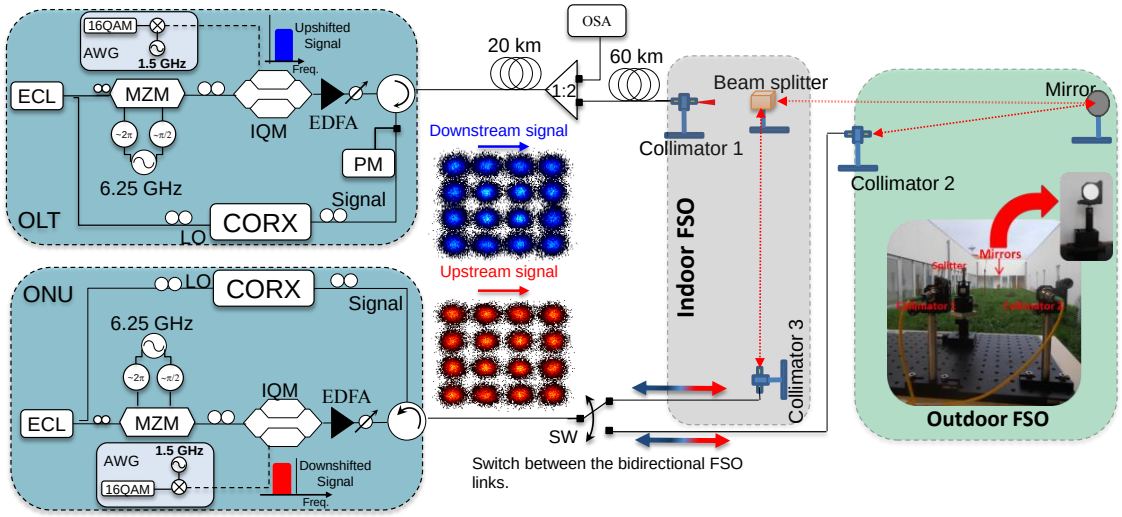

Figure 5.17 Bidirectional experimental setup. Insets: outdoor and indoor FSO setup with the picture in inset.

We started by evaluating the impact of RBS and fiber nonlinearities in the US and DS channels separately (e.g. they do not coexist in the fiber). Fig 5.18 (a) presents the sensitivity penalty @ BER=3.8 x 10^{-3} of DS signals as a function of reflected power for 12 channels in 80 km fiber plus FSO. At -30 dBm total reflected power measured by optical power meter (PM in Fig. 5.17) corresponding to -6 dBm launched power in the fiber, we achieved 0.5 dB sensitivity penalty. We note that, all connectors used in this experiment are APC. The receiver sensitivities for 80 km fiber plus FSO are presented in Fig 5.18 (b). Thanks to coherent detection, ODN budget is sufficient without the need for an EDFA. About 0.5-1 dB sensitivity penalty was achieved between bidirectional transmission over SSMF+FSO and bidirectional transmission over SSMF only.

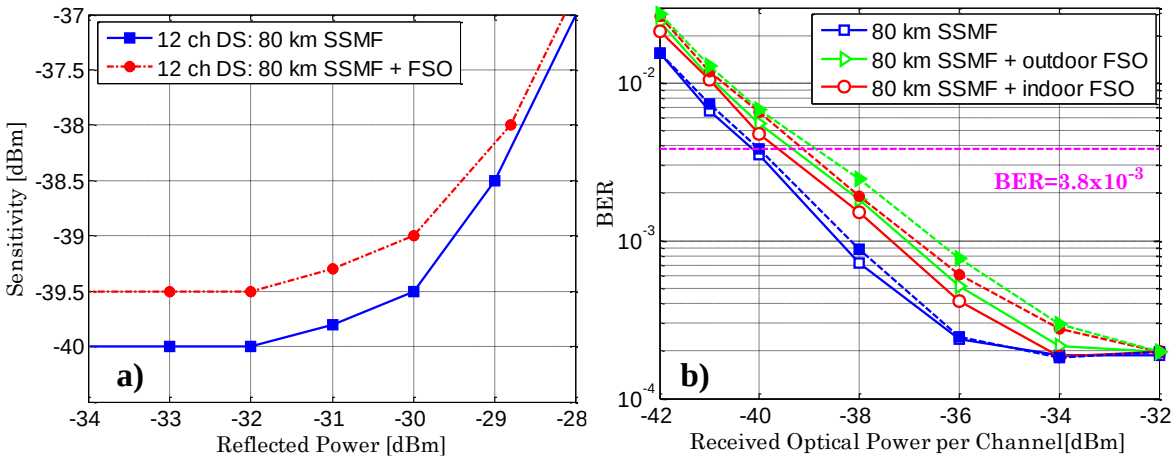

Figure 5.18 (a) Impact of back-reflection on receiver sensitivity of center channel of the 12 DS @ BER=3.8 x 10^{-3}. (b) Measured BER for the central channel of the 12 DS (solid lines+open markers) and 12 US (dashed lines + filled markers) channels.

5.5 Concluding Remarks

In this chapter, we successfully tested an ultra-broadband optical wireless link in a building to building scenario. We demonstrated that a FSO system based on DP-QPSK format with WDM and coherent detection is able to support an ultra- broadband capacity up to the record of 1.6 Terabit/s (16x100 Gb/s) over a free space link of 80 m and a propagation of 40 km of optical fiber. Also, an innovative bidirectional UDWDM-PON based on advanced modulation formats and Nyquist pulse shaping in a hybrid ODN (fiber plus PtMP-FSO) was experimentally demonstrated. Also, for the first time, an outdoor/indoor full duplex FSO link has been added to 80 km fiber without optical amplification and the desired receiver sensitivity as well as a power budget of 33.5 dB with reduced penalty (relatively to BTB case and fiber) were achieved. Hybrid splitting, based on beam splitters was also demonstrated showing a path towards FSO distribution in temporary campaigns or controlled environments.

References

[1] https://www.abiresearch.com/press/more-than-30-billion-devices-will-wirelessly-conne.

[2] D. M. Forin, G. Incerti , G.M. Tosi Beleffi , A. Teixeira, L.N. Costa, P. Andrè , B. Geiger, E. Leitgeb and F. Nadeem, "Free Space Optical Technologies" - *Chapter in Trends in Telecommunications Technologies,* Christos J Bouras, In-Tech, London, 2010.

[3] V. Jungnickel, "High-speed optical wireless communica-tions technologies," Proc. *Optical Fiber Communication Conf. (OFC)*, Anaheim, CA, March 2014, paper Th1F.5,

[4] B. Flecker, E. Leitgeb, S. Sheikh Muhammad, C. Chlestil, E. Duca, and V. Carrozzo, "Measurement of light attenuation in fog and snow conditions for terrestrial FSO links," *15th IST Mobile and Wireless Communications Summit*, June 2006.

[5] M. D'Amico, A. Leva, and B. Micheli, "Free-space optics communication systems: first results from a pilot field-trial in the surrounding area of Milan, Italy," *IEEE Microwave and Wireless Components Letters*, vol. 13, pp. 305-307, Auguest 2003.

[6] J. D. Montgomery, "Free-space optics seen as viable alternative to cable," *Lightwave (Analyst Corner)*, pp. 43-44, April 2004.

[7] G. Cossu, A. M. Khalid, P. Choudhury, R. Corsini, and E. Ciaramella "3.4 Gbit/s visible optical wireless transmission based on RGB LED," *Opt. Express*, vol. 20, n. 26, pp. B501-B506, December 2012.

[8] J. Wang, J. Yang, I. M. Fazal, N. Ahmed, Y. Yan, H. Huang, Y. Ren, Y. Yue, S. Dolinar, M. Tur and A. E. Willner "Terabit free-space data transmission employing orbital angular momentum multiplexing" *Nat. Photon.* 6, pp. 488-496, June 2012.

[9] http://en.ria.ru/science/20130129/179111471.html.

[10] D.M. Forin, G.M. Tosi Beleffi, N. Corsi, V. De Sanctis, V. Sacchieri, G. Cincotti, F. Curti, A. Teixeira, "Very high bit rates WDM transmission on a transparent FSO System," Proc. *Eur. Conf. Opt. Commun. (ECOC)*, Berlin, Germany, September 2007, paper P131.

[11] M.C. Jeong , J.S. Lee, S.Y. Kim, S. W. Namgung, J.H. Lee, M.Y. Cho, S.W. Huh ; Y.S. Ahn, J.W. Cho, J.S. Lee, "8 x 10-Gb/s terrestrial optical free-space transmission over 3.4 km using an optical repeater" *IEEE Phot. Tech. Letters*, vol. 15, no. 1, pp 171-173, January 2003.

[12] P. Chen, S. Chang, S. Shuen-Te Ji, H. Lin, H. Tsay, P. Huang, W. Chiang, W. Lin, S. Lee, H. Tsao, J.Wu, J. Wu "Demonstration of 16 channels 10 Gb/s WDM free space transmission over 2.16 km," *IEEE/LEOS Summer Topical Meetings*, Piscataway, NJ, July 2008, pp. 235-236.

[13] N. Cvijetic, D. Qian, J. Yu, Y. Huang, and T. Wang "100 Gb/s per-channel free-space optical transmission with coherent detection and MIMO processing," Proc. *Eur. Conf. Opt. Commun. (ECOC)*, Vienna, Austria, September 2009, paper 9.6.3.

[14] E. Ciaramella, Y. Arimoto, G. Contestabile, M. Presi, A.D'Errico, V. Guarino, and M. Matsumoto,"1.28 Terabit⁄s (32×40Gbit⁄s) WDM transmission system for free space optical communications," *Journal of Selelected Areas Commun.*, vol. 27, no. 9, pp. 1639-1645, December 2009.

[15] Z. Ghassemlooy, H. Le Minh, S. Rajbhandari, J. Perez, and M. Ijaz, " Performance analysis of Ethernet/fast-Ethernet free space optical communications in a controlled weak turbulence condition, " *Journal of Lightwave Technology*, vol. 30, no. 13, pp. 2188-2194, July 2012.

[16] V. Sacchieri, V. De Sanctis, N. Corsi, F. Curti, M. Guglielmucci, G.T. Beleffi, D. Forin, G. Cincotti, "DWDM transparent FSO system for in/outdoor applications at high bit rates," Proc. *International Conf. on Transparent Networks (ICTON)*, Rome, Italy, July 2007, paper M0.P.1.

[17] H.-Y Hsu, W.C Lu, H.L. Minh, Z. Ghassemlooy, Y.-L. Yu, S.-K Liaw, "2 x 80 Gbit/s DWDM Bidirectional Wavelength Reuse Optical Wireless Transmission," *Photonics Journal, IEEE* , vol. 5, no. 4, pp.7901708-7901708, August 2013.

[18] A. Shahpari, A. Abdalla, G. Parca, J. Reis, R. Ferreira, M. Lima, V. Carrozzo, G. M. Tosi Beleffi and A. Teixeira, "Ultra high capacity PON systems with free-space optical communications," *Fiber and Integrated Optics*, vol. 33, no. 3, pp. 149 -162, July 2014.

[19] I. Kim, M. Mitchel, E. Korevaar "Measurement of scintillation for free space laser communication at 785 nm and 1550 nm," *SPIE proceedings, Optical Wireless Communications II*, vol. 3850, 49-62, September 1999.

[20] R.L. Philip, L.C. Andrews "Laser beam propagation through random media," *SPIE publications*, Washington, 1998.

[21] E. Leitgeb, S. Muhammad, C. Chlestil, M. Gebgart, U. Birnbacher "Reliability of FSO links in next generation optical networks," Proc. *International Conf. on Transparent Networks (ICTON)*, Barcelona, Spain, July 2005, paperTu.B3.1.

[22] A. Shahpari, J. D. Reis, S. Ziaie, R. Ferreira, M. J. Lima, A. N. Pinto and A. Teixeira, "Multi system next-generation PONs impact on video overlay," Proc. *Eur. Conf. Opt. Commun. (ECOC)*, London, September 2013, paper Tu.3.F.3.

[23] T. Sakamoto, T. Kawanishi, and M. Izutsu, "Optimization of electro optic comb generation using conventional Mach-Zehnder modulator," Proc. *International Topical Meeting on Microwave Photonics*, Victoria, BC, October 2007, pp. 50-53.

[24] ITU-T,www.itu.int/rec/T-REC-G.989.1/e.

[25] J. D. Reis, D. M. Neves and A. L. Teixera, 'Analysis on nonlinearities on coherent ultra-dense WDM-PONs using Volterra series," *Journal of Lightwave Technology*, vol. 30, no. 2, pp. 234-241, January 2012.

[26] A. Shahpari, J. D. Reis, R. Ferreira, D. M. Neves, M. Lima and A. N. Teixeira, "Terabit+ (192×10 Gb/s) Nyquist shaped UDWDM coherent PON with upstream and downstream over a 12.8 nm band," Proc. *Optical Fiber Communication Conf. (OFC)*, Anaheim, CA, March 2013, paper PDP5B3.

[27] A. Shahpari, R. S. Luis, J. D. Reis, R. Ferreira, Z. Vujicic , J. M. D. Mendinueta, M. Lima, N. Wada and A. Teixeira, "Fully coherent self-homodyne bidirectional enhanced performance

PON," Proc. *Optical Fiber Communication Conf. (OFC),* San Francisco, CA, March 2014, paper W4G.1.

[28] D. Lavery, M. Paskov and S. J. Savory, "Spectral shaping for mitigating backreflections in a bi-directional 10 Gbit/s coherent WDM-PON," Proc. *Optical Fiber Communication Conf. (OFC),* Anaheim, CA, March 2013, paper OM2A6.

[29] F. Chang, K. Onohara, and T. Mizuochi, "Forward error correction for 100 G transport networks," *IEEE Commun. Mag.*, vol. 48, no. 3, pp. S48-S55, March 2010.

[30] http://standards.ieee.org/about/get/802/802.3.html.

CHAPTER 6 CONCLUSIONS AND FUTURE WORK

Summary

Potential paths and parameters for the optimization of the optical access requirements were addressed. Also, spectrally efficient enhanced performance coherent passive optical networks were proposed and characterized in hybrid optical distribution networks. This final chapter summarizes the salient features from these investigations. Some guidelines for future research works are also suggested.

6.1 Summary of the Contributions

The exponential growth of bandwidth-consuming Internet services such as cloud computing and online video streaming is fuelling the development of Wavelength Division Multiplexing Passive Optical Networks (WDM-PONs) with dedicated 10 Gb/s per user in next generation heterogeneous access networks and directly drives advanced R&D efforts. However, when looking ahead, the multiplicity of services, the plurality of end users and the inflexibility of cost constraints are also future challenges for practical optical access networks implementation, to develop novel and economic optical access structure.

Throughout the different chapters of this thesis we addressed potential paths and parameters for the optimization of the access requirements, technologically and economically. We started with energy consumption in optical access networks to address different theoretical techniques, providing the performance improvement in Optical Distribution Networks (ODN) topologies. It was concluded that by optimizing the ODN and type of splitter in PON we can increase the energy efficiency of optical access networks. The possibility of saving energy in the Optical Line Terminal (OLT) using different types of splitter configurations and long reach PON features was presented. The best efficiency in terms of OLT port loading and power saving for low subscription rate areas was achieved by the combination of reach extension technologies and cascaded splitter structures. From the operator point of view, for long life time and for Next Generation Optical Access Networks (NG-OAN) migration, these benefits stay without any change in deployment of network. Also, we established that the combination of transparent ODN in conjunction with tunable technology gives the best energy saving potential. In addition, some of the factors that can be considered in the analysis of energy consumption in optical access networks were addressed. These parameters were put together in a model that sets a fair and consolidated rating for each technology, taking into account the sustainability of the system for its life time. A metric was proposed to evaluate the energy efficiency of optical access technologies. The metric considered the impact of user profiles, ODN topologies and equipment characteristics.

The next step was to demonstrate high spectral efficiency and high capacity in optical access networks. The study and classification of existing Ultra Dense Wavelength Division Multiplexing PONs (UDWDM-PON) enabled us to propose an architecture with new

spectrally efficient PON in optical access networks. This work experimentally and numerically investigated the transmission capabilities of coherent UDWDM-PON scenarios employing Nyquist-shaped 16-Quadrature Amplitude Modulation (16QAM) modulated channels. By exploiting 16 channel groups spanning over only 12.8 nm in the 100 GHz frequency grid, the network capacity has been increased to 1.92 Tb/s (10 Gb/s per user). In addition, this work has shown the proof-of-concept for a fully loaded coherent PON with 24 dB ODN budget, where a single CW lightwave per user generated at the OLT was sufficient for coherent homodyne detection and generation of US and DS data. With reduced impact of the Rayleigh Back-Scattering (RBS) effect due to Nyquist-pulse shaping and frequency upshifting, the proposed system allowed us to demonstrate a fully loaded bi-directional PON handling almost 20 Tb/s in a single fiber, allowing for 1000+ terminals with a sustained data rate of 10 Gb/s, business or mobile backhaul users. In reality, since our terminals are not able to generate or consume such an humongous traffic at all times (one Blu-ray disk/s downloaded and another uploaded), traffic can be shared, and this PON would allow virtually unlimited bandwidth to more than 50 thousand terminals. In the sense of capacity and spectral efficiency, this work has demonstrated record bidirectional transmission in optical access networks and still stands as the ultimate full demo of such a high aggregated rate in a PON.

In addition, we have reviewed some of the major migration limitations in current PONs having in mind the introduction of the NGPON2. This work, firstly investigated the required guard band between UDWDM-PON scenarios (16x1.25 Gb/s coherent Quadrature Phase Shift Keying (QPSK) spaced by 3.125 GHz) and video overlay and 10 Gb/s-NRZ technologies. Experimental results show that UDWDM-PON is a promising solution for NG-OAN deployments since it is robust enough to coexist with such legacy PON technologies. In addition, we have validated a model for prediction of the dynamic Stimulated Raman Scattering (SRS) effect on RF-video based on the power spectral density of the digital baseband signal. With this model, maximum number and the launch power limits per channel of digital baseband signals for an acceptable level of carrier-to-Raman-crosstalk ratio of RF video were estimated. Besides that, the SRS of proposed spectrally efficient UDWDM system on RF-video was measured and using the model extrapolated for high number of channels. We observed that by shifting the signals from center wavelength, dynamic SRS effect on other sensitive access systems like video overlay is reduced along

with RBS, simultaneously. As the required power per up-shifted downstream channels in the fiber was lesser than -8 dBm and the signal presented reduced SRS, the overall number of channels in the proposed PON system allows high number of channels in coexisting systems.

In the last part of this work, we experimentally demonstrated a set of high capacity optical wireless links using dual-polarization QPSK and 16-QAM Nyquist pulse shaped signal in metro and access scenarios. Bidirectional (full duplex) optical wireless transmission was also investigated and allows a smooth and full integration between fiber and optical wireless access networks. These experiments demonstrated that optical wireless technology can enhance more value-added services to next-generation broadband optical metro/access networks in terms of transmitted data security and medical immunity as well as network resiliency.

The proposed system architectures and obtained results pave the way to future access networks with much higher link flexibility and increased capacity and can be very useful for further characterization and optimization of flex-grid hybrid ODN architectures and coexistence scenarios. With advanced modulation formats and pulse shaping, coherent UDWDM-PON allows a high number of users as well as enhanced network functionalities, such as load balancing and power saving. Diversity in types of modulation formats allows for pay-as-you-need dedicated bandwidth in different places and times, especially for FSO applications, where the modulation format can be changed according to the quality of signal. In addition using tuneablility in the OLT and ONU, power saving could be achieved by changing the data-rate and turning on/off OLT ports or individual ONUs. In a nutshell, we stress the immense flexibility of the proposed architecture, which enables future applications of Software-Defined Networking (SDN) and elastic optical networks.

6.2 Main Challenges and Future Work

This Ph.D. work has addressed a number of significant issues such as energy efficiency, spectral efficiency, flexibility and high capacity in optimization of next-generation optical access networks. However many other key issues require further investigations, as listed below:

- Conceptual design and implementation of innovative and energy efficient transmitters and receivers with the ability to tune data rates dynamically, according to the network state.
- Propose Digital Signal Processing (DSP) architectures for real-time applications in order to optimize the optical digital transceivers. Several problems need be solved, like the bandwidth limitations using pre-distortions filters or the power non-linear interferences, taking in to account the cost of the Analog to Digital Converter (ADC)/Digital to Analog Converter (DAC) devices.
- Conceptual design and implementation of integrated photonics transmitter and receiver for self-homodyne detection systems.
- Develop a model for estimating the static Raman crosstalk on high number of UDWDM channels as Raman nonlinearities are extremely broadband and they would nonlinearly couple all wavelengths.
- Implementing novel and reliable hybrid optical wireless networks (fiber optic plus FSO parallel with fiber optic plus RF) for higher network resiliency.
- Implementation of SDN as an orchestrator in optical wireless networks for closing the gap between bandwidth demand and revenue generation.
- Reducing complexity in DSP for both coherent and direct detections as it becomes a critical technical and economic challenge. It should be noted that the advanced SDN functionality would be implemented in the context of a DSP-based optical access platform.